UNIVERSITÀ DEGLI STUDI DI MILANO

PhD Course in

Experimental Medicine and Medical Biotechnologies – XXXIII cycle

Department of Medical Biotechnologies and Translational Medicine (BioMeTra)

"Dendritic cell subsets in the pathogenesis of High Grade Gliomas"

Tutor: Prof. Silvia DELLA BELLA

PhD Course Coordinator: Prof. Massimo LOCATI

PhD thesis of

Claudia CARENZA

R11986

Academic Year 2019-2020

Abstract

Background and aims. High grade gliomas (HGGs) are aggressive brain tumours characterized by a poor prognosis and the ability to promote an immunosuppressive tumour microenvironment that impairs anti-tumor immune responses. Therefore, there is increasing interest in developing new immunotherapeutic approaches, aimed at boosting anti-tumor immune responses in HGG patients. Because HGG has shown the highest susceptibility to dendritic cell (DC) vaccines amongst other human cancers, DC-based immunotherapeutic strategies may be particularly promising in these patients. DCs are antigen presenting cells that have the unique ability to initiate antitumor immune responses, making these cells crucial in cancer immunosurveillance. They are a rare population composed of different subsets that differ each other in origin, immunophenotype and function. The differential role of different DC subsets in HGG, and in particular the subsets specifically recruited into the tumour site and the impact of HGG on the activatory/tolerogenic properties of DCs have been poorly investigated, so far. For these reasons, in this study we performed a deep characterization of circulating and tumour-infiltrating DC subsets, and investigated possible correlations between DC parameters and histopathological and molecular HGG features, patient outcome and response to treatment. To this aim, we used multiparameter flow-cytometry and single-cell RNA sequencing (scRNAseq), which allow complex analyses on high-dimensional data.

Materials and methods. In this cross-sectional study we enrolled HGG patients undergoing surgery at their first diagnosis, and we applied an 18-colour flow-cytometry panel that allows the identification of DC-lineage DCs (pDCs, cDC1s, cDC2s) and inflammatory DCs (slanDCs, moDCs), and the characterisation of their activatory/inhibitory state. This panel was applied to DC characterization in the peripheral blood (n=23) and the tumour lesion (n=10) of HGG patients. Twelve whole blood samples obtained from healthy donors (HDs) and 3 healthy brain tissue samples were included as controls. scRNAseq experiments were performed on 7 tumoral samples and 2 healthy brain tissues obtained from HGG patients, by using 10x Genomics technology. Ingenuity Pathway Analysis (IPA) software was used to investigate the pathways and functions differentially activated or inhibited in infiltrating DCs. We also performed a longitudinal study on a second cohort of patients, diagnosed with recurrent HGG and enrolled in different immunotherapeutic early clinical trials (ieCTs), mainly containing immune checkpoint inhibitors (n=17). In these patients, we assessed the count and phenotype of circulating DC subsets before and at different time points after immunotherapy, by using the same 18-colour flow-cytometry panel described above. Multivariate analyses were used to correlate DC parameters with the patient outcome.

Results. In the cross-sectional study, we observed by flow-cytometry that the frequency of circulating pDCs, cDC1s, cDC2s and slanDCs was significantly lower in HGG patients than HDs. DC reduction was evident only in patients affected by the most severe form of HGGs (IDHwt IV grade gliomas). The analysis of tissue DCs revealed that DC subsets were absent in healthy brain parenchyma, whereas they infiltrated HGG tumour tissues. In particular all subsets of myeloid DCs (including cDC1s, cDC2s, slanDCs, and moDCs) were observed in the tumours, whereas pDCs were observed only in a few patients. Tumour-infiltrating DCs were markedly reduced in corticosteroid-receiving patients. By performing scRNAseq, we confirmed that DCs were mostly absent in healthy brain parenchyma whereas they were present in tumour samples and could be sub-divided in 2 sub-clusters. By IPA analysis, we observed a functional dichotomy between these clusters, with the largest one being characterised by an impaired/dormancy state, as assessed by the down-regulation of pathways and functions related to pro-inflammatory responses, cell motility and cell interactions, compared with the smallest cluster characterised, on the contrary, by a more active profile.
In the longitudinal study performed on relapsed HGG patients enrolled in ieCTs, we observed that patients with a positive clinical response to immunotherapeutic agents, as assessed by an increased overall survival, showed an increase in the number of circulating cDCs.

Conclusions. This study demonstrated that different subsets of DCs infiltrate human HGGs, but are mainly characterized by a transcriptomic profile suggestive of a functional impairment. These results provide novel insights into the comprehension of the molecular mechanisms of DC impairment in HGG microenvironment, and pave the way for the development of novel strategies aimed at restoring the ability of DCs to activate cytotoxic anti-tumour immune cells. Our observation in the longitudinal study that an increase of cDCs correlated with a better clinical response to immunotherapy seems to support the relevant role played by DCs in the control of HGG growth. On the other hand, our study also demonstrated that corticosteroid treatment, commonly used in HGG patients for the management of cerebral oedema, reduces the number of tumour-infiltrating DCs. Based on the above considerations, this finding may suggest a negative impact of corticosteroid treatment on anti-tumour immune responses, thus supporting the use of alternative approaches to control this clinical complication.

Altogether, our results support and encourage the study of DCs in HGG, in order to improve our knowledge on the role played by DCs within the immunosuppressive tumour microenvironment that characterises this human cancer. To this aim, in the near future we plan to apply new bioinformatic tools to the analysis of single-cell data collected in HGG tumour environment that may be particularly useful for investigating the intricate interactions occurring between DCs and other HGG-infiltrating immune cells or malignant glioma cells.

Index:

1. Introduction 8
1.1 Dendritic cells 9
1.1.1 Dendritic cell functions 9
1.1.2 DC ontogeny 12
1.1.2.1 Conventional DC subset 1 (cDC1s) 13
1.1.2.2 Conventional DC subset 2 (cDC2s) 15
1.1.2.3 Plasmacytoid DCs (pDCs) 16
1.1.2.4 Inflammatory DCs 18
1.1.3 Methods to study human DCs 19
1.2 High grade gliomas 20
1.2.1 Classification of high-grade gliomas 20
1.2.2 Oncogenic pathways 24
1.2.3 DCs in healthy brain and HGG 26
1.2.4 Immunosuppression in HGGs 28
1.2.5 Treatment options for HGGs 29
1.2.5.1 Surgery 30
1.2.5.2 First-line treatment after surgery 31
1.2.5.3 Therapeutic options for recurrent HGGs 32
1.2.5.3.1 Anti-angiogenic drugs 32
1.2.5.3.2 EGF receptor inhibitors 33
1.2.5.3.3 Immunotherapeutic strategies for HGG treatment 33
1.2.5.3.3.1 Immune checkpoint inhibitors 34
1.2.5.3.3.2 Other agents remodelling the immunosuppressive microenvironment 35
1.2.5.3.3.3 Peptide vaccines 36
1.2.5.3.3.4 DC-based vaccines 37
1.2.5.3.3.5 Reprogramming of tumour-associated DCs for anti-tumour therapies 38
2. Aim 41
3. Materials and Methods 44
3.1 Reagents 45
3.2 Subjects enrolled 47
3.2.1 First HGG patient cohort 48
3.2.2 Second HGG patient cohort 48
3.3 Sample processing 49
3.3.1 Erythrocyte lysis in whole blood samples 49
3.3.2 Enzymatical protocol for glioma dissociation 49
3.3.3 Mechanical protocol for glioma dissociation 50
3.4 Multiparametric flow-cytometry analysis 50
3.4.1 Principles 50
3.4.2 Multicolour flow-cytometry strategy 52

3.4.3 Extracellular staining for whole blood and tissue samples 53
3.4.4 Staining for absolute count 53
3.4.5 Compensation 54
3.4.6 Fluorescence Minus Ones (FMO) controls 54
3.4.7 Antibody titration 55
3.4.8 Data Analysis 56
3.4.8.1 Flow-jo analysis 56
3.4.8.2 Uniform Manifold Approximation and Projection (UMAP) analysis 57
3.5 $CD45^+$ and $CD45^-$ cell sorting and Single-cell RNAseq 59
3.5.1 Sorting 59
3.5.2 Single-cell RNA sequencing 60
3.5.3 Ingenuity pathway analysis (IPA) 61
3.6 Statistical analysis 62
3.6.1 First HGG patient cohort 62
3.6.2 Second HGG patient cohort 62
4. Results 63
4.1 Flow-cytometry characterisation of DC subsets in the whole blood of HGG patients 64
4.1.1 Frequencies and absolute counts of DC subsets in the whole blood of HGG patients and HDs 64
4.1.2 Phenotype of DC subsets in the whole blood of HGG patients and HDs 66
4.1.3 Flow-cytometry characterization of DC subsets in healthy and tumour brain tissue obtained from HGG patients 71
4.1.4 Phenotype of DC subsets in tumour brain tissues obtained from HGG patients 72
4.1.4.1 Effects of type IV collagenase treatment on TIM-3 expression 75
4.1.5 Visualisation of flow cytometric data by UMAP 76
4.1.5.1 Comparison of circulating DCs from HGG patients and HDs using UMAP analysis 77
4.1.5.2 Identification of DC subsets in tumour tissues of HGG patients 77
4.2 Single cell RNA sequencing 82
4.2.1 Identification of DC cluster 83
4.2.2 Ingenuity Pathway Analysis 88
4.2.2.1 Canonical Pathway analysis 89
4.2.2.2 Diseases and Functions (DF) Analysis 96
4.3 Analysis of circulating DC subsets in a cohort of HGG patients treated with immunotherapeutic approaches 99
5. Discussion 102
6. References 114

1. Introduction

1.1 Dendritic cells

1.1.1 Dendritic cell functions

Dendritic cells (DCs) are considered professional antigen-presenting cells (APCs) since they are provided with specialized features, such as pathogen recognition, antigen capture, processing machinery and migratory capacity (Sallusto & Lanzavecchia, 2002). DCs take up pathogens and their antigens and communicate their presence to the adaptive immune system, initiating long-lasting antigen-specific responses. DCs originate in the bone marrow, circulate in the blood, and patrol peripheral tissues, acting as sentinels that sample the environment for antigens. Beyond their crucial ability to control adaptive immune responses, DCs also play an important role in shaping the innate immune response in the peripheral tissues where they detect and capture antigens, as they can locally produce high amounts of cytokines that can affect other innate immune cells present in the microenvironment (Harizi & Gualde, 2005).

DCs can exist in two functionally distinct states, immature and mature. Immature DCs are found in blood and peripheral tissues. They are highly skilled in phagocytosis, have a low ability to present antigens and express low costimulatory molecules. However, DCs can sense invading pathogens through the expression of a variety of sensors for pathogens components called pattern recognition receptors (PRRs); these receptors can be present on the plasma membrane, like some Toll-like receptors (TLRs), or in the cytosol, like NOD-like receptors (Mellman, 2013). Upon encountering ligands for these receptors, immature DCs are triggered to mature, making them efficient in displaying MHC-peptide complexes and costimulatory molecules on the surface. Activation of DCs induces C-C chemokine receptor (CCR) CCR6 and CCR5 downregulation and CCR7 upregulation, resulting in DC migration toward draining lymph nodes (Domogalla et al., 2017). In lymph nodes, DCs enter T cell-rich regions and stimulate antigen-specific memory or naïve T cell responses. Based on the pathogen encountered, the source of the antigens and the maturation signals received, DCs not only stimulate T cells, but also polarise the nature of the T cell response (Mellman, 2013). Indeed, antigens derived from extracellular sources, such as bacteria, protozoans, allergens or dead cells are usually associated with the major histocompatibility complex (MHC) II pathway. Proteins are internalized by endocytosis and delivered to endosomes and lysosomes, where the decreasing pH and increasing hydrolytic activity causes denaturation and cleavage of antigens. Peptides are then loaded on MHC-II complexes and transferred to the surface upon DCs maturation. These complexes are recognized by naïve CD4+ T lymphocytes that based on cytokines secretion and other co-stimuli develop into effector cells (Mellman, 2013).

On the other hand, antigens derived from endogenously synthesized components, such as viral proteins produced in the cytoplasm of infected cells, are typically associated with the MHC-I pathway. In this case, proteins are ubiquitinated, cleaved by the proteasome and the peptides are translocated into the endoplasmic reticulum (ER) to be loaded onto MHC-I complex (Mellman, 2013). These complexes are expressed on almost all cells in the body and are recognized by CD8+ cytotoxic T lymphocytes (CTLs), that perform immune defence against intracellular pathogens or tumours. However, naïve CTLs need to be activated by professional APCs, usually DCs, before they can exert their cytotoxic effector functions. For this reason, DCs have a particular ability called cross-presentation, since they are capable of processing also extracellular antigens - that escape the endosome route - with the MHC-I pathway (Kurts et al., 2010) (Figure 1).

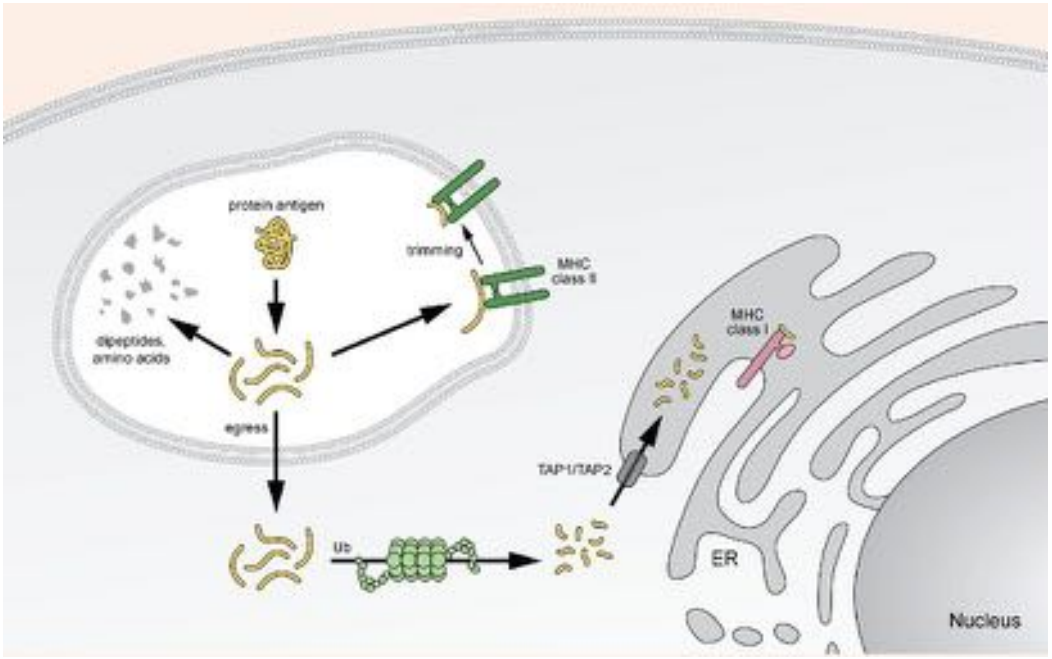

Figure 1. Pathways of antigen processing in DCs (Mellman, Cancer Immunol Res, 2013).

Another important feature of DCs is that they function as a bridge between the innate and the adaptive immune responses. Indeed, by the expression of PRRs they can sense danger and induce the expression of specialized costimulatory molecules that help to trigger T cells activation. Thus, to induce the response of a naïve T cell, three steps are required: the first one is the recognition of the MHC-peptide complex through the TCR on T cells; the second one is the binding of costimulatory molecules CD80/CD86 on DCs with CD28 present on T cells; the third one is the stimulation of T cells by DC-secreted cytokines (Domogalla et al., 2017).

Another molecule involved in DC maturation and activation is CD40, a surface receptor member of the Tumour Necrosis Factor Receptor superfamily (TNFRSF). The binding with its ligand, CD40L, which is expressed on activated T cells, induce the up-regulation of costimulatory molecules,

adhesion molecules and the production of the Th1-polarising cytokine IL-12. However, several studies demonstrated that CD40 plays a role in multiple effector T cell responses other than Th1. Moreover, it was demonstrated the CD40 expression on activated T cells, and also CD40L expression on DCs. Indeed, it was found that CD40-CD40L interactions between T cell and DCs provide reciprocal effects that both regulate T cells and DCs (Ma & Clark, 2009).

DCs are also deeply involved in the maintenance of immune tolerance, at both central and peripheral levels, by ensuring that in homeostatic conditions effector T cells do not recognise "self" antigens of the host. In the thymus tolerogenic DCs establish central self-tolerance by presenting self-antigens to developing T cells without costimulatory signals, leading to negative selection of T cells or T regulatory cell (Treg) differentiation (Domogalla et al., 2017). In the periphery, in non-inflammatory conditions, DCs encounter and present self-antigens and non-pathogenic environmental antigens to T cells. In this condition, the production of Tregs is favoured; these "induced" Tregs, that are not produced in the thymus, help to prevent immune responses against environmental antigens entering from the gut or the airways (Mellman, 2013).

Tolerogenic DCs can exploit different immunosuppressive mechanisms to induce tolerance (Figure 2). They can display an immature phenotype characterised by low expression of co-stimulatory and MHC molecules and altered cytokine production, leading to T cell anergy or Tregs promotion. Also, secretion of anti-inflammatory cytokines, like IL-10 or TGF-β, and reduced production of pro-inflammatory cytokines induce tolerance. Another mechanism relies on the induction of apoptosis of T cells via Fas cell surface death receptor (FasL/Fas) interactions. Tolerogenic DCs can also express inhibitory receptors such as programmed cell death ligand (PDL)-1, inhibitory Ig-like transcripts (ILT) and T cell/transmembrane, immunoglobulin, and mucin (TIM) receptors, which act on T cells by dampening TCR signalling. In addition, tolerogenic DCs alter T cell responses by modulating metabolic parameters; for example, the release of indoleamine 2,3-dioxygenase (IDO) reduces T cell proliferation (Domogalla et al., 2017).

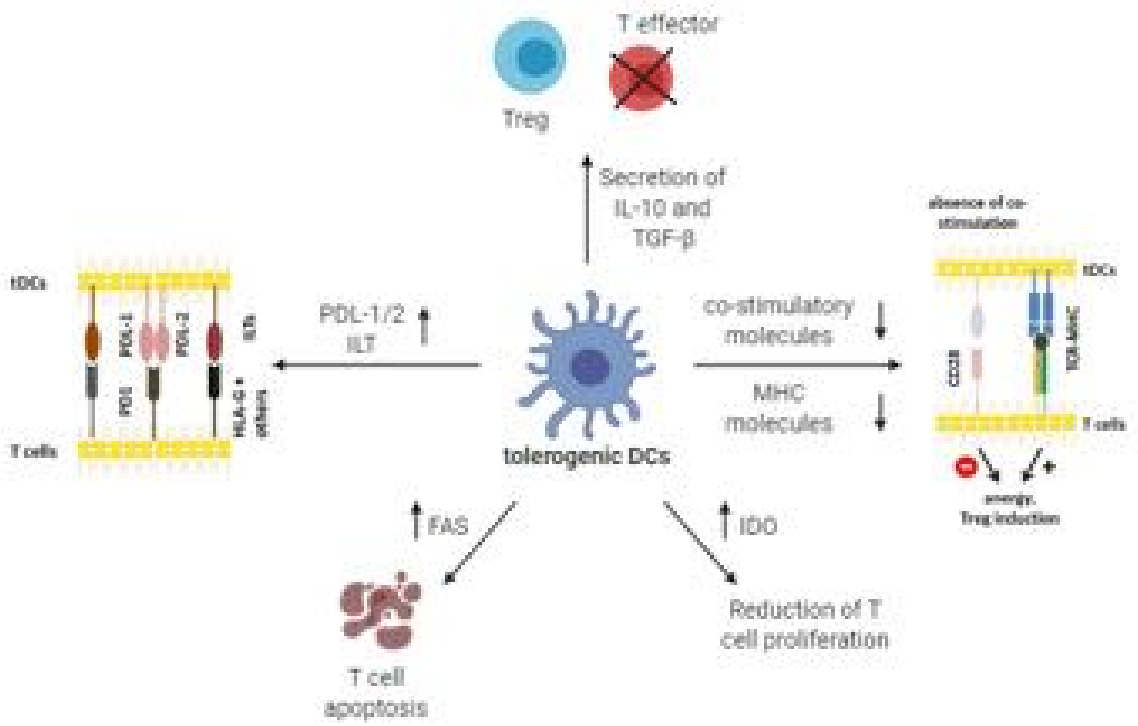

***Figure 2**. Immunosuppressive mechanisms of tolerogenic DCs (Adapted from Domogalla et al, Front Immunol., 2017).*

1.1.2 DC ontogeny

DC ability to activate different arms of adaptive immunity relies not only on their state of activation, as discussed above, but also on their belonging to different subsets that are each endowed with functional specialization (Collin & Bigley, 2018). Studies on human DCs unveiled the presence of subsets that differ for ontogeny, transcription factors requirement, migration patterns and immunological functions. In the bone marrow, CD34+ hematopoietic stem cells (HSCs) can generate multipotent progenitors (MPPs), which can either differentiate into common myeloid progenitors (CMPs) and common lymphoid progenitors (CLPs). Then, CMPs expressing fms-related tyrosine kinase 3 (Flt3) differentiate into the macrophage-DC progenitor (MDP) that is the common precursor for monocytes, macrophages and DCs (Eisenbarth, 2019). Common DC progenitors (CDPs), derived from MDPs, generate a precursor DC population (pre-DC), which does not yet express the full phenotype of differentiated DCs. This precursor is released in peripheral blood and reaches terminal differentiation in 2 subsets of conventional (or myeloid) DCs (cDCs), namely cDC1 and cDC2, in lymphoid organs and peripheral tissues; these subsets are characterized by the expression of myeloid markers, including CD11c. In addition, CDP can give rise to another subset called plasmacytoid DCs (pDCs), which complete their differentiation in the bone marrow and are then released to circulate in

the blood and peripheral or lymphoid tissues (Carenza et al., 2019; Reizis, 2019). Several studies have demonstrated that pDCs can actually differentiate from progenitors committed to both myeloid and lymphoid lineages (Reizis, 2019). Altogether, the subsets of cDC1s, cDC2s and pDCs are commonly known as DC-lineage DCs and are present in homeostatic conditions in both blood and tissues (Eisenbarth, 2019).

Moreover, there are subsets classified as inflammatory DCs, such as monocyte-derived DCs (moDCs) and a small population of 6-sulfo-LacNAc (slan)-positive cells, called slanDCs. Transcriptomic analyses suggest that these subsets derive from monocyte precursors and under inflammatory conditions, they rapidly proliferate and infiltrate the site of inflammation, where they are involved in antigen presentation to T cells, pathogen clearance and cytokine production (Carenza et al., 2019; Collin et al., 2013; Eisenbarth, 2019) (Figure 3).

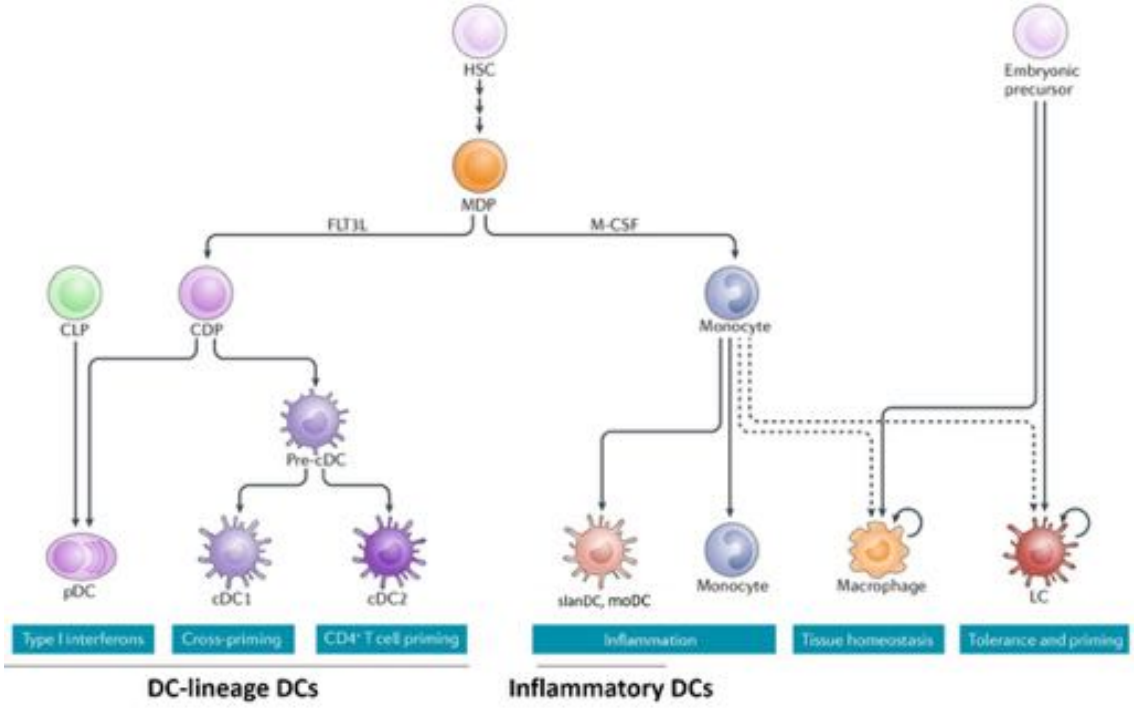

Figure 3. *Functionally specialized conventional and non-conventional dendritic cell subsets and related lineages (adapted from Eisenbarth, Nat Rev Immunol., 2019).*

1.1.2.1 Conventional DC subset 1 (cDC1s)

Human cDC1s represent the 0.02-0.03 % of total peripheral blood mononuclear cells (PBMCs) (Carenza et al., 2019; O'Keeffe et al., 2015). They were originally described as a subset of blood DCs with a high expression of CD141 (BDCA-3, thrombomodulin), a membrane receptor for thrombin, but also characterized by myeloid marker expression, as CD11c, CD13 and CD33. To discern cDC1s from cDC2s, other markers have been considered, such as CLEC9A, the C-type lectin receptor for actin exposed during cell necrosis; CADM1, a cell adhesion molecule; indoleamine 2,3-dioxygenase

(IDO), which is an enzyme implicated in immune modulation (Villani et al., 2017)). Several studies reported the presence of human cDC1s in blood and among resident DCs of lymph nodes, tonsils, spleen and bone marrow, but also in non-lymphoid tissues, like skin, lung, intestine and liver, with evidence of enrichment in tissues compared to blood (Collin & Bigley, 2018).

The development of human cDC1s is mainly dependent upon Interferon Regulatory Factor 8 (IRF8) and Basic leucine zipper transcription factor (BATF3). IRF8 is considered a fundamental factor in promoting DC potential over other lineages during haematopoiesis. In fact, IRF8 limits CEBPA-mediated granulocytic differentiation; interacting with KLF4, IRF8 modulates the balance between DCs and monocytes differentiation; by competing with IRF4, IRF8 controls the output between cDC1 and cDC2; also, BATF3 ensures that IRF8 transcription maintains cDC1 maturation (Tamura et al., 2015).

An important feature of human cDC1s is the high expression of TLR3, which recognize dsRNA, and the chemokine receptor XCR1. Unlike the mouse counterpart, human cDC1s lack in the expression of TLR4 and TLR9, thus they do not produce high levels of IL-12. Another difference stands in the high expression levels of TLR8 in human cDC1s, which binds bacterial ssRNA and mammalian mitochondrial ribosomal RNA; nonetheless, even in response to TLR8 ligation, human cDC1s fail to produce appreciable amounts of IL-12, suggesting that they are not the main producers of this cytokine (Macri et al., 2018).

Instead, human cDC1s are considered the major producers of type III IFNs (IFN-λ) in response to TLR3 ligation. The IFN-λ family consists of four members that are functionally related to type I IFNs, hence being involved in protection against viruses (O'Keeffe et al., 2015).

Regarding their role in immunity, cDC1s have been described as the subset that has a higher intrinsic capacity to cross-present antigens via MHC class I to activate CD8+ T cells and induce cytotoxic responses (Collin & Bigley, 2018). In particular, human cDC1s excel in cross-presenting cellular antigens, immune complexes and antigens specifically targeted to late endosomes, thanks to their high expression of CLEC9A, TLR3 and XCR1. The ligand of XCR1, which is XCL1, is secreted by activated CD8+ T cells and act as a powerful chemoattractant. These features point out the crucial role of cDC1 in anti-tumour and anti-viral CTL responses. Moreover, human cDC1s can polarize CD4+ cells towards a Th1 phenotype, especially after ligation with TLR3. However, unlike the mouse counterpart, human cDC1s do not possess a specialized capacity to induce Th1 responses, since several studies reported that human cDC2s also have a similar ability. This is probably concordant with the findings that human cDC1s are not the major producer of IL-12, which has an important role in Th1 induction (O'Keeffe et al., 2015).

At last, in mice, cDC1s have been reported to exert tolerogenic functions, even though this potential is not well documented in humans. Recent studies in human cDC1s found a selective expression of TLR10, which is an anti-inflammatory TLR with inhibitory properties (Jiang et al., 2016). For this reason, further investigations are needed to better understand the role of human cDC1 in tolerance mechanism.

1.1.2.2 Conventional DC subset 2 (cDC2s)

Human cDC2s are the major DC population in blood, representing up to 0.5-1% of total PBMCs. This subset is also present in lymph nodes, tonsils, spleen, skin, liver, kidneys, lungs and gut (Carenza et al., 2019; Macri et al., 2018). Transcriptome analyses suggested conserved functions between mice and humans cDC2s, however, tissue-specific discrepancies suggest that human cDC2s are more readily influenced by the local environment, therefore they can acquire different functions in different tissues (O'Keeffe et al., 2015).

A fundamental marker for human cDC2s characterization is CD1c, which is a human-specific non classical MHC that presents mycobacterial glycolipid antigens to T cells. Other useful markers are CD2, a cell adhesion molecule, SIRPA, a glycoprotein involved in the negative regulation of RTK signalling process, and myeloid antigens CD11b, CD11c, CD13 and CD33. Also, transcriptional profiling has identified the alpha subunit of the high-affinity IgE receptor (FCER1A), CD301, signal regulatory protein alpha (CD172a), CLEC10A, VEGFA and FCGR2A as consistent cDC2 markers (Collin & Bigley, 2018; Dutertre et al., 2019; O'Keeffe et al., 2015).

The development of human cDC2s depends on many transcription factors, even though there is not a single factor that has exclusive control over their development. Only IRF4, that has been found at high expression levels, is considered a lineage-defining factor (O'Keeffe et al., 2015).

Regarding pattern recognition receptor expression, human cDC2 express TLR2, TLR3, TLR7, TLR8 and TLR9. Unlike the mouse equivalents, several evidence support the role of cDC2s as major producers of IL-12, especially in response to TLR8 stimulation. So, although cDC1s and cDC2s produce similar amounts of TLR8 transcript and upregulate costimulatory molecules after TLR8 stimulation, only cDC2 produce IL-12p70, IL-1β, TNF and IL-6, suggesting a role in Th1 responses. The stimulation of TLR8 also induce the production of IL-23, and this was specifically observed in lung and intestinal cDC1s, suggesting a specific capacity to induce Th17 responses against bacterial and fungal pathogens (O'Keeffe et al., 2015).

Studies on human blood cDC2s revealed that multiple inflammasome related components are highly expressed, including NLRP4, NLRC4 and IL-1β, consistent with data in the mouse. These findings

suggest that cDC2s have a shared specialization for cytoplasmatic viral detection and inflammasome responses (Macri et al., 2018).

Regarding their role in immunity, numerous studies reported the ability of human cDC2s to induce Th1, Th2 and Th17 responses, suggesting a high level of plasticity. They display a similar capacity to induce Th1 and Th2 responses as cDC1s, thus, the capacity of human DCs to polarize CD4+ T cell responses does not appear to be restricted to a particular subset and is likely to be influenced by the environmental stimuli. However, it was reported that cDC2s are able to induce higher levels of IL-17, in line with their ability to produce IL-23. Therefore, they are concordant with the mouse cDC2s counterparts in the induction of Th17 immunity to counteract bacterial and fungal pathogens (Macri et al., 2018).

There are also evidence that demonstrate the capacity of human circulating cDC2s to induce CTL responses. It has been demonstrated that, without TLR activation, cDC2s can cross-present soluble antigens at least as well as activated cDC1s, but they are inferior to cDC1s when cross-presenting necrotic cell-associated antigens. Thus, neither the generation of CD8+ T cell responses appear to be restricted to any particular human DCs subtype (Macri et al., 2018).

Ultimately, it was also studied the role of human cDC2s in the regulation of immune responses and the maintenance of tissue homeostasis, given the role of their mouse counterparts. It was shown that human intestinal cDC2s express CLEC4A, a negative regulator of DC expansion that is critical in preventing autoimmunity. Moreover, they express CD101, an immune regulatory molecule, the inhibitory receptors PILRA and TGFBR2, IRAK3, a negative regulator of TLR signalling, and VSIG4, a negative regulator of T cell activation. These genes suggest a role for cDC2s in the regulation of diverse regulatory responses. Also, it was reported a higher ability of cDC2s in the liver to secrete IL-10 and low pro-inflammatory cytokines in response to *E. coli* and lipopolysaccharide (LPS) and to induce T cells with immunosuppressive functions, implying a role in the maintenance of immune tolerance in this organ. These observations suggest the possibility that in non-lymphoid tissues, environmental stimuli precondition cDC2s towards an immune-regulatory phenotype in the steady-state (O'Keeffe et al., 2015).

1.1.2.3 Plasmacytoid DCs (pDCs)

In non-inflammatory conditions, human pDCs are found in blood and lymphoid organs, where they represent 0.2-0.8% of peripheral blood mononuclear cells (PBMCs), but rarely they are present in healthy non-lymphoid tissues (Cao & Bover, 2010; Carenza et al., 2019). The development of pDCs in mammals is dependent on several transcription factors, such as IKZF1 and IRF8. However, there is a key axis that regulates the balance of pDC and cDC differentiation, based on the antagonism between ID2, which is an inhibitor of DNA binding, and TCF4, which is a lineage-determining factor

for pDCs that is negatively regulated by ID2. TCF4 directly activated multiple pDC-enriched genes, including transcription factors involved in pDC development and function (Reizis, 2019).

Unlike cDCs, pDCs do not express myeloid antigens such as CD11c, CD11b and CD33, but they maintain the expression of the CDP markers CD123 (IL-3R) and CD45RA, which are downregulated when pre-DC differentiate into cDCs. They are characterized by the expression of CD303, CD304, CD85k (ILT3), CD85g (ILT7) and Death Receptor 6 (DR6). These surface receptors are involved in the regulation of the major physiological function of pDCs, which is the production of type I interferon (IFN-I). In fact, pDCs are specialized to sense and respond to viral infection thanks to the expression of TLR7 and TLR9. These TLRs are the key endosomal pattern recognition receptors that sense ssRNA and dsDNA, respectively. Stimulation of TLRs induces the rapid production of high quantities of type I-III IFN and the secretion of cytokines. The IFN-I-producing capacity of pDCs is dependent on interferon response family (IRF) transcription factors, such as IRF7, whereas the production of the tumour necrosis factor (TNF) and IL-6 is based on the nuclear factor-kB (NF-kB) pathway; these pathways are regulated by ligation with surface receptors that can induce activation or tolerance. For instance, the binding of CD303 or ILT7 inhibits IFN-α production via ITAM signalling; also, sphingosine-1-phosphate signalling interacts with ILT7 to limit TLR-induced IFN production (Collin et al., 2013; Reizis, 2019). Even if human pDCs can produce large amounts of type III interferon, which is important in mucosal anti-viral responses, cDC1s are considered the main productors of these proteins (Macri et al., 2018). Even though pDCs are considered the most important IFN-I producing cells in anti-viral responses, they are involved also in other functions. For example, pDCs are able to produce high levels of IFNs in response to non-viral pathogens. Indeed, the human fungal pathogen Aspergillus fumigatus induces IFN-I production by pDCs in a Dectin-2 dependent manner (O'Keeffe et al., 2015). In addition, unlike the mouse pDCs, human pDCs can prime CD4+ T cells and to cross-present antigens to cytotoxic lymphocytes, even if they are not as efficient as cDCs (Macri et al., 2018)

Although pDCs play important pro-inflammatory functions, they have also been associated with protection from allergy and oral and transplant tolerance. These mechanisms of immunosuppression are probably linked to their capacity to produce IDO and to induce regulatory T cells. In fact, pDCs found in tumour-draining lymph nodes and in the periphery of solid tumours express high levels of IDO and have been associated with worse clinical outcomes (Macri et al., 2018; Munn et al., 2004).

1.1.2.4 Inflammatory DCs

Upon inflammatory conditions, other subsets of DCs can infiltrate the site of inflammation. Although there are difficulties in addressing their ontology, transcriptomic studies revealed that they derive from monocytes rather than from DC precursors (Collin et al., 2013; Dutertre et al., 2019). Monocytes derive from embryonic precursors and their further differentiation is strongly driven by the microenvironment, conversely to cDCs or pDCs, whose developmental programs are primed at an early stage, independently of their tissue of residency. When entering tissues, monocytes can differentiate either in macrophages or monocyte derived DCs (moDCs). Studies on both in vitro human monocyte differentiation models and in vivo mouse models showed how moDCs and macrophages do not represent different states of polarised macrophages but are actually distinct lineages controlled by two sets of molecular regulators. In fact, in the presence of M-CSF, monocytes differentiate by default into macrophages; however, if monocytes are exposed to certain cytokines (such as IL-4 and TNF-α) in concomitance with aryl hydrocarbon receptor (AHR) ligands, they differentiate into moDCs (Goudot et al., 2017). However, moDCs represent a phenotupically heterogenous population, whose ontology is still under debate, as recent data obtained by high dimensional single-cell protein and RNA analysis suggest that moDCs may be related to cDC2s rather than monocytes (Dutertre et al., 2019; Sander et al., 2017). moDCs retain the expression of myeloid markers as CD13, CD33, CD11b and CD11c, but they can be distinguished from human monocytes mainly for their expression of CD1a, which is a member of the CD1 family of transmembrane glycoproteins, that mediate the presentation of lipid and glycolipid antigens of self or microbial origin to T cells; other characterizing markers include CD14, CD206, FceRI, IRF4, SIRPα, MAFB and ZBTB46, which is a DC lineage-specific transcription factor (Collin & Bigley, 2018; Segura & Amigorena, 2013).

Human moDCs have been found in steady-state tissues, including skin, lung and intestine. This resident population expands many-fold during inflammation and functions mainly at the inflammatory site (Collin & Bigley, 2018). They are characterized by an activated phenotype, with a high production of pro-inflammatory cytokines, like IL-12, IL-23, and the capacity to induce both IL-17 and IFN-γ production by CD4+ T cells. The dual induction of Th1 and Th17 response has been observed in several autoimmune pathologies, suggesting a key role for infiltrating DCs in the pathogenesis of these diseases (O'Keeffe et al., 2015).

Inflammatory DCs also include a small population identified using a specific monoclonal antibody (M-DC8) recognizing the 6-sulfo-LacNAc carbohydrate modification of PSGL-1. Blood circulating slanDCs have a transcriptional profile that overlaps with $CD16^{+}$ non-classical monocytes, thus suggesting a monocytes origin of these cells; however, they share many phenotypic and functional

characteristics with cDCs. Indeed, slanDCs in the peripheral tissues are endowed with DC-specialized functions including efficient antigen presentation, capacity to activate naive T cells and promote Th1/Th17 immune responses (Carenza et al., 2020). Different studies highlighted the pro-inflammatory nature of circulating slanDCs, based on their capacity to produce large amounts of TNF-α and IL-12 upon stimulation with TLRs. They also promote proliferation, cytotoxicity and IFN-γ production by NK cells and induce strong antigen-specific T cell responses. (Micheletti et al., 2016; Schlitzer et al., 2015).

1.1.3 Methods to study human DCs

The past decades have witnessed a large increment in the number of parameters analysed in single-cell cytometry and transcriptome studies. Parameter numbers currently reach ~30 for flow-cytometry, and >20,000 in single-cell RNA sequencing (scRNAseq).

The most common technique used to identify and study human DCs is flow-cytometry; this technique has been employed not only for the analysis of blood cells but also for the analysis of single-cell suspension from tissues. Flow-cytometry allows the characterisation of a high number of antigens simultaneously, facilitating the identification of distinct populations and the study of phenotype of a specific subset. Indeed, we recently optimised an 18-color flow-cytometry panel that could be applied both in whole blood and tissues for the identification of both DC-lineage DCs and inflammatory DCs and the evaluation of their activation/inhibitory state. in particular, this panel was designed for the assessment of the expression of three costimulatory molecules (CD40, CD80, CD86) and three inhibitory molecules (PD-L1, ILT2, TIM-3) (Carenza et al., 2019).

Also, recently computational tools have been developed to scale and represent these high dimensional data, such as the t-distributed Stochastic Neighbor Embedding (tSNE) or Uniform Manifold Approximation and Projection (UMAP) tool (McInnes et al., 2018; Van Der Maaten, 2015). These tools by an algorithm of dimensionality reduction allow to analyse in a unsupervised manner complex high dimensional datasets (such as those deriving from flow-cytometry or scRNAseq data) and to visualize them in a two-dimensional space. This enables to understand large datasets because it is able to gather in the same geographical position of high dimensional space similar cells, forming clusters, proving a simpler method to visualise how different cell clusters are. Indeed, the algorithm calculate reciprocal interactions among cells, connecting similar cells each other in the same cluster. In the UMAP space, contrary to tSNE space, also distances among clusters are worthy because similar clusters localize closer than dissimilar ones.

If the big limitation of flow-cytometry is the finite number of parameters that the machine is able to measure simultaneously (up to 30 parameters), this issue has been overcome by transcriptomic analyses that has evolved rapidly, from the analysis of data of bulk populations to single-cell RNA sequencing. This technique can lead to the discovery of novel surface markers whose expression can be validated by flow cytometry; it can also reveal the heterogeneity between subsets and identify small DC precursor populations, but also potential new subpopulations with specialized functions (Collin & Bigley, 2018).

1.2 High grade gliomas

1.2.1 Classification of high-grade gliomas

Gliomas are tumours formed by the glial cells of nervous tissue. These can be benign or malignant. In particular, malignant or high grade gliomas (HGGs) represent about 80% of all malignant brain tumours (Hart et al., 2019; Suárez-García et al., 2020).

Before 2016, gliomas were classified solely by histology. In May 2016 the World Health Organization (WHO) revised their classification system, incorporating also molecular criteria for a better distinction of different subtypes, in order to provide to oncology clinicians guidelines to more accurately diagnose, predict efficacy of treatments, and enhance individualized therapeutic plans for patients (Davis, 2018; Louis et al., 2016).

According only to histopathological classification, based on light microscopy and immunohistochemistry techniques, the majority of HGGs are of the subtype of anaplastic astrocytoma (AA), anaplastic oligodendroglioma (AO) or glioblastoma multiforme (GBM) (Hart et al., 2019).

- Anaplastic astrocytoma (AA) is a diffusely astrocytic, primary brain tumour that constitutes 4% of all malignant CNS tumours and 10% of all gliomas. The median overall survival of patients that underwent standard treatment is 3 years and the 5-years survival rate is 28%. The median age of onset of AA is at 41 years. Roughly a quarter of AA arise as a de novo tumour, whereas it is estimated that three quarters are a consequence of transformation from a lower-grade astrocytoma (Grimm & Chamberlain, 2016).
- Anaplastic oligodendrogliomas (AOs) represent the third most common type of glioma and comprise 4%-15% of all gliomas. The prevalence of AOs varies from 3.5% of all malignant gliomas to 20%-54% of all oligodendroglial tumours. AOs primarily occur in adults, with a median age at diagnosis ranging from 45 to 50 years and median overall survival (OS) of

approximately 4.5 years. AOs frequently tend to gradually grow and evolve from a low-grade, well-differentiated glioma into HGG with anaplastic features (Simonetti et al., 2015).

- GBM (WHO grade IV glioma) is the most common malignant primary brain tumour making up 54% of all gliomas and 16% of all primary brain tumours (Ostrom et al., 2013). This tumour is associated with a median survival of only 3 months in untreated patients (Tamimi et al., 2017) and a mean overall survival of about 14.6 months in patients treated with standard therapy, consisting of maximally safe surgical resection followed by combined radiotherapy and adjuvant chemotherapy with temozolomide (Seliger et al., 2019).The diagnosis of GBM occurs primarily at a median age of 64 at the diagnosis. The incidence increases with age, peaking at 75–84 years and drops after 85 years. As for the anatomical localization, GBM most commonly develops in the supratentorial region (frontal, temporal parietal, and occipital lobes), with the highest incidence in the frontal lobe (Tamimi et al., 2017).

The initial detection of GBM is based on standard magnetic resonance imaging (MRI) that is the current imaging gold standard, being the most sensitive tool; however, once a GBM definable lesion is identified with MRI, the tumour is already at an advanced state. Then, the validation of the diagnosis is commonly made with formalin-fixed, paraffin-embedded tissue from resected or biopsied tumours (Alexander & Cloughesy, 2017).

Lately, positron emission tomography (PET) gained an increasing relevance because it provides additional insight beyond MRI into the biology of gliomas and a non-invasive method of grading; for example, it can be useful for the differential diagnosis of HGG from other types of brain tumours (Verger et al., 2017).

Up to date, the cause of the disease is still unknown for the majority of GBM patients. In fact, only a small percentage of patients (5%) presented a critical germline alteration and less than 20% of GBM patients have a strong family history of cancer. The only well-established causative exposure is from ionizing radiation, but only a small fraction of the cranial tumours caused by radiation exposure are GBMs. Other causative factors have been explored without finding a clear connection, such as the use of mobile phones, viral triggers (cytomegalovirus) or lifestyle characteristics (cigarette smoking and alcohol consumption) (Alexander and Cloughesy 2017; Tamini et al., 2017).

On the other hand, there are established prognostic factors that affect the survival of GBM patients, including the resectability of the tumour, its location, size, multifocality, as well as advanced age, comorbidities, and the patient's general condition (Tamimi et al., 2017).

On the other hand, according to the 2016 WHO classification gliomas are graded on a scale from I to IV, based on both histopathological and molecular criteria. HGGs belong to grades III or IV and share an aggressive and infiltrating nature (Dolecek et al., 2012). Besides this classification, GBM can be

also divided into primary GBMs (pGBM) and secondary GBMs (sGBM). pGBMs and sGBMs are histologically indistinguishable, since they are both characterized by a central area of necrosis surrounded by palisading cells and marginal proliferation of endothelial cells (microvascular hyperplasia). Other general features are increased mitosis, hypercellularity and cellular pleiomorphism. All of these characteristics result in histological heterogeneity, suggesting that the tumour can grow rapidly even if the core undergoes necrosis (Bradshaw et al., 2016). pGBM arise "de novo" and account for 80% of total GBMs. pGBM occur in older patients (mean age = 64 years) and present an aggressive and highly invasive phenotype. More typical genetic alterations for pGBM consist of EGFR overexpression, PTEN deletion or mutation, CDKN2A (p16) deletion and loss of chromosome 10. Conversely, sGBMs originate from a pre-existing lower grade glioma (LGG) and are less common (20%). These tumours occur in younger patients (mean age = 45 years), often present TP53 mutations or 1p/19q co-deletion and are often associated with a slower progression (Mansouri et al., 2019).

In 2008 Parsons and colleagues reported for the first time the mutation in the isoform 1 of the isocitrate dehydrogenase (IDH1) in sGBMs; recent studies have since confirmed recurrent somatic mutations in the IDH1 and IDH2 genes in a significant proportion of patients with gliomas, leading to distinct disease characteristics when compared with patients with wild-type IDH genes (Parsons et al., 2008). IDH mutations were found very frequent in WHO grade II/III gliomas and sGBM (>80%), but very rarely in pGBM (<5%) (Mansouri et al., 2019).

It is now agreed that IDH mutation is a critical biomarker of sGBM, leading in 2016 to a new WHO classification of GBMs based on the IDH status:

- GBM, IDH-wild type (about 90% of cases) corresponding most frequently to the clinically defined pGBM, predominant in patients aged over 55 years and associated with a poor prognosis.
- GBM, IDH-mutant (about 10% of cases) corresponding closely to the so-called sGBM, with a history of prior lower grade diffuse glioma, preferentially occurring in younger patients and associated with a better outcome and an increase in overall survival (Parsons et al., 2008).
- GBM, NOS, a diagnosis that is reserved for those tumours for which full IDH evaluation cannot be performed (Wesseling & Capper, 2018).

The IDH1 gene encodes for isocitrate dehydrogenase 1, an enzyme localized in the cytoplasm and peroxisomes, whereas the IDH2 gene encodes for the mitochondrial isocitrate dehydrogenase 2 (Parsons et al., 2008). These enzymes participate in protection from oxidative stress because they catalyse the oxidative carboxylation of isocitrate to α-ketoglutarate (α-KG), resulting in the

production of nicotinamide adenine dinucleotide phosphate (NADPH), that in turn maintain an adequate pool of reduced glutathione (GSH) and peroxiredoxin (Mansouri et al., 2019).
Also, the reaction driven by IDH1 produces as much as 65% of the brain's NADPH, being the main source of these molecules in the human brain (Kaminska et al., 2019).
Mutations in IDH1 and IDH2 genes comprise mostly missense variants that lead to a single amino-acid substitution of arginine residues at codon 132 in exon 4 of the IDH1 gene or codons 172 of the IDH2 gene. These mutants, besides losing their catalytic activity, gain the function of catalysing the reduction of α-KG to its (R)-enantiomer of 2-hydroxyglutarate (2-HG). In this way the oncogenic effect of IDH mutation is potentially twofold. First, 2-HG is considered an oncometabolite that may play a role in the process of glioma development and progression. In fact, recent studies have demonstrated that increased levels of 2-HG result in increased activity of HIF-1-α and increased level of its downstream targets, such as VEGF (Figure 4). Moreover, 2-HG is also involved in collagen maturation, causing defects in basement membranes that can potentially facilitate glioma progression (Sasaki et al., 2012).

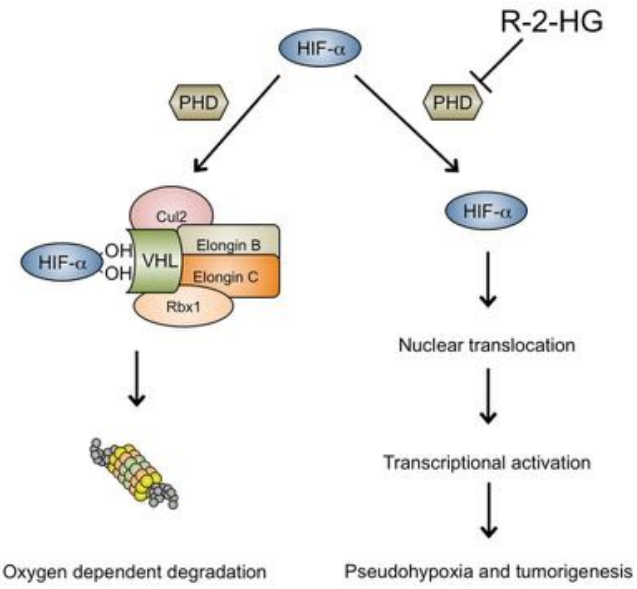

Figure 4. *Hydroxylation of HIF1-a by PHD is inhibited by high levels of R-2-HG (Dimitrov et al., Int J Med Sci, 2015).*

Second, IDH mutation results in a decreased production of α-KG, which impairs the function of many α-KG-dependent dioxygenases, including methylcytosine dioxygenase TET2 and histone demethylases (Figure 5). Under normal conditions, TET2 utilizes α-KG as a substrate to hydroxylate 5-methylcytosine to 5-hydroxymethylcytosine during DNA demethylation. α-KG also binds to the JmjC domain of histone demethylases, which function to demethylate lysine residues on histone tails and subsequently regulate gene transcriptional activity. 2-HG produced by the mutant IDH1 protein acts as a competitive inhibitor of TET2 and JmjC, promoting a hypermethylation phenotype that

interferes with the terminal differentiation of cells and may predispose cells carrying mutant IDH to malignant transformation (Dimitrov et al., 2015; Lu et al., 2012).

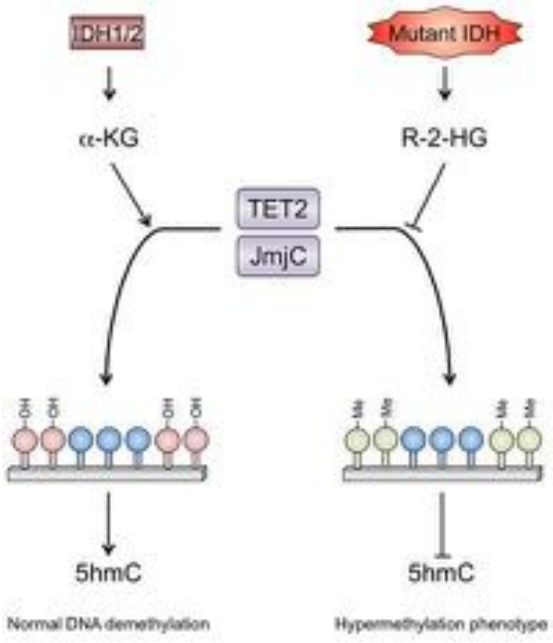

Figure 5. *R-2-HG acts as a competitive inhibitor of TET2 and JmjC (Dimitrov et al., Int J Med Sci, 2015).*

Moreover, recent studies have reported an association between IDH1R132H mutation and the methylation status of the MGMT promoter (Mansouri et al., 2019). The O6-methylguanine-DNA methyl-transferase (MGMT) gene encode for a ubiquitously expressed enzyme involved in DNA repair. The enzyme acts by removing alkyl adducts from the O6 position of guanine at DNA level, thus antagonizing the effects of alkylating agents. Defective MGMT functions result in the persistence of the O6-methylguanine adduct, causing base mismatch and leading to cell cycle arrest and apoptosis. For example, epigenetic modifications could silence the MGMT gene by methylation of cytosine-phosphate-guanine (CpG) island at specific CpG sites within the MGMT gene promoter, reducing the level of MGMT functional protein and leading to inadequate repair of DNA in response to alkylating agents that in turn could drive cells to apoptosis (Mansouri et al., 2019). So, MGMT promoter methylation is considered a relevant prognostic marker and can also be used to predict therapeutic response to alkylating agents, such as temozolomide (TMZ) (Lombardi & Assem, 2017).

1.2.2 Oncogenic pathways

The causes of GBM onset are still unknown. Approximately 5% of patients show predisposing germline alterations. Mutations such as somatic chromosomal aberrations, copy number changes and gain or loss of function events in oncogenes and tumour suppressor genes are mainly involved in

gliomagenesis. Genes significantly mutated include epidermal growth factor receptor (EGFR), PTEN, retinoblastoma (RB), and TP53.

The pathway that is most frequently altered involves receptor tyrosine kinases (RTKs), cell-surface receptors that bind growth factors (GFs) (Network CGAR, 2008). In particular, EGFR signalling is important for the proliferation, migration, differentiation and survival of all types of CNS cells. EGFR is considered an oncogene because alterations in EGFR signalling lead to uncontrolled increases in phosphorylation activity. The majority of GBMs that overexpress EGFR also have alterations of the EGFR gene, such as amplification of the EGFR locus (mainly in 7p11.2) and receptor mutations. The most common mutation is the EGFRvIII, which corresponds to the loss of exons 2–7, leading to a deletion of 267 amino-acids in the extracellular domain making the receptor ligand independent and constitutively active, driving to an uncontrolled increase in phosphorylation activity. This mutation is never observed in healthy tissues (Sugawa et al. 1990; Lombardi & Assem, 2017).

GBM can also show high levels of activity of the Ras pathway, even if Ras mutations are rare in this tumour; this can be explained by the increased activation of upstream factors, such as the EGFR. The increase of the Ras activity promotes tumour progression fostering the cell cycle, survival and migration through a cascade of downstream effectors (Lombardi et al., 2017).

Alterations in the PI3K/PTEN/Akt pathway have been implicated in GBM pathogenesis. Indeed, in GBMs, the tumour suppressor function of PTEN is frequently inactivated, either by loss of heterozygosity (LOH) or mutation-induced constitutive activation of PI3K; this results in an increase of PI3K activity, leading to PIP3 generation and activation of Akt, which is involved in cell proliferation and inhibition of apoptosis (Koul, 2008).

The RB pathway plays a crucial role in the cell cycle. RB is an important tumour suppressor gene because it works preventing the transcription of genes involved in mitosis and cell cycle. This pathway is negatively regulated by cyclin-dependent kinase inhibitor proteins (CDKN), such as CDKN2A-p16INK4a that can be found mutated in GBMs. In other cases, GBM cells can override this negative regulation via methylation of the RB promoter and gene silencing. These alterations lead to uncontrolled cell cycle proliferation (Knudsen & Wang, 2010).

The TP53 pathway also functions in cell cycle control, DNA damage response, cell death, and differentiation. When DNA damage occurs, the cell becomes stressed and activates the TP53 pathway that controls cell cycle progression and apoptosis. In human gliomas, TP53 mutations are often missense mutations that target exons crucial for DNA binding. Other alterations seen in GBMs are MDM2 and MDM4 amplifications, which are molecules that negatively regulate TP53 activity (McLendon et al., 2008).

Currently, there is no defined sequence of mutational events that lead to glioma pathogenesis. Any combination of these pathways may contribute to the development of this tumour, whose complexity is enhanced by high levels of variability both between different tumours, as well as within the same tumour. However, the identification of these alterations can help to improve early diagnosis, prognosis and treatment prediction, even though several of these biomarkers are in deep need of validation to be used in clinical routine.

1.2.3 DCs in healthy brain and HGG

Normal brain differs from other tissues for some important features. In particular it is composed by unique tissue-resident cell types including microglia, astrocytes and neurons, and it is physically protected from external agents by the blood-brain barrier (BBB). Indeed, the normal brain has long been considered one of the ‘‘immune privileged’’ organs in the body that must be shield from immune cell entry and/or attack because activated immune cells produce inflammatory factors that can be cytotoxic leading to neurodegeneration. Therefore, interactions with the immune system need to be finely regulated within the brain (Quail & Joyce, 2017). While it is clear that microglia represents the major innate immune cell component of the brain, several studies indicate the presence of bone marrow-derived perivascular macrophages and other peripheral immune cells at the interface between the blood and the interstice of the brain or between the blood and the cerebral spinal fluid (CSF). Moreover, over the years, many cells have been described as APCs, including astrocytes, vascular endothelial cells, microglia and macrophages (Srivastava et al., 2019), but as regards the presence of DCs within healthy brain parenchyma, it still remains under debate, especially in humans. Indeed, our knowledge related to the presence of DCs in the brain mainly relies on studies conducted in mice or on autoptic specimens of human brain with techniques, like immunohistochemistry that allows only a limited exploration of markers for DC identification, which is also complicated by the fact that DCs share several markers with other myeloid populations, making their recognition difficult (Lande et al., 2008; Serot et al., 1997). Therefore, it remains matter of debate how CNS-antigens are exactly transferred to secondary lymphoid organs in humans. Studies on murine brain have described how the CNS parenchyma is largely devoid of DCs under steady-state conditions (Ransohoff & Engelhardt, 2012; Worbs et al., 2017). However, these cells were found within the interstice of the choroid plexus, between the fenestrated capillaries and the basal surface of the choroid epithelium. The choroid plexus is a secretory tissue found in each of the brain ventricles, the main function of which is to produce CSF (Lun et al., 2015). The invasion of circulating haematopoietic cells in this area is easier because the blood-CSF barrier does not rely on endothelial tight junctions in blood vessels to restrict entry in the interstice. Endothelial cells of this region are also fenestrated and lack

an astrocyte layer, leading to a high degree of capillary permeability. Instead, the epithelial layer is characterized by the presence of tight junctions between cells, creating a primary barrier for the passage of material (Johanson et al., 2011). For this reason, the stromal interstice of choroid plexus is the ideal region for antigen uptake by DC subsets. These cells were also found in the epithelial surface facing the CSF and in the CSF itself, especially in the lateral ventricles. It was demonstrated that DCs of this region respond to immune signals and can migrate to cervical lymph nodes (Carson et al., 2006).

Furthermore, DCs are present in the perivascular spaces of the murine brain, that correspond to the interstitial spaces between the basement membrane of the astrocyte layer and the capillary endothelial layer, in the context of the BBB. These spaces have been proved to act as a lymph-like drainage system in the CNS. In fact, interstitial fluid from the brain parenchyma drains along the basement membranes of capillaries, reaching cervical lymph nodes in the neck. The drainage of this region contains tissue debris and soluble antigens that are accessible for the uptake by DCs and presented to T cells within the perivascular space (R. O. Weller et al., 2009). The presence of DCs in locations near blood vessels support the idea that endogenous DCs in homeostatic conditions are most likely to arise from circulating pre-DCs that enter the brain perivascular regions at an early stage (Colton, 2013). These findings together with the recent discovery of a functional lymphatic vasculature in the meningeal dura mater of mice linking the venous sinuses of the dura mater to deep cervical lymph nodes, has been revising the concept of CNS as an immune-privileged site (Aspelund et al., 2015; Louveau, Harris, et al., 2015; Louveau, Smirnov, et al., 2015).

In the context of pathological conditions, such as in inflammatory and tumour conditions, the BBB is compromised and there could be a robust infiltration of multiple immune cell types from the peripheral circulation to the brain parenchyma (Srivastava et al., 2019). However, the presence and the possible role of DC subsets in HGGs have been poorly investigated, so far. In particular, one study assessed the infiltration of $BDCA2^{+}$ cells by immunohistochemistry, and demonstrated that tumour-infiltrating pDCs progressively increased in human glioma from grade I to III, but they were negligible in grade IV (Dey et al., 2015). Another study performed single-cell transcriptomic analysis of tumor and stromal cells in human GBM samples, and demonstrated the presence of DCs in glioma microenvironment (GME), but did not provide any further characterization of these cells (Darmanis et al., 2017). In addition Wang and colleagues studied immunological changes in GME according to three different GBM-intrinsic transcriptional subtypes (proneural, classical, and mesenchymal), finding out, among other immune populations, two sub-populations of tumour-associated DCs (TADCs), one charcaterised by a resting profile, and one by an activated profile. However, they did not perform any further investigation on these cells (Q. Wang et al., 2017). Altogether, it is evident

that DCs do infiltrate human HGGs, but a phenotypic and functional characterization of these cells is still lacking.

1.2.4 Immunosuppression in HGGs

Over the natural defences of the CNS, including the BBB, malignant gliomas exhibit features that limit the efficacy of current treatments. In particular, high heterogeneity, low mutational burden and resulting low immunogenicity, and a strong immunosuppressive TME configure HGGs, and in particular GBM, as the paradigmatic "immune desert cancer" (Locarno et al., 2020). Indeed, aggressive tumours, in particular GBM, use specific mechanisms to avoid immune recognition and tumour cell killing, blocking the anti-tumoral response in favour of tumour growth and progression. Beside tumoral cells, myeloid cells recruited in this GME display properties directly sustaining tumour growth and shaping the adaptive immune response, with inhibition of cytotoxic $CD8^+$ T cells and promotion of Tregs recruitment. These immune escape mechanisms are summarised in figure.

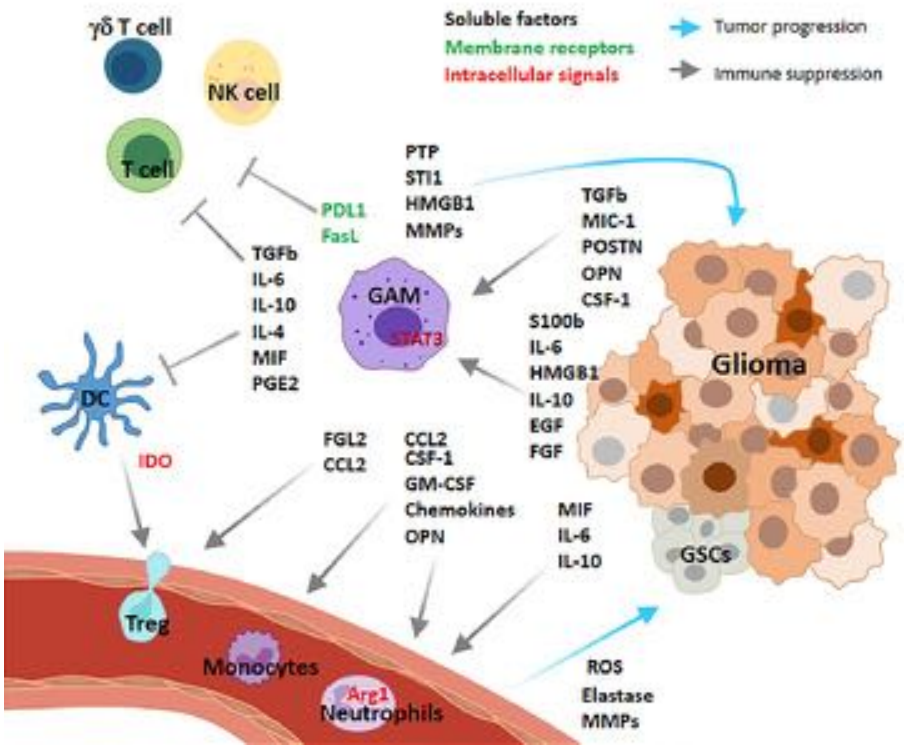

Figure 6. *Myeloid cell and tumour immunosuppressive mechanisms (adapted from Locarno et al., 2020). [NK cell, Natural killer cell; PTP, Protein Tyrosine Phosphatase; STI1, Stress-Inducible Protein 1; HMGB1, High Mobility Group Box Protein 1; MMPs, Matrix Metalloproteinases; TGFb, Transforming growth factor beta; MIC-1, Macrophage Inhibitory Cytokine-1; POSTN, Periostin; OPN, Osteopontin; CSF-1, (macrophage) colony stimulating factor 1; IL-6, Interleukin 6; IL-10, Interleukin 10; GSCs, Glioma Stem Cells; ROS, Reactive oxygen species; MIF, Macrophage migration inhibitory factor; EGF, Epidermal Growth Factor; FGF, Fibroblast Growth Factor; CCL2,* chemokine ligand 2; PGE2, *Prostaglandin E2].*

HGGs are known for their dual immunosuppressive role, because they act both at local and systemic levels, impairing any possible antitumour response. Immunosuppressive mechanisms acting within HGG microenvironment include: down-regulation of MHC-I complexes on tumoral cells, thus

becoming “invisible” to immune system attacks; overexpression of immunosuppressive factors, such as cytokines (TGF-β, IL-10), prostaglandin E2, VEGF, indoleamine 2,3-dioxyhenase (IDO) and STAT3, that in turn influence macrophage polarization towards an M2 phenotype, DC maturation, regulatory T cell and myeloid-derived suppressor cell recruitment, and inhibition of NK cell functions (Locarno et al., 2020). Moreover, the overexpression of IL-6 by tumour-associated macrophages (TAMs) and the production of proteases and metalloprotease by TAMs and tumour infiltrating polymorphonucleated cells (PMNs), support tumour growth, angiogenesis and invasiveness (Locarno et al., 2020). Lastly, tumoral cells can induce a dysregulation of the normal immune checkpoint dynamic homeostasis, through the expression of checkpoint molecules, like PD-L1, that inhibit anti-tumoral T cell functions (Locarno et al., 2020; Simonelli et al., 2018).

Given these powerful mechanisms of immunosuppression acting within the tumour, together with the poor knowledge on what drive it, especially in human, and the particular organ that harbour this type of tumours, there is a formidable challenge to overcome for the successful application of immune-oncology strategies (Quail & Joyce, 2017).

1.2.5 Treatment options for HGGs

Therapeutic options for HGG patients remain challenging because all treatments are symptomatic, but not curative (Berger et al., 2014). Currently, even if there is a better understanding of molecular mechanisms and gene mutations leading to more tailored therapeutic approaches, overall mortality rates remain high in glioma patients. Indeed, HGG management is challenging, especially due to tumour heterogeneity, its location, and its rapid and aggressive relapse. For this reason, first-line treatment of malignant gliomas generally encompasses maximal surgical resection (when feasible), radiotherapy and chemotherapy (Preusser et al., 2011).

The aim of the 2016 WHO classification of CNS tumours was to integrate histological and molecular factors, to offer clinicians a common tool to tailor treatment. In particular, in HGG patients, the features that should be routinely tested and that have proved to be clinically significant are IDH1/2 mutations, codeletion of chromosomes 1p/19q, ATRX loss and methylation of MGMT promoter (Pellerino, 2018) (Figure 7).

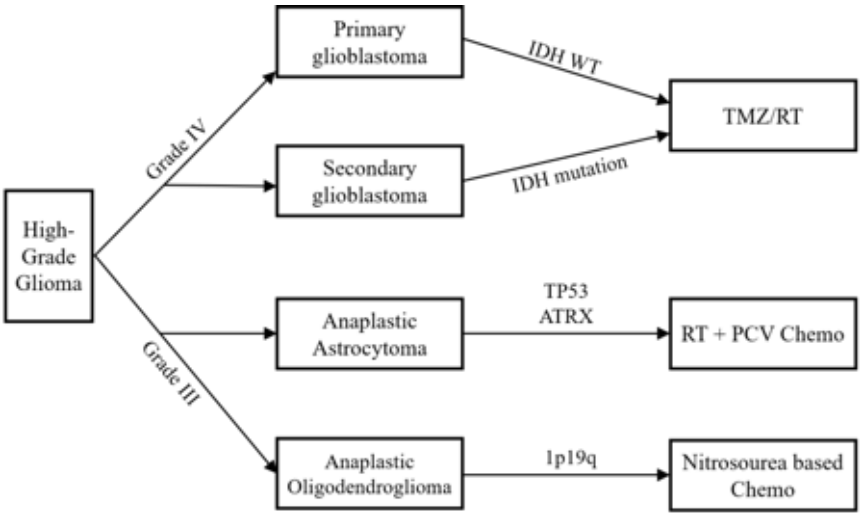

***Figure** 7. Treatment options for High Grade Gliomas.*

1.2.5.1 Surgery

Surgery is the initial therapeutic approach in HGGs and has multiple goals: (1) maximal safe resection, which means to remove as much of the tumour mass as possible while preserving the neurological status of the patient; (2) tissue specimen for pathological diagnosis; (3) to ease neurological symptoms, as intracranial hypertension, and improve seizure control, altogether delaying clinical worsening and improving quality of life; (4) to ameliorate conditions for complementary treatments (Pellerino, 2018; Fernandes et al., 2017).

One of the most important treatment-related predictors of a patient outcome is the extent of resection (EOR). A more extensive surgical resection is associated with longer life expectancy, where the longest survival is obtained in patients undergoing gross total resection followed by adjuvant therapies (Fernandes et al., 2017). In order to minimize the neurological deficits after surgery for tumours located within the eloquent cortex, which are areas of the brain necessary for language, motor, and sensory functions, several techniques have been employed to maximize the extent of surgery and facilitate the impact of complementary therapies. For instance, one possible non-invasive imaging procedure is the functional MRI, which allows localizing speech, language and motor centres through contrast imaging, depending on blood oxygenation levels (Pellerino, 2018). It was reported by Mueller and colleagues that postoperative neurological deficits occurred in 0% of cases when the resection margins were over 2 cm of the eloquent cortex, while in 50% of cases when resection margins were less than 1 cm (Mueller et al., 1996). Similar to this technique, the intraoperative MRI allows to obtain real-time images of the brain tumour during surgery, to evaluate the extent and the risk of resection in eloquent areas; however, high cost and time consumption limits its utilization (Ronkainen & Tervonen, 2006).

Other techniques, besides avoiding neurological defects, are aimed to improve the EOR by enhancing the visualization of tumour margins. Fluorescence-guided surgery, for example, exploits properties of fluorescent molecules systematically administered. The most used approach is the 5-aminolevulinic acid-induced porphyrin fluorescence (5-ALA-PpIX). 5-ALA is a natural amino acid that following systemic administration, is metabolized in mitochondria of tumoral cells and emits a red fluorescent signal. It has been demonstrated that the use of 5-ALA increases the rate of gross total resection (GTR) and progression-free survival (PSF) (Eljamel et al., 2008).

1.2.5.2 First-line treatment after surgery

Considering the high infiltrative nature of HGGs, surgery alone is not able to prevent recurrence, which tends to occur close to the resection margins; for this reason, adjuvant treatments are mandatory. Thus, newly diagnosed HGG patients will undergo surgery or biopsy (to confirm the diagnosis); then, based on molecular lesions and features of the tumour, the treatment options can vary. IDH mutations and 1p/19q codeletion are markers of oligodendroglial tumours, that are associated with a prolonged survival following nitrosureas-based chemotherapy (Cairncross et al., 2013). Instead, IDH mutations and TP53 mutations/ATRX loss are related to AA, for which the most effective treatment regimen is represented by radiotherapy followed by PCV chemotherapy, based on procarbazine, lomustine (CCNU), and vincristine (Pellerino et al., 2018). Moreover, when dealing with GBM patients, independently from the IDH status, the alkylating agent temozolomide (TMZ) is used as first-line treatment. In particular, the regimen of radiotherapy with concomitant daily TMZ followed by 6 cycles of TMZ (Stupp regimen) has proven to have better overall survival (OS) and PSF when compared to radiotherapy alone (Stupp et al., 2005). TMZ induces DNA methylation and tumour cytotoxicity through cell cycle arrest by the formation of O6-methylguanine DNA adducts, which are repaired by the enzyme MGMT, when its promoter is not methylated. In this regard, MGMT methylation represents a strong predictive factor in response to alkylating agents. In fact, when the MGMT promoter is methylated the functions of the enzyme are defective, resulting in the persistence of the O6-methylguanine adduct, causing base mismatch and leading to cell cycle arrest and apoptosis. However, the clinical utility of MGMT remains poor, because of the lack of therapeutic options for patients with unmethylated MGMT promoter. For this reason, the Stupp regimen is considered the standard of care for all newly diagnosed GBM (nGBM) following surgery (Fernandes et al., 2017). In this context, dose-dense schedules of TMZ (ddTMZ) have been designed, after completion of concomitant RT-TMZ, to reduce tumour MGMT levels and exhaust activity, thereby improving the cytotoxic function of TMZ, especially in the MGMT unmethylated patients. However, when compared to the Stupp regimen, there were no significant differences between treatments in terms of median OS and PSF, but there was increased toxicity in ddTMZ arm (Le Rhun et al., 2015).

1.2.5.3 Therapeutic options for recurrent HGGs

Currently, there is no standard of care established for recurrent or progressive GBM (rGBM). The identification of effective therapies is complex and treatment options include supportive care, re-operation, re-irradiation, systemic therapies, and combined modality therapy. These options need to be weighted considering also tumour size and location, age, previous treatments, and prognostic factors. Considering the poor prognosis and limited therapeutic options, patients can be advised to enrol in clinical trials to get access to novel targeted therapies (Pellerino, 2018); even though, the treatment of rGBM should consider in first place the preservation and the improvement of the quality of life of the patient (Fernandes et al., 2017).

1.2.5.3.1 Anti-angiogenic drugs

HGGs are among the most vascularized tumours, especially when considering GBM since it has been demonstrated that the necrotic core gives rise to angiogenic pathways leading to abnormal vasculature formation and an increase in aggressiveness (Cheray et al., 2017). For this reason, anti-angiogenic therapeutic strategies are very attractive.

Bevacizumab is a monoclonal antibody that inhibits angiogenesis targeting VEGF ligand, thus preventing its binding to VEGFR. This results in a reduction of endothelial proliferation and vascular growth in the tumour (Lombardi et al., 2017). Studies have reported a significant improvement in PFS when comparing Bevacizumab over radiotherapy alone in rGBM. Moreover, two large phase III trials compared standard treatment alone versus bevacizumab added to standard treatment, resulting in an increase in PFS without differences in OS (Pellerino, 2018). Combination therapy studies are ongoing, but with many challenges. For example, many trials evaluated the combination of bevacizumab and irinotecan in HGGs, resulting in an increase in PFS and median OS, despite the development of severe side effects (Vredenburgh et al., 2007). Given the improvement in patient survival with respect to other drugs, bevacizumab was approved by the FDA for the treatment of rGBM and nGBM patients who had disease progression on prior therapy; up to date, bevacizumab is the only targeted therapy approved for GBM treatment. However, several studies reported that long-term use of bevacizumab is associated with the emergence of resistance, recurrence, disease progression, and failure in response to other chemotherapy. One possible explanation could be that anti-angiogenic drugs create a hypoxic environment, that induces autophagy in the CSC population, leading to cell survival and aggressiveness (Cheray et al., 2017).

1.2.5.3.2 EGF receptor inhibitors

There are many growth factor receptor inhibitors in use across several cancer types. They can be divided into two main categories:

- mAbs, that act by targeting either the ligand growth factor or the transmembrane tyrosine kinase receptor and induce cell death through apoptosis, complement activation or effector cell activation;
- Small molecules, that can penetrate the cell membrane and act on the cytoplasmatic tyrosine kinase domain to inhibit its activity and disrupt signalling.

Specifically, it has been demonstrated that EGFR constitutive activation or amplifications are associated with high-grade malignancies and poor prognosis (Pellerino, et al 2018). EGFR mutations have been found especially in IDH WT GBMs and are associated with an oncogenic activity or have predictive power. Several clinical trials have tried to translate the clinical importance of these mutations into therapy. Cetuximab is a mAb that targets EGFR, preventing receptor dimerization, while gefitinib and erlotinib are small molecules that avoid phosphorylation of tyrosine residues, blocking downstream signalling; none of these compounds have been proven effective in monotherapy, and clinical trials are ongoing studying combinations of these drugs with other tyrosine kinase inhibitors or standard therapy (Mansouri et al., 2019).

1.2.5.3.3 Immunotherapeutic strategies for HGG treatment

Cancer immunotherapy, with its own concept of boosting antitumor immunity beyond directly targeting cancer cells, has recently emerged as a cornerstone of modern oncology achieving regulatory approvals for a number of other “historically” resistant cancers (Locarno et al., 2020).

The advent of immunotherapy for glioma treatment has brought great expectations for HGG patients and the spectrum of immunotherapeutic approaches for HGG patients is rapidly growing and includes different strategies, comprising immune checkpoint modulators, peptide vaccine and cell-based therapies. Additionally, there are immunotherapeutic early-phase clinical trials (ieCTs) which adopt innovative approaches characterized by a rapid dose-escalation of novel agents to determine the safety and the recommended dose/schedule, followed by large multiple expansion cohorts evaluating anti-tumour activity across different tumour types. They could include the administration of immunomodulator drug as monotherapy or in a combinatorial regimen and for some of them the inclusion of patients with a diagnosis of malignant glioma is allowed.

1.2.5.3.3.1 Immune checkpoint inhibitors

The maintenance of immune homeostasis is fundamental to avoid inflammatory tissue damage and autoimmune diseases. For this reason, physiological immune responses are based on the equilibrium between stimulatory and inhibitory signals. The inhibitory signals are referred to as immune checkpoints, such as programmed cell death 1 (PD-1)/ programmed cell death ligand 1 (PD-L1) and cytotoxic T-lymphocyte antigen 4 (CTLA-4) (Buchbinder & Desai, 2016).

The aim of checkpoint inhibitors is to block the inhibition signal and allow the immune system to generate a response. They were initially studied in patients with melanoma. In particular, ipilimumab, an anti-CTLA-4 mAb, and nivolumab, an anti-PD1 mAb, led to promising results and consequently approved by FDA respectively in 2011 and 2014 for metastatic melanoma (Larkin et al., 2015); (Hodi et al., 2010).

At a functional level, tumour cells express PD-L1, which binds PD1 on T cells, inhibiting their activation and production of cytokines (such as IFN-γ and IL-2). Several studies conducted on GBM specimens reported high PD-L1 expression in both newly diagnosed and recurrent GBM, while the expression in the healthy tissue that surrounds GBM is very low (Preusser et al., 2015).

CheckMate-143 is a randomized phase 3 clinical trial comparing nivolumab with bevacizumab in patients with rGBM, but it did not meet the primary endpoint of improved OS. Other trials are evaluating the safety and efficacy of nivolumab in combination with the current standard of care. CheckMate-548, for example, is a phase 3 randomized trial comparing nivolumab with radiation therapy and TMZ versus patients who received only the standard of care in nGBM with MGMT methylation. Instead, CheckMate-498 is a similar phase 3 trial for patients with unmethylated MGMT. Results from both these trials are still awaited (Buchbinder & Desai, 2016; Simonelli et al., 2018).

An immune checkpoint that has also been explored in immunotherapy is CTLA-4, which is expressed on naïve T lymphocytes and interact with CD80/CD86 present on the surface of APCs, resulting in the reduction of T cell activation and responsiveness. This molecule is also constitutively expressed on T regulatory cells, contributing to their immunosuppressive role (Simonelli et al., 2018). CheckMate-143 also investigated the safety and efficacy of nivolumab alone versus the combination of nivolumab plus ipilimumab for rGBM. Results were encouraging in terms of OS, however, 90% of patients who received the combination therapy had grade 3 or 4 adverse events leading in most of the cases to interruption of treatment (Pellerino et al., 2018).

Another molecule that has recently come to the attention is T-cell immunoglobulin and mucin-domain containing-3 (TIM-3), a surface protein expressed on CD4+ T-helper 1 and CD8+ T cytotoxic cells. The binding to its ligand galectin-9 on tumour cells induces a repressive pathway in the cells

expressing TIM-3, resulting in immune suppression. “Exhausted” lymphocytes that co-express PD-1 and TIM-3 are no longer able to exert their effector function and represent the most affected tumour-infiltrating lymphocytes (TILs) population in GBM (Kim et al., 2017; Simonelli et al., 2018). Another ligand of TIM-3 that is expressed in the tumour microenvironment is HMGB1, a damage-associated molecular pattern protein expressed also by necrotic cells. HMGB1 plays a critical role in the transport of nucleic acids into endosomal vesicles. After the binding to TIM-3 expressed on immune infiltrating cells, the transport of nucleic acids into endosomes is blocked, suppressing pattern-recognition receptor-mediated innate immune responses to tumour-derived nucleic acids. (Chiba et al., 2012).

An anti-TIM-3 mAb, MBG453, has been developed and its safety and efficacy are under investigation in several clinical trials, alone or in combination with other inhibitors. For example, NCT03961971 is a phase I trial currently enrolling patients with rGBM to determine the safety of MBG453 when given in combination with anti-PD-1 mAb and stereotactic radiosurgery; results are awaited in the next years.

1.2.5.3.3.2 Other agents remodelling the immunosuppressive microenvironment

Beyond the classic immune checkpoint modulators, several novel agents designed to reshape the immunosuppressive tumour microenvironment are now entered in ieCT development.

These compounds act on targets expressed mainly by myeloid cells or on soluble factors driving their functional activities (Simonelli et al., 2018). The purpose of these compounds is to re-educate TAMs and microglia since they represent one of the major contributors to GBM immunosuppression. Ongoing clinical trials aim at testing inhibitors of the CSF-1 receptor (CSF-1R), molecules targeting TGF-β1 signalling and CD38 signalling.

As regards anti-CSF-1R antibodies, it has been observed in glioma mouse models that they are able to block glioma progression, markedly suppress tumour cell proliferation and reduce tumour grade. Two phase I trials exploring safety and activity of CSF-1R inhibitors alone or in combination with PD-1 blockade across multiple tumour types including GBM are currently ongoing (Simonelli et al., 2018).

TGF-β1 signalling represents a key immunosuppressor driver in malignant gliomas, impairing cytotoxic T cells proliferation and activation, as well as maturation and functions of antigen-presenting cells and NK cells. After failure of single-agent approaches targeting activity of TGF-β1 pathway in malignant gliomas, clinical trials investigating the combinations of molecules aimed at inhibit both PD-1/PD-L1 and TGF-β1, in combination with RT and CT are ongoing (Mariathasan et al., 2018; Tauriello et al., 2018).

CD38 is a type II glycosylated membrane protein that functions as a receptor binding to CD31 and is involved in cell adhesion and signal transduction. The expression of CD38 in healthy humans can be detected on NK cells, monocytes, DCs, macrophages, PMNs, activated T and B cells, and plasma cells. CD38 overexpression has been observed in several haematological malignancies as well as in many solid tumours, such as prostate cancer and GBM. In particular in glioma mouse models, it has been observed that the administration of micromolar doses of CD38 inhibitors blocks tumour progression and prolong the lifespan of the glioma-bearing mouse. Based on this observation, a phase I trial exploring PD-L1 blockade combined with isatuximab (a mAb against CD38) in different tumour types including GBM is currently ongoing (Blacher et al., 2015; Locarno et al., 2020).

1.2.5.3.3.3 Peptide vaccines

Peptide vaccines are designed to induce an immune response by activating DCs, that are professional APCs. The selection of the target antigen is based on approaches targeting a single tumour-specific mutant protein (IDH Arg132IHis or EGFRvIII), a predefined panel of tumour-associated antigens (TAAs), or patient-specific antigen cluster acquired from tumour lysate. The choice of the antigen is fundamental because, for example, TAAs are less prone than tumour-specific antigens (TSAs) to induce an immune response, since T cells with a high affinity for TAAs undergo negative selection during thymic development. Also, using peptides from altered proteins that are expressed only in tumours is convenient, being tumour-specific and less likely to induce autoimmunity. (Weller et al., 2017).

However, there are only few antigens specific for HGGs. Among peptide vaccines it is possible to include Rindopepimut. It is a single antigen-based peptide vaccine that has been extensively studied in the clinical setting for GBM treatment. It targets the 13 amino acid sequence of EGFRvIII, which is the mutant form of EGFR that harbours in about 30% of HGG patients. Three phase 2 trials showed increased PFS and OS in nGBM, leading to a phase 3 trial of Rindopepimut/GM-CSF in nGBM, which, despite the generation of a strong humoral immune response, failed to provide survival benefits. The ReACT trial was another study investigating the effect of Rindopepimut in patients with rGBM, in which OS seemed to be improved, but there was no improvement in terms of PFS (Platten et al., 2018).

Given the relevance of IDH1/2 mutation in gliomagenesis, other studies are focused on the therapeutic efficacy of IDHR132H-specific vaccines. IDHR132H neoepitope represents an interesting target because it is a TSA expressed in all tumour cells. The NOA-16 trial is a phase I study evaluating IDHR132H vaccine in newly diagnosed HGG patients when given in combination with standard therapy. The study met its primary endpoints by demonstrating safety and immunogenicity (Platten et al., 2018).

However, targeting a single tumour antigen can be a limitation, because it elicits the response against only a subset of tumour cells and the tumour can develop resistance by shedding the targeted antigen. (M. Weller et al., 2017); (Pellerino et al., 2018).

On the contrary, IMA950 is a multi-peptide therapeutic vaccine used in nGBM patients, that include 11 tumour-associated peptides and a synthetic hepatitis B virus marker peptide. The vaccine was tested in a phase I trial to test safety and immunogenicity. It was injected with GM-CSF after surgery, either before or after chemotherapy initiation. The vaccine results safe and many patients responded to the stimulation, leading to further developments of the study (Rampling et al., 2016).

1.2.5.3.3.4 DC-based vaccines

One of promising strategies in the treatment of HGG patients is the administration of DC-based vaccine, as among different tumours in which their efficacy have been proved, HGGs have shown the highest susceptibility (Garg et al., 2017; Prins et al., 2011).

Instead of administering peptides directly, autologous DCs can be used to vehicle antigens deriving from the tumour. In fact, DCs are specialized immune cells that play a critical role in promoting an immune response against antigens, which can be both foreign pathogenic or self-tumour antigens. DCs are capable of boosting a memory T cell response but most importantly they are effective initiators of naïve T cell responses, making them the best choice for the generation vaccines based on tumour antigens (Santos, 2018).

Autologous DCs can be loaded ex vivo with either single or multiple tumour antigens and administered back to the patient. When the patient undergoes primary surgery, the tumour lysate is isolated from a surgical specimen. The same patient undergoes leukapheresis to collect DCs that are then pulsed with tumour antigens; these cells are then primed to stimulate the expression of major histocompatibility complex (MHC) molecules presenting tumour antigens and reinjected into the patient as a vaccine (Santos, 2018).

One strategy is based on the exposure of DCs to a single antigen. Several studies reported that human cytomegalovirus (CMV) proteins are expressed in more than 90% of GBMs, whereas viral proteins have not been detected in normal brain tissues surrounding the tumour, making them TSAs. For this reason, Mitchell and colleagues generated vaccines by pulsing DCs with pp65 CMV antigen. In particular, pre-conditioning the vaccine site with a potent recall antigen, like tetanus-diphtheria toxoid, they reported promising results in terms of PFS and OS (Mitchell et al., 2015).

Other DC-based vaccine trials have exposed DCs to multiple tumour antigens, providing several possible targets to the immune system. One example is ICT-107 trial, which is based on the exposure of autologous patient-derived DCs to peptides from proteins linked to glioma CSC signature and predicted to be abundant in GBM (gp100, MAGE1, AIM2, HER2, IL-13Rα2, TRP2). Safety was

assessed in phase I trial that enrolled patients with newly diagnosed and recurrent GBM, showing encouraging data in terms of median PFS for both groups (M. Weller et al., 2017).

So, despite the promising molecular and immunological rationale and the strong preclinical evidence of activity, most of the time the use of single-agent immunotherapies in HGG patients failed to meet clinical efficacy. On the other hand, the most encouraging response rates in the treatment of solid malignancies, in general, were reached with combinatorial approaches. For this reason, combinatorial approaches as CTLA-4/PD-1 blockade or combining checkpoint inhibitors with antigen-specific vaccines seem more interesting strategies.

However, these type of vaccines is time consuming, expensive, and bears potential risks due to autoimmunity. The advent of nanomedicine seems to provide a better option. Indeed with their tailored properties, nanoparticles (NPs) can specifically deliver antigens or adjuvants to DCs, preventing their degradation and promoting the efficient activation of DCs, directly reprogramming DCs in vivo. Therefore, the investigation of the presence and the function of DCs in the tumour microenvironment, the understanding of DC role in the context of glioma immunosuppression could provide a fruitful substratum to develop and improve new therapeutic strategies aimed at re-educating DCs directly in patients.

1.2.5.3.3.5 Reprogramming of tumour-associated DCs for anti-tumour therapies

The presence of DCs in the stroma of various types of cancer has been well-established (Baleeiro et al., 2008; Benencia et al., 2014). Interestingly, often these cells do not exert a positive immune influence, because cancer cells and their products present in TME or released in circulation are able to dampened DC immunostimulatory functions that potentially could exert against tumour. Indeed TADCs, albeit carrying tumour antigens, express low levels of co-stimulatory molecules (Benencia et al., 2014). Thus, upon DCs encounter antigen-specific naïve T cells, they can induce an anergic state in these cells favouring tumour immune-escape. In particular, tumour-associated cytokines such as VEGF, IL-10, prostaglandinE-2 (PGE2), and TGF-β can profoundly affect the activation state of DCs not only locally but also at a systemic levels (Benencia et al., 2014). For instance, it has been demonstrated that VEGF induces a potent systemic effect on both primary and secondary immune organs. Here, DCs could be influenced by tumour factors and/or immunosuppressive leukocytes that can affect their properties switching their phenotype towards a tolerogenic one (D. I. Gabrilovich et al., 1996). In addition, TADCs could also contribute to tumour growth and progression through the release of angiogenic factors (Curiel et al., 2004).

Collectively, if on one hand these studies provide ample evidence in support of tumours' capability to reprogram the biology of DCs towards a pro-tumoral phenotype, on the other hand the fact that TADCs are professional APCs harbouring tumour antigens that could present and potentially activate

CTLs, provides foundations for the reprogramming of TADCs in vivo. This could be a compelling therapeutic strategy that could be transform DCs into effective APCs capable of promoting anti-tumour immunity and combating tumour growth.

At present there are several strategies under development based on the use of NPs and that are reviewed in (Yang et al., 2021). In comparison with classical immunotherapeutic drugs discussed above, NPs, extensively designed as drug delivery systems, can prolong retention time and achieve targeted delivery, thus reducing toxicity. In addition they tend to accumulate in tumour much more than in normal tissue because of the leaky tumour vasculature and damaged lymphatic drainage (Prabhakar et al., 2013). This accumulation in TME is also favoured by the fact that they are conjugated with specific ligands, facilitating their delivery. Numerous nanostructures with different compositions, sizes, shapes, and functions have been developed (Yang et al., 2021), but the underlying principle is common to different NPs. In order to promote DC maturation and activation, NPs, reaching TME, are engineered with antigens and antibodies targeting different molecules express on DC surface (CD40, CD11c, CD205, mannose receptor). Moreover NPs are decorated with adjuvants, like TLR ligands, which have the function to induce the maturation of DCs and strong immune responses by activating CD4+ and CD8+ T cells that acquire cytotoxic abilities or helper functions (such as IFN-γ secretion). In vivo tumour models have shown how the delivery of these NPs is able to induce an inhibition of tumour growth. Apart from extra addition of adjuvants in nanocomplex, there are also NPs, like Fe3O4 NPs, which could promote the maturation of DCs, potentiating immune responses (Saeed et al., 2019; Yang et al., 2021). A summary of the role of DCs and the function of NPs in the tumour immunity is represented in Figure 8.

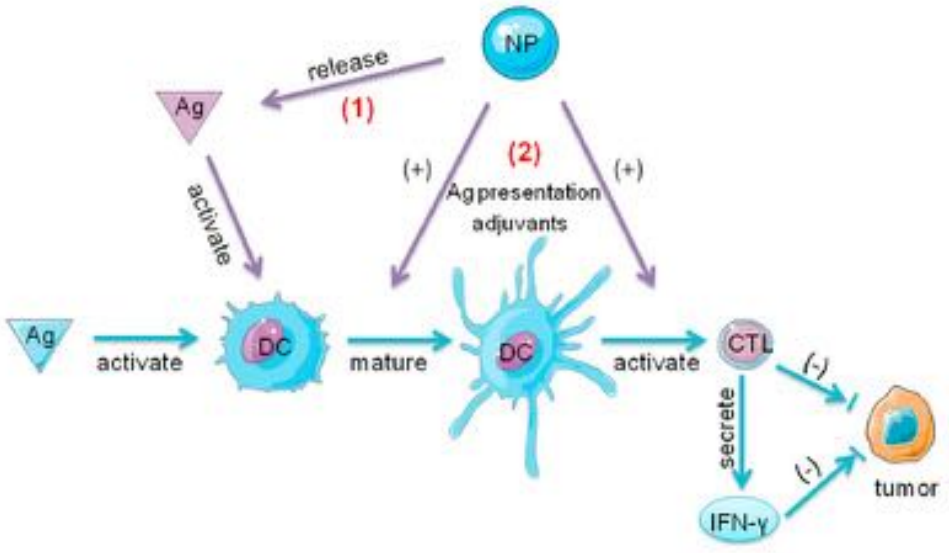

Figure 8. *The role of DCs and the function of NPs in the tumour immunity (Yang et al., 2021).*

For these reasons NPs could represent an efficient strategy aiming at reprogramming DCs directly in vivo. However, the therapeutic efficacy of nanomedicine largely depends on proper carriers and antigens. In addition, the variation of DC subsets (e.g., plasmacytoid or myeloid) has not been fully elucidated. So more extensive studies and a fully characterisation of different TADC subsets are needed in order to clarify the most appropriate design of NPs and the functions of different DC subsets before they can be translated to clinical practice.

2. Aim

Gliomas represent the 80% of malignant primary brain tumours. Among high grade gliomas (HGGs), IV grade glioma IDH wt represents the most aggressive primary brain tumour in adults, characterized by a very poor prognosis despite standard of care treatments (Hart et al., 2019; Stupp et al., 2005). Therefore, based on the recent successes of cancer immunotherapy, there is increasing interest in using immunotherapeutic approaches in the treatment of HGG patients. In particular, DC-based immunotherapy represents a promising strategy in the treatment of GBM, which is the human cancer that showed the highest susceptibility to DC-based vaccines (Garg et al., 2016; Prins et al., 2011). However, our knowledge on the mechanisms underlying the efficacy of these immunotherapeutic interventions, as well as the effects of HGG microenvironment on DCs, the subsets of DCs specifically recruited to the tumour site and the impact of HGG on the activatory/tolerogenic profile of DCs is extremely poor. Yet, a detailed comprehension of the specific DC subsets and the molecular pathways of DC activation impaired in these patients would bring novel insights into the comprehension of the intricate interactions between HGGs and the immune system, and would provide the basis for improving the efficacy of DC vaccines and for a therapeutic reprogramming of tumour-associated DCs.

For these reasons, in this study we performed a deep characterization of circulating and tumour-infiltrating DC subsets in a cohort of HGG patients undergoing surgery at their first diagnosis. In particular, we aimed to:

- characterize circulating DCs in HGG patients compared with healthy donors, by using an 18-color flow cytometry panel, set-up in our laboratory (Carenza *et al.*, 2019), that allowed a direct comparison of frequencies and phenotype of all DC subsets in a single tube;
- characterize tumour-infiltrating DCs compared with DCs in healthy brain tissues obtained from patients with gliomas, by using the same 18-color flow cytometry panel;
- correlate the above results with HGG histopathological/molecular features and dexamethasone treatment, in order to investigate the impact of biological tumor features and steroid treatment on the frequency and phenotype of DC subsets in HGG patients;
- perform a single-cell RNA sequencing of HGG samples compared with healthy brain tissues, in order to confirm with a different experimental approach the presence of different DC subsets in tumour samples;
- analyse the transcriptomic profile of tumour-infiltrating DCs, in order to investigate possible DC features related to the immunosuppressive tumour microenvironment that typically characterizes HGG.

In this study we also included a second cohort of patients composed of relapsed HGG patients, who were enrolled in multi-cohort immunotherapeutic early clinical trials (ieCTs). Given the importance

of immunotherapeutic strategies in modulating the immune responses against cancer and the crucial role played by DCs in the activation of anti-tumor immune responses, in this part of the study we aimed to:

- investigate whether ieCTs may have an impact on the number and phenotype of circulating DCs at different time points after the administration of the therapy, by using the same 18-color flow-cytometry panel applied for the study of the first patient cohort;
- analyse possible correlations between circulating DC parameters and patient clinical outcome, in order to investigate whether peripheral blood DC features may predict response to treatment, or may be useful in the patient follow-up.

3. Materials and Methods

3.1 Reagents

The following reagents were used for cytofluorimetric characterization of dendritic cells:

- FACS tubes, BD, New Jersey, USA
- Mouse monoclonal antibody anti-human CD45 AF700-conjugated, BD, New Jersey, USA
- Mouse monoclonal antibody anti-human CD3 FITC-conjugated, BioLegend, California, USA
- Mouse monoclonal antibody anti-human CD19 FITC-conjugated, BD, New Jersey, USA
- Mouse monoclonal antibody anti-human CD20 FITC-conjugated, BD, New Jersey, USA
- Mouse monoclonal antibody anti-human CD56 FITC-conjugated, BD, New Jersey, USA
- Mouse monoclonal antibody anti-human CD14 BV570-conjugated, BioLegend, California, USA
- Mouse monoclonal antibody anti-human CD16 BUV496-conjugated, BD, New Jersey, USA
- Mouse monoclonal antibody anti-human HLA-DR BUV661-conjugated, BD, New Jersey, USA
- Mouse monoclonal antibody anti-human CD123 PE-Cy7-conjugated, BD, New Jersey, USA
- Mouse monoclonal antibody anti-human CD11c PE-Cy5-conjugated, BD, New Jersey, USA
- Mouse monoclonal antibody anti-human CD141 BV605-conjugated, BioLegend, California, USA
- Mouse monoclonal antibody anti-human CD1c BV421-conjugated, BioLegend, California, USA
- Mouse monoclonal antibody anti-human M-DC8 APC-conjugated, Milteny Biotec, Germany
- Mouse monoclonal antibody anti-human CD1a BUV395-conjugated, BD, New Jersey, USA
- Mouse monoclonal antibody anti-human CD40 BV650-conjugated, BD, New Jersey, USA
- Mouse monoclonal antibody anti-human CD80 BV510-conjugated, BD, New Jersey, USA
- Mouse monoclonal antibody anti-human CD86 BUV737-conjugated, BD, New Jersey, USA
- Mouse monoclonal antibody anti-human CD274 (PD-L1) PE-CF594-conjugated, BD, New Jersey, USA
- Mouse monoclonal antibody anti-human CD85j (ILT2) PE-conjugated, BioLegend, California, USA
- Mouse monoclonal antibody anti-human CD366 (TIM-3) BV711-conjugated, BD, New Jersey, USA
- Fixable Viability Stain 780 (FVS780), BD, New Jersey, USA
- MACS buffer solution: HBSS w/o Ca2+ and Mg2+ + FBS 2% v/v + EDTA 2mM
    - HBSS w/o Ca2+ and Mg2+, Lonza, Switzerland
    - Fetal Bovine Serum (FBS), Lonza, Switzerland

    - Ethylenediaminetetraacetic acid (EDTA), VWR INTERNATIONAL s.r.l., UK
- Fixative solution: Paraformaldeyde (PFA) 1% in PBS w/o Ca^{2+} and Mg^{2+}
    - PBS w/o Ca^{2+} and Mg^{2+}, Lonza, Switzerland
    - PFA, Sigma-Aldrich, Missouri, USA
- Comp-Beads™, BD Biosciences, New Jersey, USA

The following reagents were used for tissue dissociation:

- Falcon 50 ml conical tubes, BD, New Jersey, USA
- Falcon 15 mL collection tube, BD, New Jersey, USA
- gentleMACS™ C tubes, Milteny Biotec, Germany
- Glioma medium: Dulbecco's Modified Eagle Medium + 1% L-Glutamine + 1% Penicillin-Streptomycin:
    - Dulbecco's Modified Eagle Medium (DMEM) high glucose, Lonza, Switzerland
    - 1% L-Glutamine, Lonza, Switzerland
    - 1% Penicillin-Streptomycin Mixture, Lonza, Switzerland
- RPMI 1640 and 1% FBS:
    - Roswell Park Memorial Institute (RPMI) 1640, Euroclone SpA, Italy
    - FBS, Lonza, Switzerland
- Type IV Collagenase, Merck KGaA, Germany
- Type I DNase, Merck KGaA, Germany
- 70 µm and 100 µm filters, BD, New Jersey, USA
- FACS buffer solution: HBSS w/o Ca^{2+} and Mg^{2+} + FBS 2% v/v
    - HBSS w/o Ca2+ and Mg2+, Lonza, Switzerland
    - FBS, Lonza, Switzerland
- Myelin Removal Beads II, Milteny Biotec, Germany
- LS columns, Milteny Biotec, Germany
- MidiMACS™ Separator, Milteny Biotec, Germany
- gentleMACS Dissociator, Milteny Biotec, Germany
- Tumour Dissociation kit, Milteny Biotec, Germany
- Trypan Blue, Sigma-Aldrich, Missouri, USA
- ACK 1X in distillated water:
    - Ammonium chloride (NH4Cl) 0,83% w/v, Merck KGaA, Darmstadt, Germany
    - Potassium Bicarbonate (KHCO3) 0,1% w/v, Merck KGaA, Darmstadt, Germany
    - Titriplex (EDTA disodium salt) 0,004% w/v, Merck KGaA, Darmstadt, Germany

The following reagents were used for dendritic cell absolute count:

- Pharm Lyse™ lysing solution, BD, New Jersey, USA
- CountBright™ absolute counting beads, ThermoFisher Scientific, Massachusetts, USA
- Mouse monoclonal antibody anti-human CD45 AF700 conjugated, BD, New Jersey, USA
- Fixative solution: Paraformaldeyde (PFA) 1% in PBS w/o Ca^{2+} and Mg^{2+}
    - PBS w/o Ca^{2+} and Mg^{2+}, Lonza, Switzerland
    - PFA, Sigma-Aldrich, Missouri, USA

The following reagents were used for cell-sorting experiments:

- Falcon 50 ml conical tubes, BD, New Jersey, USARPMI 1640 and 1% FBS:
    - Roswell Park Memorial Institute (RPMI) 1640, Euroclone SpA, Pero, Italy
    - FBS, Lonza, Switzerland
- Type IV Collagenase, Merck KGaA, Darmstadt, Germany
- Type I DNase, Merck KGaA, Darmstadt, Germany
- 70 µm filters BD, New Jersey, USA
- ACK 1X in distillated water:
    - Ammonium chloride (NH4Cl) 0,83% w/v, Merck KGaA, Darmstadt, Germany
    - Potassium Bicarbonate (KHCO3) 0,1% w/v, Merck KGaA, Darmstadt, Germany
    - Titriplex (EDTA disodium salt) 0,004% w/v, Merck KGaA, Darmstadt, Germany
- FACS buffer solution: HBSS w/o Ca^{2+} and Mg^{2+} + FBS 2% v/v
    - HBSS w/o Ca2+ and Mg2+, Lonza, Switzerland
    - FBS, Lonza, Switzerland
- Mouse monoclonal antibody anti-human CD45 FITC conjugated, BD, New Jersey, USA
- Fixable Viability Stain 700 (FVS700), BD, New Jersey, USA
- Hoechst DAPI, ThermoFisher Scientific, Massachusetts, USA.

3.2 Subjects enrolled

This study evaluated two cohorts of patients. The first one was composed by HGG patients at their first diagnosis of which circulating DCs before surgery and tumour-infiltrating DCs were evaluated. The second cohort was composed by relapsed HGG patients who were eligible for the enrolment in multi-cohort immunotherapeutic early phase clinical trials (ieCTs). The enrolment was conducted by unit of Neuro-Oncology at Humanitas Research Hospital, IRCCS, Rozzano, Milan, Italy. For each sample histology and molecular profile of the tumour (IDH wild type/mutated, methylation status of MGMT, ATRX loss and 1p-19q codeletion) were evaluated.

3.2.1 First HGG patient cohort

In the first part of this study we evaluated 27 patients with a clinical-radiological diagnosis of HGGs. 23 blood samples were collected at baseline (the day before surgery) and of these, 10 tumoral tissues derived from the central core of the pathological lesion were collected right after surgery. 4 healthy cerebral tissues were collected from a distal area of the pathological tissue and were macroscopically free of any disease. For each sample, information about frequency and phenotype of DC subsets were assessed in the blood and tissue samples. The absolute count of DC subsets was performed just for whole blood samples. Moreover 7 tumoral tissues and 2 healthy tissues, from 8 patients, were used for single cell-RNA sequencing analyses. This study also enrolled 12 healthy controls, from which were collected blood samples to evaluate information about the absolute number, frequency and phenotype of DC subsets (see Table 1).

	Healthy controls	**HGG patients**	**Healthy brain tissues**
Total number of enrolled subjects	12	27	4
Whole blood	12	23	-
Core	-	13	-
Age, years (mean, range)	47 (25-69)	58 (36-74)	55 (46-69)
Sex, males:females (n)	7:5	13:14	3:1
Histotype (n)	-	AA (III, IDH wt) (4) AA (III, IDH mut) (3) OA (III, IDH mut) (1) GBM (IV, IDH wt) (17) GBM (IV, IDH mut) (1) Gliosarcoma (IV, IDH wt) (1)	

Table 1 | *List of healthy donors and patients enrolled.*

3.2.2 Second HGG patient cohort

We evaluated 17 patients with a diagnosis of recurrent HGG who were enrolled in different ieCTs, as indicated in Table 2, and were followed from July 2018 to February 2020. For each sample, information about absolute count and phenotype of DC subsets were assessed before the treatment (T0) and at different time points after the treatment (T1, T2, T3, T4, T5).

	HGG patients
Total number of enrolled subjects	17
Age, years (mean, range)	50 (43-71)
Sex, males:females (n)	13:4
Histotype (n)	GBM (IV, IDH wt) (15) GBM (IV, IDH mut) (2)
ieCT (n)	anti CSFR1 (2) anti CSFR-1 + anti PD-1 (5) anti CD38 + anti PD-L1 (10)
Dexamethasone (1-4 mg), treated:untreated	11:6

Table 2 | *List of relapsed HGG patients enrolled.*

The study protocol was approved by the institutional review boards (IRB) of Humanitas Research Hospital (ONC-OSS-04-2017; 29/19). Written informed consent were provided by all participants before inclusion in the study in compliance with the Declaration of Helsinki.

3.3 Sample processing

3.3.1 Erythrocyte lysis in whole blood samples

1,5 mL of blood of each subject was incubated with ammonium chloride (ACK) 1X for 10 minutes to lyse erythrocytes. Samples were then centrifuged at 400 relative centrifugal force (rcf) for 10 minutes and cells were washed in Dulbecco's phosphate-buffered saline (DPBS -/-) 1X without Calcium (Ca), Magnesium (Mg) and Phenol Red. Samples were again centrifuged at 400 rcf for 10 minutes to obtain cells for flow-cytometry experiments.

3.3.2 Enzymatical protocol for glioma dissociation

Before processing, tissues were collected and stored at 4°C in Glioma medium. After an initial shredding with a scalpel, tissues were digested with an enzymatic procedure. Type IV Collagenase at a final concentration of 1.6 mg/mL and type I DNase at a final concentration of 0.4 mg/ml were added to RPMI 1640 and incubated with samples at 37°C for 1 hour. Then, homogenates were smashed on a 70 μm filter, washed with RPMI added with 2%FBS and collected in 50 mL collection tubes. Samples were then centrifuged at 290 rcf for 7 minutes and pelleted cells were incubated for 2 minutes with 1 mL of ACK 1X to lyse erythrocytes. After, samples were washed with FACS buffer and centrifuged for 290 rcf for 7 minutes. Since processing of cerebral tissue liberates large quantities of myelin debris that can impair cell count with Trypan blue and antibody binding, specimens were incubated with FACS buffer and Myelin Removal Beads II for 15 minutes at 4°C. Samples were then washed with FACS buffer and centrifuged at 290 rcf for 7 minutes. Pelleted cells were then resuspended in FACS buffer and applied onto LS Column. Columns were previously rinsed with FACS buffer, since they do not run dry. The matrix of the LS Columns is composed of ferromagnetic spheres, that when placed within the magnetic field of a MidiMACS^{TM} Separator, amplify the

magnetic field by 10,000-fold, inducing a high gradient within the column. This allow the negative selection of cells that are eluted in a 15 mL collection tube , while Myelin Removal Beads II bound to myelin debris remain in the LS column. Afterwards, samples were centrifuged, and pelleted cells were counted in Trypan blue. Cells were then used for flow-cytometry experiments.

3.3.3 Mechanical protocol for glioma dissociation

Before processing, tissues were collected and stored at 4°C in Glioma medium. After an initial shredding with a scalpel, samples were transferred in C tubes, containing RPMI 1640 supplemented with 1% FBS. C tubes were loaded on gentleMACS™ Dissociator and samples were mechanically disintegrated with the protocol mSpleen_01. Then, homogenates were smashed on a 100 μm filter, washed with FACS buffer and collected in 50 mL collection tubes. Samples were then centrifuged at 290 rcf for 7 minutes and pelleted cells were incubated for 2 minutes with 1 mL of ACK 1X to lyse erythrocytes. After, samples were washed with FACS buffer and centrifuged for 290 rcf for 7 minutes. As for enzymatic digestion (see paragraph 3.3.2), samples were incubated with FACS buffer and Myelin Removal Beads II for 15 minutes at 4°C, then washed with FACS buffer and centrifuged at 290 rcf for 7 minutes. Pelleted cells were then resuspended in FACS buffer and applied onto LS Column. Afterwards, samples were centrifuged, and pelleted cells were counted in Trypan blue. Cells were then used for flow-cytometry experiments.

3.4 Multiparametric flow-cytometry analysis

3.4.1 Principles

Flow-cytometry is a technology that allows the simultaneous investigation of physical, phenotypical and functional characteristics of single cells, but also the characterization of different cell types in a heterogenous populations.

The flow cytometer used in this work is a FACSymphony™ (BD Biosciences). The machine present in our cytometry facility at Humanitas Research Hospital is equipped with 5 different lasers (blue, red, violet, ultraviolet, and yellow-green) and enables the simultaneous measurement of up to 28 different parameters on a single cell. It is composed by a benchtop flow cytometer and a workstation equipped with the BD FACSDiva software to operate the cytometer functions. The machine is composed by three main structures, which are the fluidic component, the optical system and the electronic part.

The **fluidic component** allows the single cell suspension to pass in a stream, cell-by-cell, in front of the laser beam for interrogation. To obtain a single cell suspension and so an accurate measure of optical properties, the cytometer hydrodynamically focuses the cell suspension through a small nozzle in order to move the cells one by one through the laser beam.

Another important component of the machine is the **optical system**, that includes lasers that excite fluorochromes and allows the selection and separation of emission wavelengths. Before the acquisition of the sample, to detect the expression of extracellular molecules, the single cell

Marker	Description	Clone	Conjugate	Manufacturer	Batch
CD45	Leukocyte common antigen	HI30	AF700	BD Biosciences	8186553
CD3	Lineage marker—T cells	HIT3A	FITC	Biolegend	B218086
CD19	Lineage marker—B cells	4G7	FITC	BD Biosciences	8162764
CD20	Lineage marker—B cells	2H7	FITC	BD Biosciences	3291707
CD56	Lineage marker—NK cells	NCAM 16,2	FITC	BD Biosciences	61126
CD14	Lineage marker—monocytes	M5E2	BV570	Biolegend	B225361
CD16	Lineage marker—NK cells and granulocytes	3G8	BUV496	BD Biosciences	8116651
HLA-DR	Major histocompatibility complex class II molecule	G46-6	BUV661	BD Biosciences	7249926
CD123	pDC marker	7G3	PE-Cy7	BD Biosciences	8060955
CD11c	mDC marker	B-ly6	PE-Cy5	BD Biosciences	80859
CD141 (BDCA-3)	$CD141^+$ mDC marker	M80	BV605	Biolegend	B239279
CD1c (BDCA-1)	$CD1c^+$ mDC marker	L161	BV421	Biolegend	B227045
M-DC8 (anti-slan)	slanDC marker	DD-1	APC	Milteny Biotec	5180403606
CD1a	moDC marker	HI149	BUV395	BD Biosciences	7227951
CD40	Costimulatory molecule	5C3	BV650	BD Biosciences	8163659
CD80	Costimulatory molecule	L307	BV510	BD Biosciences	8228546
CD86	Costimulatory molecule	2331	BUV737	BD Biosciences	7240739
CD274 (PD-L1)	Inhibitory molecule	MIH1	PE-CF594	BD Biosciences	7191550
CD85j (ILT2)	Inhibitory molecule	GHI/75	PE	Biolegend	B222938
CD366 (TIM-3)	Inhibitory molecule	7D3	BV711	BD Biosciences	7348783
Fixable Viability Stain 780	Viability marker		APC-Cy7	BD Biosciences	6174894

Table 3 | List of monoclonal antibodies used in this study.

suspension is stained with specific fluorochrome-conjugated monoclonal antibodies (mAb). When the cell suspension is run through the cytometer, the single cell is interrogated by different laser beams that excites the fluorochrome conjugated with the specific mAbs used. Every fluorochrome is excited by a specific laser and has a precise emission wavelength. Many fluorochrome with specific excitation and emission wavelengths and conjugated to different mAbs are commercially available, allowing to detect expression levels of a high number of molecules at the same time on a single cell.

When a single cell is interrogated by a laser beam, it scatters light in all directions. The light that is scattered in the forward direction (along the same axis of the laser path) is detected in the Forward Scatter Channel (FSC) and the intensity of this signal is proportional to cell size and membrane permeability. Instead, the light that is scattered in the perpendicular direction (at 90° to the axis of the laser path) is detected in the Side Scatter Channel (SSC) and the intensity of the signal is proportional to the internal complexity of the cell.

In addition, flow cytometers are equipped with various filters to direct photons of the correct wavelength to each detector, limiting the range of wavelength measured by a specific detector. However, spectral overlap could occur when two or more fluorochromes emitting at similar wavelength and, as consequence, light emitted from one fluorochrome can be collected also by a detector optimized for a different fluorochrome. This effect is called spillover and can be corrected by using the compensation.

The last important component of the flow cytometer is the **electronic part**, which comprises detectors that convert the fluorescence signal into proportional electrical pulses and display them on a computer. There are two types of signal detectors: Photomultiplier tubes (PMTs), used to detect the SSC and the signals generated by all fluorescence channels; Photodiodes, less sensitive to light signals compared to PMTs, that allows the detection of the FSC signal.

3.4.2 Multicolour flow-cytometry strategy

An 18-color flow-cytometry panel optimised by Carenza and colleagues (Carenza et al., 2019) was applied to study the frequency and the phenotype of DC subsets in the peripheral blood of HDs and HGG patients; the panel was also applied to study DC subsets in healthy cerebral tissues and in tumour tissues of HGG patients. mAbs used for the staining are listed in Table 3.

To design a polychromatic flow-cytometry panel the grade of compensation between channels, the mAb titrations, the levels of expression of antigens and the brightness of the conjugated fluorochromes should be taken into consideration. In a polychromatic experiment, in which a high number of parameters are analysed simultaneously, the compensation procedure could be complex. This is due to the high number of pair wise combinations between fluorochromes, which increase

exponentially with the number of parameters analysed. Moreover, since it increases the chance of operator error, to avoid manual compensation, we used Software-assisted compensation. In particular, the compensation was performed during acquisition using the Diva software, and manually adjusted.

3.4.3 Extracellular staining for whole blood and tissue samples

Cells were stained in the dark at room temperature (RT) for 15 minutes with the Fixable Viability Stain (FVS) 780 in a final volume of 250 µl (for a maximum of $10x10^6$ cells). The dye was diluted 1:4000 in DPBS-/- 1X. FVS 780 reacts with and covalently binds to cell-surface and intracellular amines. Permeable plasma cell membranes, such as those present in necrotic cells, allow for the intracellular diffusion of the dye and covalent binding to higher overall concentrations of amines than in non-permeable live cells, therefore enabling the identification of non-viable cells and their exclusion from the analysis. After the incubation, samples were washed with 5 mL of MACS buffer and centrifuged for 5 minutes at 400 rcf. Then, pelleted cells were incubated with a specific monoclonal antibody cocktail in the dark for 20 minutes at 4°C, to avoid unspecific binding, in a final volume of 50 µl (for a maximum of $10x10^6$ cells). Antibodies were used at concentrations gained by titration experiments and are listed in Table 3. Afterward, samples were washed with 2 mL of MACS buffer and centrifuged for 5 minutes at 400 rcf. Next, each cell pellet was fixed with 100 µl of 1% PFA for 20 minutes at RT in the dark, under fume hood. Lastly, samples were washed with 2 mL of MACS buffer and resuspended in 100-150 µl of MACS buffer. Samples were then acquired at BD FACSymphony™ flow cytometer (BD Bioscience).

3.4.4 Staining for absolute count

50 µl of peripheral blood were incubated in the dark for 20 minutes at RT with a monoclonal antibody anti-human CD45 AF700-conjugated. Antibodies were used at concentrations gained by titration experiments. After incubation, samples were fixed 4% PFA) for 15 minutes at RT in the dark, under fume hood. Then, 500 µl of BD Pharm Lyse™ lysing solution were added to each sample and incubated for 10 minutes at RT. BD Pharm Lyse™ lysing solution is a buffered, concentrated (10X) ammonium chloride-based lysing reagent. When diluted to a 1X concentration it lyses red blood cells following monoclonal antibody staining. Before the acquisition of samples at BD FACSymphony™ flow cytometer (BD Bioscience), 25 µl of CountBright™ absolute counting beads were added to obtain the concentration of each sample as cells/µl. CountBright™ absolute counting beads are a calibrated suspension of microspheres that are brightly fluorescent across a wide range of excitation and emission wavelengths and contain a known concentration of microspheres. For absolute counts, a specific volume of the microsphere suspension is added to a specific volume of sample, so that the ratio of sample volume to microsphere volume is known. The volume of sample analysed can be

calculated from the number of microspheres events, and can be used with cell events to determine cell concentration. To calculate cell concentration:

$$\frac{A}{B} \times \frac{C}{D} = concentration\ of\ sample\ as\ cells/\mu L$$

Where A is the number of cell events; B is the number of bead events; C is the assigned bead count of the lot (beads/50 µL); and D is the initial volume of the sample (50 µL).

3.4.5 Compensation

MAbs conjugated to different fluorochromes can be used to detect specific antigens, expressed on the extracellular membrane of the cell, in a multicolour flow-cytometry panel. To design a panel, two important points must be considered: the brightness of the fluorochrome and the level of antigen expression. The fluorescence from more than one fluorochrome may be detected by the same detector, especially with fluorochromes which emit at similar wavelengths. Therefore, proper fluorescence compensation is essential, to avoid spectral overlap and to ensure that the fluorescence detected in a particular detector derives from the fluorochrome that is being measured.

A correct compensation can be reached by using a paired single-stained control, one for each fluorochrome-conjugated mAb used in the panel. Different rules should be following to obtain a good compensation: (1) single-stained control samples must be bright at least as the test staining; (2) each compensation control must have a paired negative control of the same source, cells or beads, given that auto-fluorescence can vary depending on the source used.

For this reason, Comp-Beads™ were used in stainings to optimize fluorescence compensation settings for multicolor flow-cytometryic analyses. These beads are conjugated to a mAb specific for the K light chain of Immunoglobulins, from mouse, rat, or rat/hamster.

3.4.6 Fluorescence Minus Ones (FMO) controls

In order to discriminate positive cells for the following markers, CD40, CD80. CD86, PD-L1, ILT2, TIM-3 and M-DC8, Fluorescence Minus One (FMO) controls were implemented to the experiment. An FMO control is a tube of cells stained with all fluorochromes used in the experiment except one. FMO controls are used to determine the cut-off point between background fluorescence and positive populations in multicolour flow-cytometry experiments. They are needed when a positive cell population is presented as a smear instead of being distinctly separate from the negative population. The lack of distinction between positive and negative populations is exacerbated by “spreading” of the negative populations due to the contributions of fluorescence overlap compensation from multiple fluorochromes.

3.4.7 Antibody titration

Manufacturer's instructions often recommend a specific dilution for each fluorochrome-conjugated mAbs. However, the suggested dilution not always allows the optimal detection of the antigen and the right separation of positive and negative signals. Therefore, to select the right amount of reagent to be used in a flow-cytometry experiment, titration experiments are performed for every mAb. The main aspects to consider when making a titration experiment are the level of antigen expression (which could be bright or dim) and the type of cell population to be investigated.

Titration experiments of mAbs were performed on cryopreserved PBMCs that were thawed and stained for the viability marker FVS 780. After 15 minutes of incubation in the dark at RT, cells were washed and stained with 7 serial dilutions of the mAb of interest: from titer reported on datasheet, to 1:2, 1:4, 1:8, 1:16, 1:32, and 1:64 dilution.

The tube number 8 is the FMO and represents the background due to unspecific signal. It is made with cells stained only with FVS 780, without the mAb to be titrated, and it is considered the negative population.

The correct titer is chosen because it gives the best separation between the negative population and the positive one, with the lowest background. Moreover, the right titer can be mathematically calculated by dividing the median of fluorescence of positive and the negative signal. The best separation corresponds to the highest ratio.

3.4.8 Data Analysis

3.4.8.1 Flow-jo analysis

Flow-cytometry Standard (FCS) 3.0 files, acquired through BD FACSymphony^{TM} flow cytometer, were analysed using the FlowJo software (TreeStar Inc, Ashland, Oregon, USA), versions 9.9.6 and 10.7.

Gating strategies for whole blood and tissue samples were shown in Figures 8 and 9 (WB and tissue, respectively).

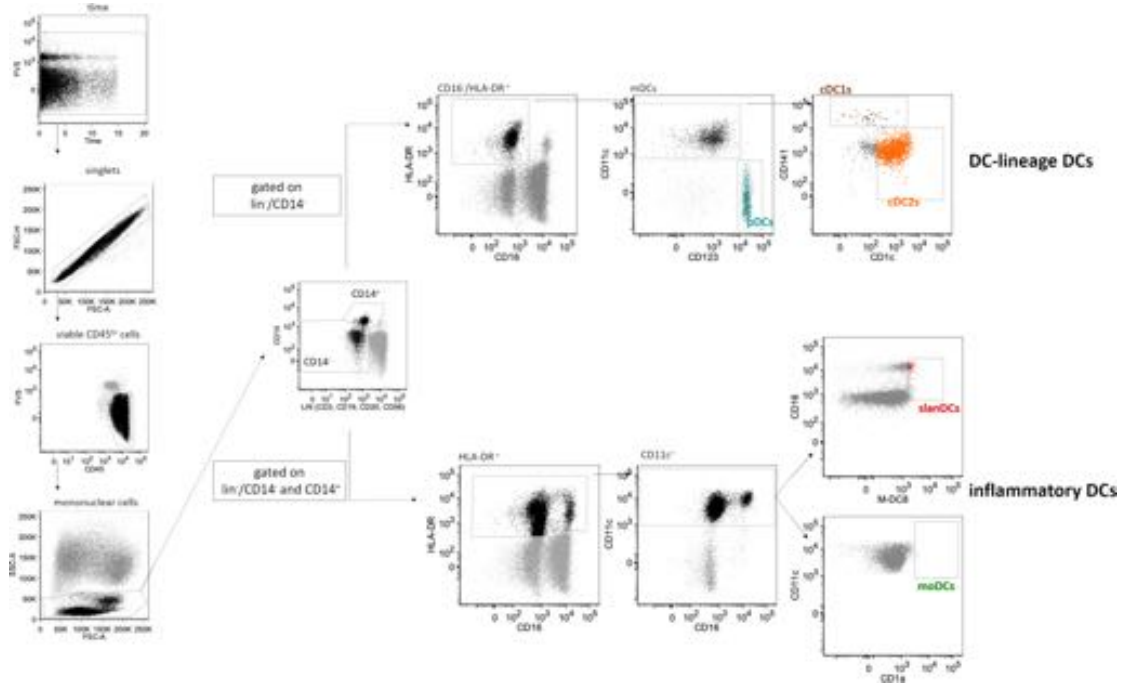

Figure 9. *Gating strategy used for the identification of 5 distinct DC subsets in the peripheral blood of healthy donors. DCs were analyzed within the gate of single viable mononuclear cells. Lineage-DCs were identified in the gate of lin^{-}/CD14^{-}/CD16^{-}/HLA-DR^{+} cells. Within lineage-DCs, pDCs (CD123^{+}/CD11c^{-}), cDC1s (CD123^{-}/CD11c^{+}/CD141^{+}) and cDC2s (CD123^{-}/CD11c^{+}/CD1c^{+}) were identified. Inflammatory DCs were identified as lin^{-}/HLA-DR^{+}/CD11c^{+} that could be negative or positive for CD14 and CD16. Within inflammatory DCs, slanDCs, and moDCs were identified based on positive staining of M-DC8 and CD1a, respectively. As expected, moDCs were undetectable in most samples.*

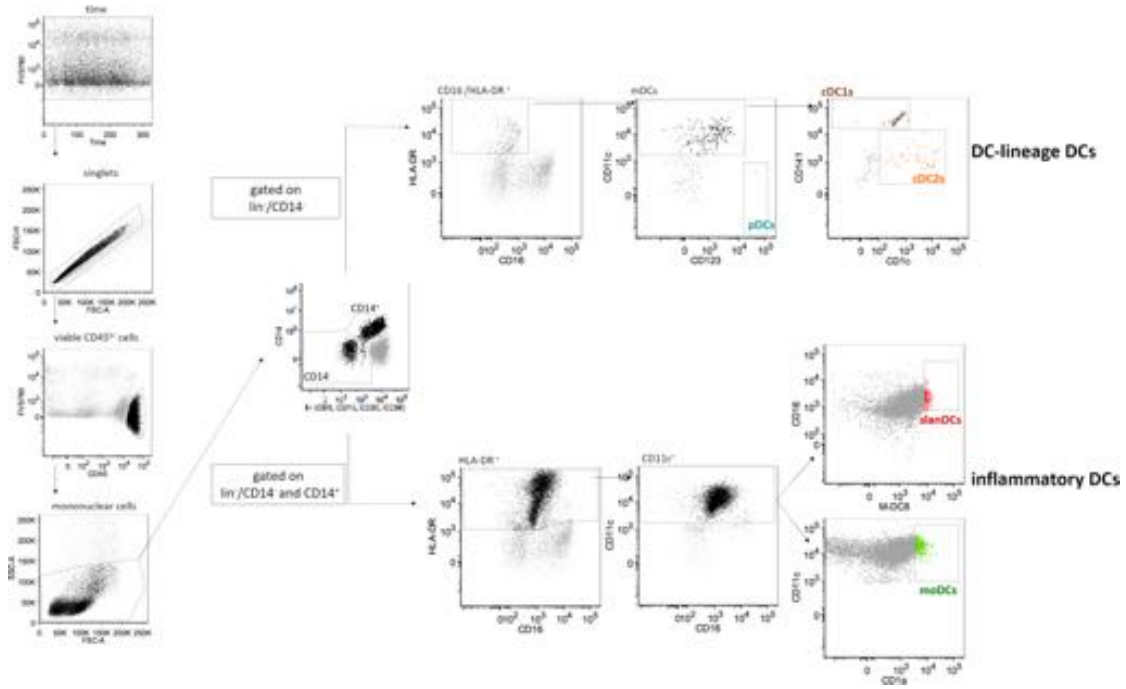

Figure 10. *Gating strategy used for the identification of 5 distinct DC subsets in the tumour tissue of HGG patients. DCs were analyzed within the gate of single viable CD45^{br} mononuclear cells. Lineage-DCs were identified in the gate of lin$^-$/CD14$^-$/CD16$^-$/HLA-DR$^+$ cells. Within lineage-DCs, pDCs (CD123$^+$/CD11c$^-$), cDC1s (CD123$^-$/CD11c$^+$/CD141$^+$) and cDC2s (CD123$^-$/CD11c$^+$/CD1c$^+$) were identified. Inflammatory DCs were identified as lin$^-$/HLA-DR$^+$/CD11c$^+$ that could be negative or positive for CD14 and CD16. Within inflammatory DCs, slanDCs, and moDCs were identified based on positive staining of M-DC8 and CD1a, respectively.*

3.4.8.2 Uniform Manifold Approximation and Projection (UMAP) analysis

UMAP is a new technique developed by McInnes and colleagues (McInnes et al., 2018). It is an unsupervised clustering algorithm that allows to reduce the dimensionality of complex data and visualize them in a two-dimension space, evaluating, at single cell level, differences/similarities of marker expression. For the multiparametric analysis of flow-cytometry data, we used UMAP plugin provided by FlowJo v10.7 software. The algorithm is based on two main parameters: the *n_neighbors* and the *min_dist.* The *n_neighbors* is the number of approximate nearest neighbors used to construct the initial high-dimensional graph. It effectively controls how UMAP balances local versus global structure, where local and global structures mean distances among data points within clusters or among clusters, respectively. Low values will push UMAP to focus more on local structure by constraining the number of neighboring points considered when analyzing the data in high dimensions, while high values will push UMAP towards representing the big-picture structure while losing fine detail. The second parameter is *min_dist*, or the minimum distance between points in low-dimensional space. This parameter controls how tightly UMAP clumps points together, with low values leading to more tightly packed embeddings. Larger values of *min_dist* will make UMAP pack points together more loosely, focusing instead on the preservation of the broad topological structure.

Initially, a unique computational barcode was assigned to single samples that were divided in 3 groups. Groups contained samples deriving respectively from whole blood of HDs (n=12), whole blood of HGG patients (n=21) and tumour tissue of HGG patients (n=8). Since the number of samples for each group was uneven, a down-sample operation was performed. First, 3 different concatenate files were created containing live $CD45^+/lin^-/HLA\text{-}DR^+$ cells deriving respectively from whole blood of HDs (n=12), whole blood of HGG patients (n=21) and tumour tissue of HGG patients (n=8). Then, on each concatenated file was applied the down-sample gate, imposing the maximum number of events from the group with the lowest numerosity. Then, the 3 down-sampled files were concatenated in a single file and visualised with UMAP dot plot (distance function, Euclidean; nearest neighbors, 15; minimum distance, 0.5). The expression of the following markers was considered: CD45, CD14, CD16, HLA-DR, CD11c, CD123, CD141, CD1c, M-DC8, CD1a, CD40, CD80, CD86, PD-L1, ILT2, TIM-3.

3.5 CD45^{+} and CD45^{-} cell sorting and Single-cell RNAseq

3.5.1 Sorting

The cell sorting technology exploits flow-cytometry to isolate and purify a specific cell population according to physical parameters and the expression of specific markers, starting from a heterogeneous suspension of cells. Indeed, based on user-defined parameters, individual cells can so be diverted from the fluid stream and collected into homogeneous fractions with a purity that approaches 100%.

More in detail, after the cell staining, samples are introduced in the injection chamber. Hydrodynamic focusing forces particles through the cuvette in a single-file stream, where laser light intercepts the stream at the sample interrogation point, as in a normal flow cytometer (Figure 11). The sorter is set up so that each individual cell enters a single droplet as it leaves the nozzle tip. This drop is given an electronic charge, depending on the fluorescence of the cell inside the drop. Single particles pass then through the sort block where they are either transported to waste via the waste aspirator or sorted into a collection device in the sort collection chamber. The sort block houses the high-voltage deflection plates, which are used to deflect side streams during sorting and attract or repel the cells accordingly into collection tubes.

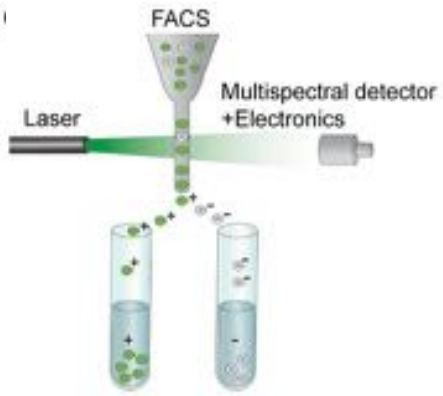

Figure 11. *FACS sorting scheme.*

Sorting experiments were performed using the BD FACSAria II (BD Biosciences) flow cytometer, a high-speed fixed-alignment benchtop cell sorter. It can perform a multicolour analysis of up to 13 fluorescent markers and two scatter parameters at the same time.

9 Samples (7 from tumour tissues and 2 from healthy cerebral tissues) were sorted for CD45^{+} and CD45^{-} cells to then perform single cell RNA sequencing experiment. Briefly, after tissue dissociation with type IV collagenase (1,6 mg/mL) and type I DNase (0,4 mg/mL) in DPBS-/- 1X at 37°C for 1 hour, homogenates were sequentially smashed on a 100 µm, 70 µm and 40 µm filter, washed with FACS buffer and centrifuged at 290 rcf for 7 minutes. Pelleted cells were incubated at 4°C for 2 minutes with 1 mL of ACK 1X to lyse erythrocytes. After, samples were washed with FACS buffer, centrifuged for 290 rcf for 15 minutes at 4°C and resuspended in RPMI 1640 for the nuclear staining with Hoechst dye at 37°C for 15 minutes. Then cell suspension was stained for viability marker (Fixable Viability Stain 700) and anti-human mAb CD45 FITC-conjugated, at 37°C for 20 minutes. After, cells were sorted.

3.5.2 Single-cell RNA sequencing

Mapping genotypes to phenotypes is one of the long-standing challenges in biology and medicine, and a powerful strategy for tackling this problem is performing transcriptome analysis. However, even though all cells in our body share nearly identical genotypes, transcriptome information in any one cell reflects the activity of only a subset of genes. Furthermore, because the many diverse cell types in our body each express a unique transcriptome, conventional bulk population sequencing can provide only the average expression signal for an ensemble of cells (Hwang et al., 2018). On the contrary, high-throughput technologies enable the profiling of hundreds of thousands of cells in parallel, providing an unbiased view of the heterogeneity of single cells within a population (Kolodziejczyk et al., 2015).

To sequence mRNA from a single cell, one has to overcome two challenges that are not present in standard population-level methods: (1) capturing single cells and (2) amplification of small amounts of mRNA from a cell. Although it may seem trivial, capturing single cells quickly and accurately with high efficiency is one of the main challenges of single-cell sequencing. To increase throughput, cells from a tissue can be dissociated, suspended in a buffer and loaded into microfluidics platforms. Optionally, after dissociation, cells can be stained and sorted to enrich a specific population of interest. After the steps of lysis of single cells, each scRNA-seq protocol may be divided into three steps: (1) reverse transcription to obtain complementary DNA (cDNA), (2) cDNA amplification, and (3) sequencing library preparation. scRNA-seq can be affected by multiple technical artifacts arising from cell capture, library preparation, and sequencing procedures. Quality control to discard poor quality libraries is therefore essential for reliable downstream analyses (Kolodziejczyk et al., 2015).

In this work, single-cell RNA sequencing experiments were performed on 7 tumoral samples and 2 healthy cerebral tissues (of which one was matched) derived from HGG patients. After sorting experiments (as described in 3.5.1) for each patient were added 10% in volume of $CD45^-$ cells to $CD45^+$ cells. Sorted cells were resuspended in 1mL PBS plus 0.04% BSA and washed two times by centrifugation at 450 rcf for 7min. After the second wash cells were resuspended in 30 µL and counted with an automatic cell counter (Countess II, Thermo Fisher) to get a precise estimation of total number of cells recovered. Afterwards we loaded about 20.000 cells of each sample into one channel of the Single Cell Chip A using the Single Cell 3' v2 reagent kit (10X Genomics) for Gel bead Emulsion generation into the Chromium system. Following capture and lysis, cDNA was synthesized and amplified for 14 cycles following the manufacturer's protocol (10X Genomics). 50 ng of the amplified cDNA for each sample were then used to construct sequencing libraries. Libraries were sequenced via NovaSeq6000 (Illumina, San Diego, CA) for 8 samples and NextSeq500 (Illumina, San Diego, CA) for 1 healthy cerebral sample. An average sequencing depth of at least ~ 50,000

reads/cell was obtained for each sample. Following the sequencing, the raw data from each sample were demultiplexed and FastQC quality control checks on raw sequence data were performed. Then raw data from each sample were aligned to the hg38 reference genome, and single cell feature counts were quantified. All these steps were performed by using the 10X Genomics Cell Ranger pipeline (v3.0.1 10, 10XGenomics), obtaining a matrix of gene expression. Then, we continued the data analysis with the filtered barcode matrix files using the Seurat package (v3.0.2) in R (v3.5.1). For the initial QC step, we filtered out the cells that expressed <200 genes and the genes that were expressed in less than 3 cells. We also removed cells with >10% mitochondrial transcripts content. After removal of low-quality cells, gene expression matrices were normalized by the NormalizeData function and then were scaled by the ScaleData function of Seurat.

Clustering analysis was performed by using the FindNeighbors and FindClusters functions provided by Seurat package and non-linear dimensional reduction with the RunUMAP function was performed for graphic visualization of data, selecting Louvain algorithm that was settled at different resolution levels, to choose the optimal parameter of resolution through cluster-tree visualization. The choice of resolution influences the number of clusters. Cluster annotation was performed in silico using the automatic annotation method for scRNAseq data, SingleR which used different databases (Human Primary Cell Atlas (HPCA), Novershtern Hematopoietic Data, Monaco Immune Data). Moreover the DC annotation was performed manually basing on literature data obtained by scRNAseq analyses of sorted DC subsets (Breton et al., 2016; Collin & Bigley, 2018; Villani et al., 2017).

Correlation heat map of gene expression between clusters was generated by calculating Pearson correlation coefficient ($0 \leq \rho \leq 1$) by R Pheatmap function.

Then we performed re-clustering of DC cluster, using singleR, and the R package Clustree was used to visualise and choose the resolution of our analysis.

Sequencing data were analysed by the laboratory of Leukocyte biology in collaboration with unit of Bioinformatics at Humanitas Research Hospital.

3.5.3 Ingenuity pathway analysis (IPA)

Lists of differentially expressed genes (DEGs) for cluster 0 and 1 of infiltrating DCs, containing gene identifiers and corresponding expression values (adjusted p-value < 0.01; 0.58 < average logFold-Change (FC) < -0.58), were uploaded into the IPA software (Qiagen). The “core analysis” function included in the software was performed on each cluster, applying the “immune cell” filter. The “comparison analysis” was then performed between the “core analysis” of the two clusters of infiltrating DCs and used to interpret the differentially expressed data, which included canonical pathways (CPs) and disease and functions (DFs). Only statistically significant CPs and DFs were

considered (p-value <0.05; 1.5 < z-score < -1.5) Each gene identifier was mapped to its corresponding gene object in the Ingenuity Pathway Knowledge Base (IPKB).

3.6 Statistical analysis

3.6.1 First HGG patient cohort

The statistical analyses were performed using OpenStat (version September 11 2008) software.

The significance of data between paired patients was valued using nonparametric Wilcoxon Matched Test, Signed Ranks test statistical analysis. The significance of data between HDs and patients was valued using Mann Whitney U test statistical analysis. P values were considered statistically significant when $p < 0.05$.

3.6.2 Second HGG patient cohort

Differences in immunological markers count were calculated as follow $\Delta(T1,T0)/T0$ and $\Delta(TF,T0)/T0$.

Follow-up time was estimated with the inverse Kaplan–Meier method. Survival curves were generated using the Kaplan–Meier method. Differences between groups were evaluated using the log-rank test.

The Cox proportional hazards regression model was used to calculate the hazard ratios (HRs) and their 95% confidence intervals (CIs). A p-value <0.1 was set as statistically significant in the univariable model. Only factors statistically significant at level 0.05 were included in the final multivariable model. All analyses were carried out with SAS software, version 9.4 (SAS Institute, Cary, NC).

4. Results

4.1 Flow-cytometry characterisation of DC subsets in the whole blood of HGG patients

In order to assess whether circulating DCs undergo any changes in HGG patients, we compared DCs in the peripheral blood of 23 HGG patients before surgery and 12 healthy donors (HDs), by using an 18-color flow cytometry panel recently optimized in our laboratory that allows a direct comparison of different DC subsets within the same tube (Carenza *et al.*, 2019). In addition, by using CountBright^{TM} Absolute Counting Beads, we assessed and compared the absolute count of DC subsets in whole blood samples from HDs and HGG patients.

In order to investigate the impact of disease severity and corticosteroid treatment on DC counts and phenotype, we further analysed DC features in HGG patients stratified according to the histopathological/molecular features of the tumour, and corticosteroid medication.

4.1.1 Frequencies and absolute counts of DC subsets in the whole blood of HGG patients and HDs

We first compared the frequencies and absolute counts of circulating DCs between HGG patients and HDs. As shown in Figure 12A, we observed a significant decrease in the frequencies of all the subsets of DC-lineage DCs (pDCs, cDC1s and cDC2s) in HGG patients when compared with HDs. The same results were confirmed when the absolute counts of DCs were analysed (Figure 12B). Regarding inflammatory DCs, we observed only a slight increase in the frequency of slanDCs in HGG patients compared with HDs that was not confirmed when the absolute counts of these cells were considered. moDCs were undetectable in the peripheral blood of HDs and HGG patients, as expected.

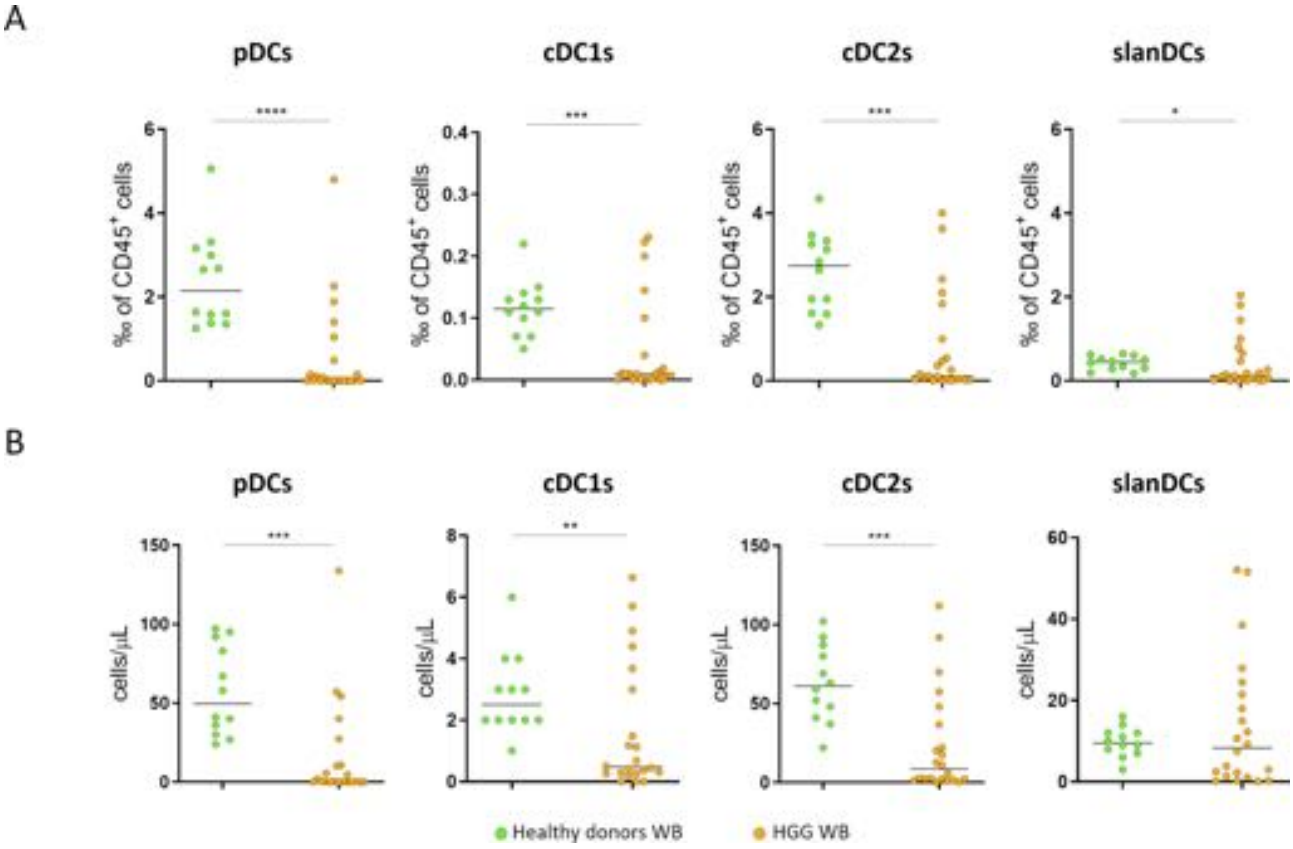

Figure 12. *(A) The frequency of DC subsets in whole blood samples obtained from healthy donors (green circles, n = 12) and HGG patients (orange circles, n = 23), was expressed as per thousand (‰) of CD45-positive cells. (B) The absolute count of DC subsets in whole blood samples obtained from healthy donors (green circles, n = 12) and HGG patients (orange circles, n = 22), was expressed as number of cells per µL of whole blood. Each symbol represents a single sample. In each series, the median is also shown. *p < 0.05, **p < 0.01, ***p < 0.001. Statistical significance calculated using the Mann-Whitney U test.*

Because HGG patients are often treated with corticosteroids (usually, dexamethasone) before surgery in order to manage tumor-induced cerebral edema and its neurological manifestations, we wondered whether this treatment may have any impact on peripheral blood DCs. Therefore, in order to investigate the effects of steroid treatment on circulating DCs in HGG patients, we stratified patients on the basis of pre-surgery steroid administration, dividing 12 untreated patients from 11 patients treated with different doses of steroids (from 4 to 16 mg/die).

The group of untreated patients included a cohort of patients affected by either III grade glioma (n=5), or IV grade glioma with IDH mut (n=1), or IV grade glioma IDH wt (n=6). Because this last type of glioma is characterized by the highest severity and worst prognosis among all HGGs, in our analyses we split the group of untreated patients into "untreated III+IVmut" (n=6) and "untreated IVwt" (n=6), for a direct comparison. The group of dexamethasone-treated ("dex-treated") patients was composed of 11 patients, 10 of which were affected by IV grade glioma IDH wt, and only 1 by III grade glioma. As shown in (Figure13A), among untreated patients we observed that the reduction in the frequency of all DC subsets was much more marked in the "untreated IVwt" group compared with the "untreated

III+IVmut" group. This last group showed indeed DC frequencies similar to HDs, suggesting that peripheral blood DCs are affected only in HGG patients affected by the most severe disease. As shown in the same figure, "dex-treated" patients showed a marked reduction of all DC subsets, with frequencies similar to those observed in the "untreated IVwt" group. Because almost all patients in the "dex-treated" group were affected by IV grade IDHwt glioma, it was not possible from these results to ascribe DC reduction to corticosteroid treatment or disease severity.

As shown in (Figure 13B), roughly similar results were observed when DC absolute counts, rather than DC frequencies within CD45-positive cells, were considered.

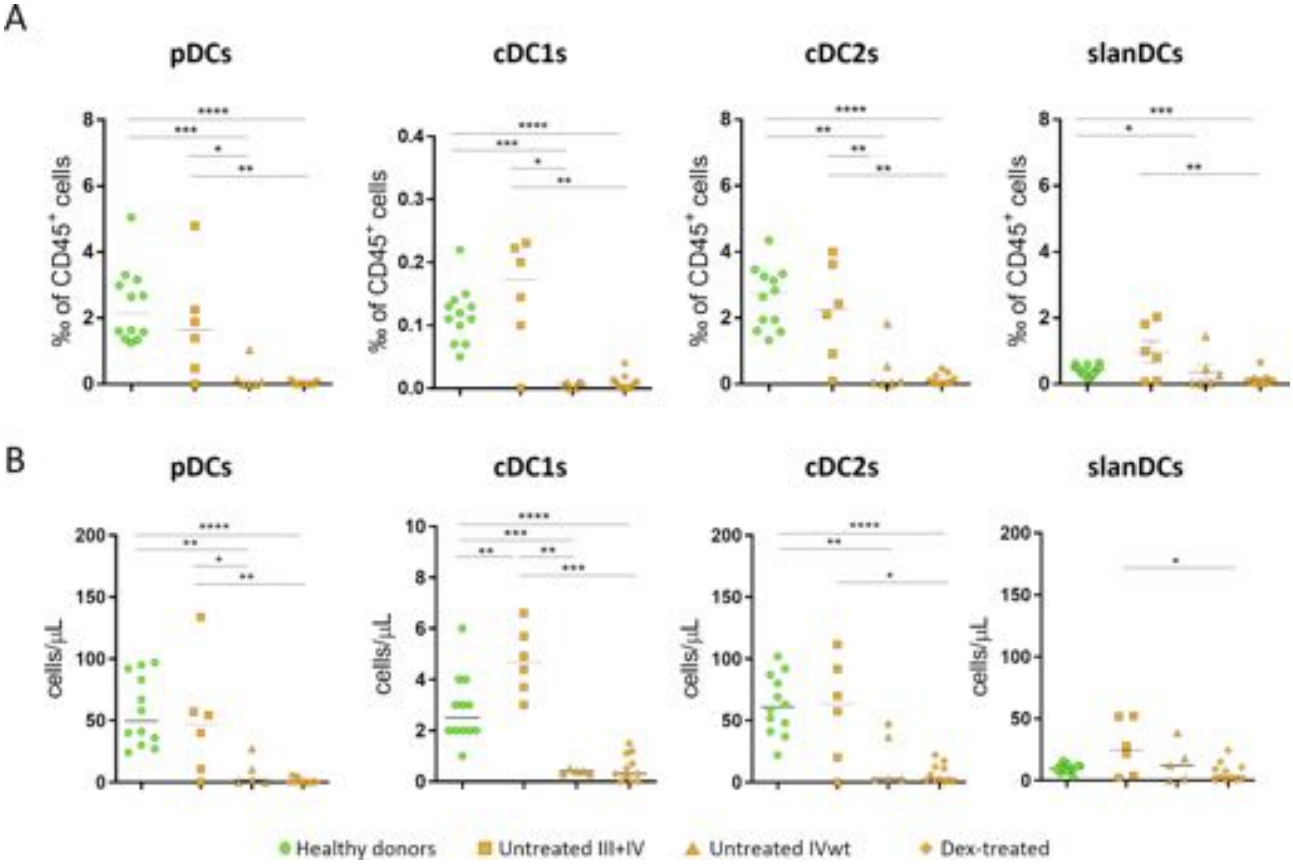

Figure 13. *(A) The frequency of DC subsets in whole blood samples obtained from healthy donors (green circles, n = 12) and HGG patients stratified based on histopathological/molecular features and corticosteroid treatment was expressed as per-thousand (‰) of CD45-positive cells (orange squares, "untreated III+IVmut", n = 6; orange triangles, "untreated IVwt", n = 6; orange diamonds, "dex-treated", n = 11), (B) The absolute count of DC subsets in whole blood samples obtained from the same individuals was expressed as number of cells per µL of whole blood. Each symbol represents a single sample. In each series, the mean ± SEM is also shown. *p < 0.05, **p < 0.01, ***p < 0.001, ****p < 0.0001. Statistical significance calculated using the Mann-Whitney U test.*

4.1.2 Phenotype of DC subsets in the whole blood of HGG patients and HDs

In order to investigate possible changes in the state of activation of DCs in HGG patients, we compared the phenotype of all DC subsets between HGG patients and HDs, analysing the expression of the activation markers CD40, CD80, CD86, HLA-DR, and the immune checkpoints PD-L1, ILT2

and TIM-3. As shown in (Figure 14), we did not observe any consistent differences in the expression of costimulatory molecules and HLA-DR between HDs and patients, not even when we divided patients according to HGG histopathological/molecular features and corticosteroid treatment (Figure 15).

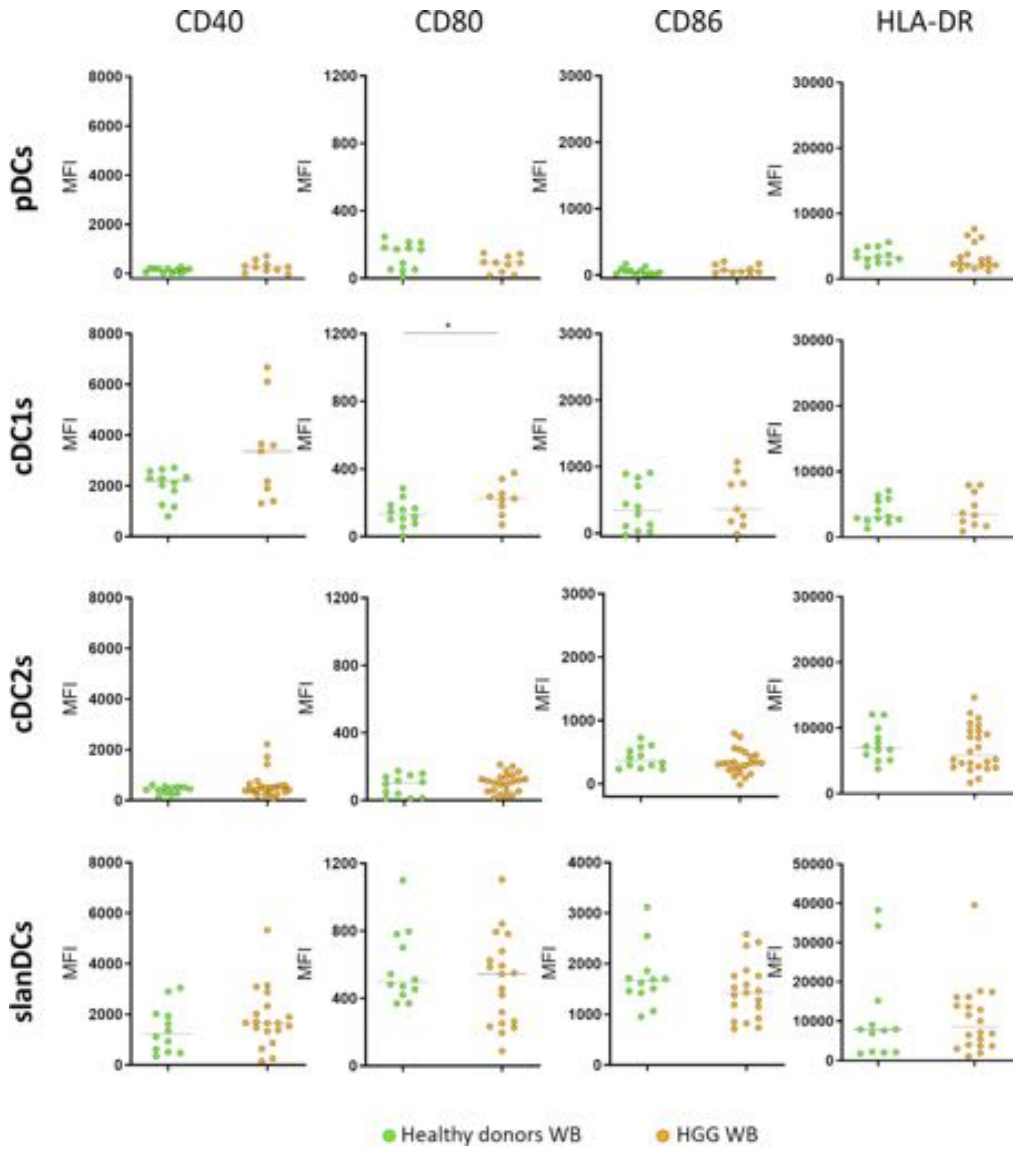

Figure 14. *Surface expression of the activation markers CD40, CD80, CD86 and HLA-DR on DC subsets in whole blood samples obtained from healthy donors (green circles, n =12) and HGG patients (orange circles, n= 23). The expression of the activation markers was assessed on pDCs, cDC1s, cDC2s, and slanDCs, and expressed as Mean Fluorescence Intensity (MFI). Each symbol represents a single sample. In each series, the median is also shown. *p < 0.05. Statistical significance calculated using the Mann-Whitney U test.*

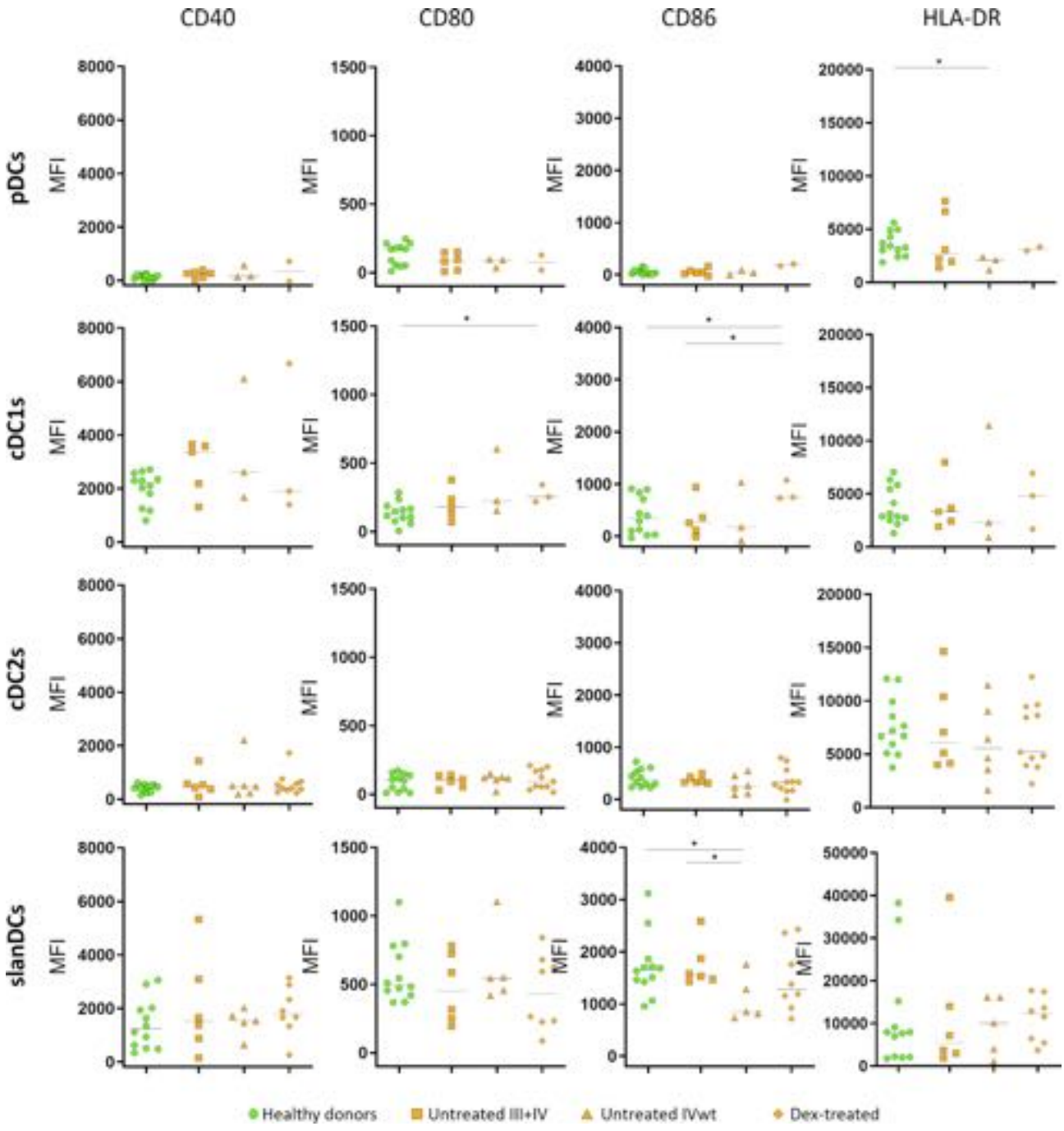

Figure 15. *Surface expression of the activation markers CD40, CD80, CD86 and HLA-DR on DC subsets from whole blood of healthy donors (green circles, n =12), and HGG patients stratified based on histopathological/molecular features and corticosteroid treatment (orange squares, "untreated III+IVmut", n = 6; orange triangles, "untreated IVwt", n = 6; orange diamonds, "dex-treated", n = 11).The expression levels of the activation molecules were assessed on pDCs, cDC1s, cDC2s, and slanDCs, and expressed as Mean Fluorescence Intensity (MFI). Each symbol represents a single sample. In each series, the median is also shown. *p < 0.05. Statistical significance calculated using the Mann-Whitney U test.*

The analysis of immune checkpoint expression showed a significant reduction in the expression of ILT2 on pDCs and cDC2s in HGG patients compared with HDs (Figure 16). This reduction in ILT2 expression was similarly observed in all subgroups of patients, suggesting that it was not affected by histopathological or molecular HGG features, nor by corticosteroid treatment (Figure 17). As shown

in the same figures, the expression of PD-L1 on cDC1s was higher in the group of "dex-treated" compared with "untreated III+IVmut" patients, although PD-L1 expression on cDC1s in the whole group of HGG patients did not differ significantly from HDs.

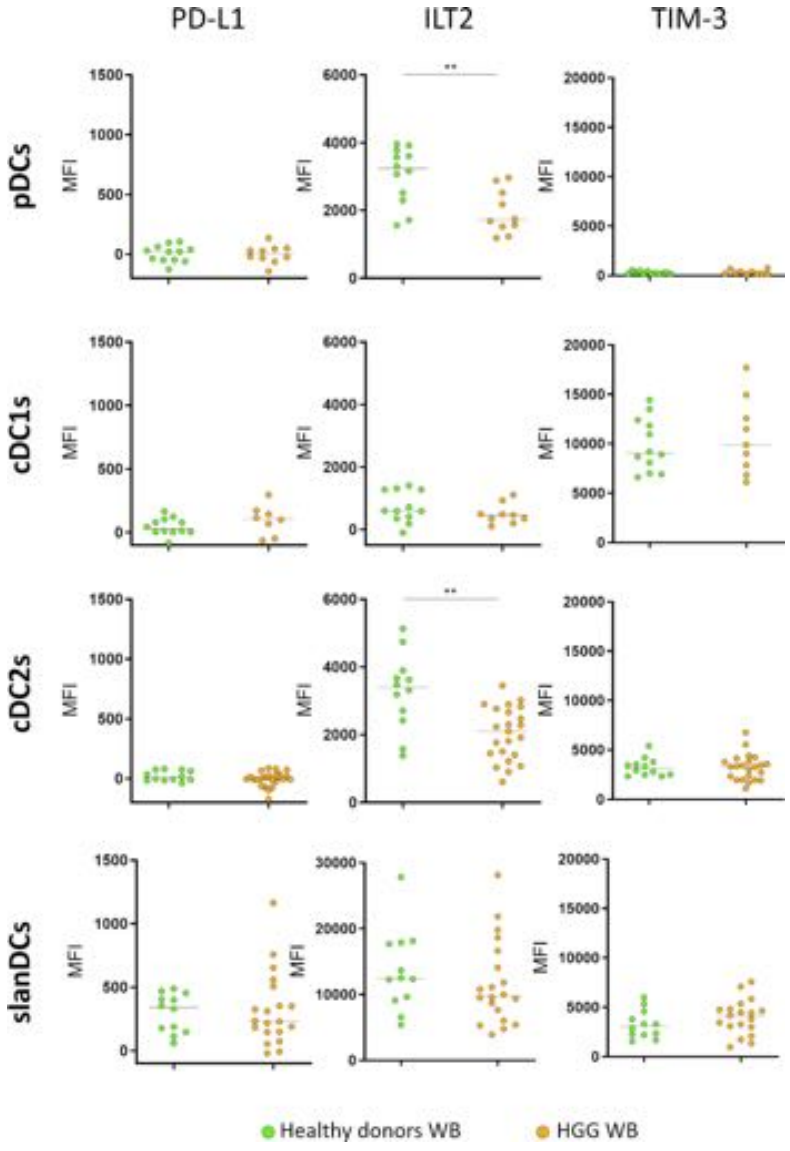

Figure 16. *Surface expression of inhibitory molecules on DC subsets from whole blood of healthy donors (green circles, n =12) and HGG patients (orange circles, n= 23). The expression levels of the inhibitory molecules PD-L1, ILT2, and TIM-3 were assessed on pDCs, cDC1s, cDC2s, and slanDCs, and expressed as Mean Fluorescence Intensity (MFI). Each symbol represents a single sample. In each series, the median is also shown. *p < 0.05, **p < 0.01. Statistical significance calculated using the Mann-Whitney U test.*

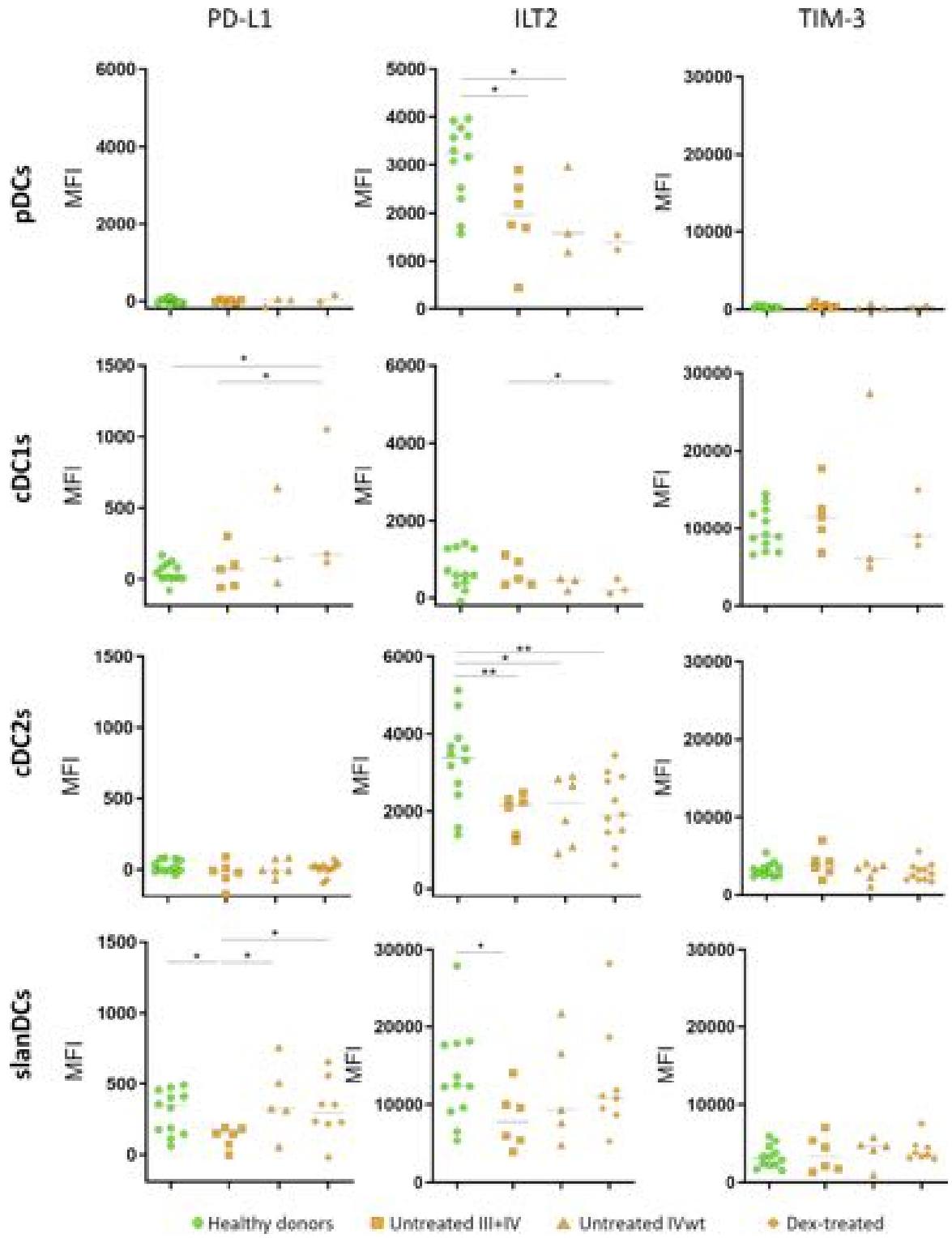

Figure 17. *Surface expression of inhibitory molecules on DC subsets from whole blood of healthy donors (green circles, n =12) and HGG patients stratified based on histopathological/molecular features and corticosteroid treatment (orange squares, "untreated III+IVmut", n = 6; orange triangles, "untreated IVwt", n = 6; orange diamonds, "dex-treated", n = 11). The expression levels of the inhibitory molecules PD-L1, ILT2 and TIM-3 were assessed on pDCs, cDC1s, cDC2s, and slanDCs, and expressed as Mean Fluorescence Intensity (MFI). Each symbol represents a single sample. In each series, the median is also shown. *p < 0.05, **p < 0.01. Statistical significance calculated using the Mann-Whitney U test.*

4.1.3 Flow-cytometry characterization of DC subsets in healthy and tumour brain tissue obtained from HGG patients

In order to investigate the ability of DCs and their subsets to infiltrate the tumour in HHG patients, we applied the same 18-color flow cytometry panel used for peripheral blood DC characterization to the analysis of the mononuclear cells obtained from 10 tumour tissue samples resected from the central core of the pathological lesions of HGG patients. Three healthy brain tissue samples obtained from HGG patients from a macroscopically disease-free area distal from the tumour were also included, as controls. As observed in (Figure 18), the presence of any subsets of DC-lineage and inflammatory DCs was negligible in healthy brain parenchyma. However, a significant increase in the frequency of all myeloid DC subsets, including cDC1s, cDC2s, slanDCs and moDCs, was observed in the tumour samples, indicating that all these DC subsets are able to infiltrate HGG lesions. Notably, pDCs were observed only in 2 tumour samples, whereas they were negligible in the vast majority of HGG lesions.

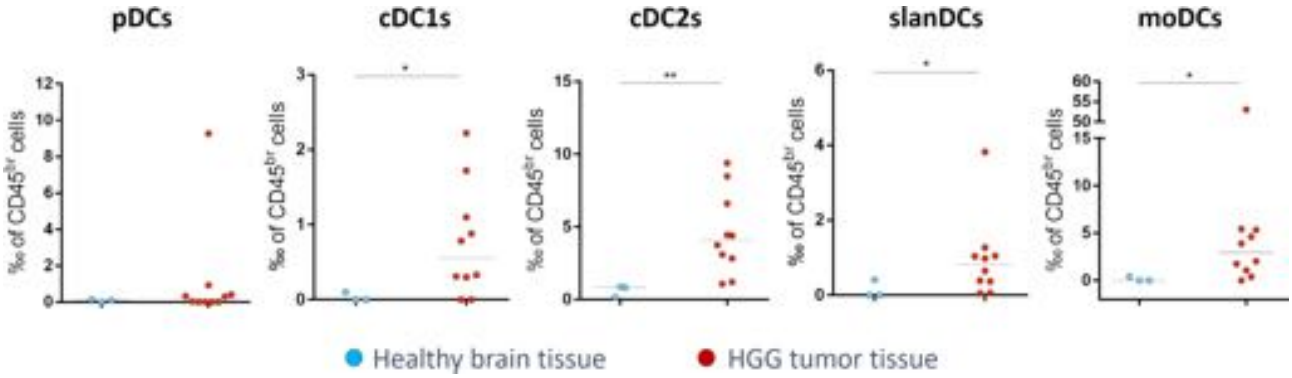

Figure 18. *The frequency of DC subsets in healthy tissues (light blue circles, n = 3) and tumor tissues (red circles, n = 10) obtained from HGG patients, was expressed as per-thousand (‰) of CD45-bright cells. Each symbol represents a single sample. In each series, the median is also shown. *p < 0.05, **p < 0.01. Statistical significance calculated using the Mann-Whitney U test.*

We further analysed the frequency of tumour-infiltrating DC subsets in HGG patients stratified according to HGG histopathological/molecular features and corticosteroid treatment. As shown in (Figure 19), we observed that all myeloid tumour-infiltrating DC subsets were significantly higher than HDs in the group of "untreated IVwt", but not in "untreated III+IVmut" patients, likely suggesting that a higher number of myeloid DCs is recruited into the tumour site of the most severe HGG type. Moreover, the analysis of cDC1s, which are mostly involved in the activation of anti-tumoral cytotoxic T cell responses, showed a significantly lower frequency of tumour-infiltrating cDC1s in the group of "dex-treated" patients, indicating that corticosteroid treatment affects the ability of cDC1s to infiltrate the tumour. As shown in the same figure, a similar trend was observed when analysing the other myeloid DC subsets.

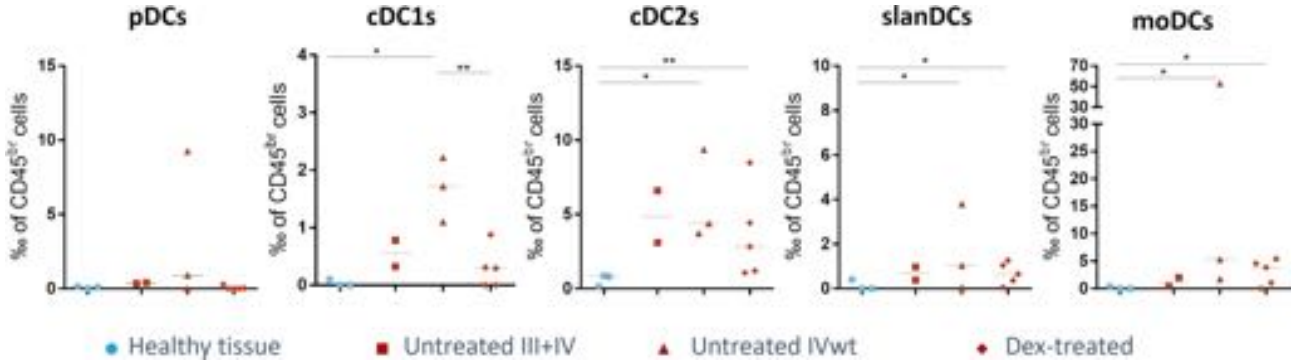

Figure 19. *The frequency of DC subsets in healthy tissues (light blue circles, n = 3) and tumor tissues from HGG patients stratified based on histopathological/molecular features and corticosteroid treatment (red squares, "untreated III+IVmut", n = 2; red triangles, "untreated IVwt", n = 3; red diamonds, "dex-treated", n = 5)was expressed as per-mille (‰) of CD45 bright cells. Each symbol represents a single sample. In each series, the median is also shown. *p < 0.05, **p < 0.01. Statistical significance calculated using the Mann-Whitney U test.*

4.1.4 Phenotype of DC subsets in tumour brain tissues obtained from HGG patients

Given the lack of DCs in healthy brain tissues, it was not possible to compare the phenotype of tissue-infiltrating DC subsets between healthy and tumour tissues. We could just investigate possible changes in the state of activation of DCs in HGG patients stratified according to tumour histopathological/molecular features and corticosteroid treatment, assessing the expression of the activation markers CD40, CD80, CD86, HLA-DR, and the immune checkpoints PD-L1, ILT2 and TIM-3. As shown in (Figure 20), we did not observe any consistent differences in the expression of costimulatory molecules and HLA-DR, just a significant decrease of CD40 in cDC2s between "dex-treated" and "untreated IVwt" patients. As regards inhibitory molecules, we just observed a slight increase in the expression of PD-L1 in tumour-infiltrating cDC2s and moDCs in the group of "dex-treated" patients compared with the group of "untreated IVwt" patients and a slight increase of both PD-L1 and ILT2 in cDC1s either in "dex-treated" patients compared with "untreated IVwt" patients and in "untreated IVwt" patients compared with "untreated III+IVmut" patients (Figure 21). This modest increase of inhibitory molecules could support the immunosuppressive role that GME exert on infiltrating DCs, however, given the exiguity of tumoral samples, these data needed further confirmations.

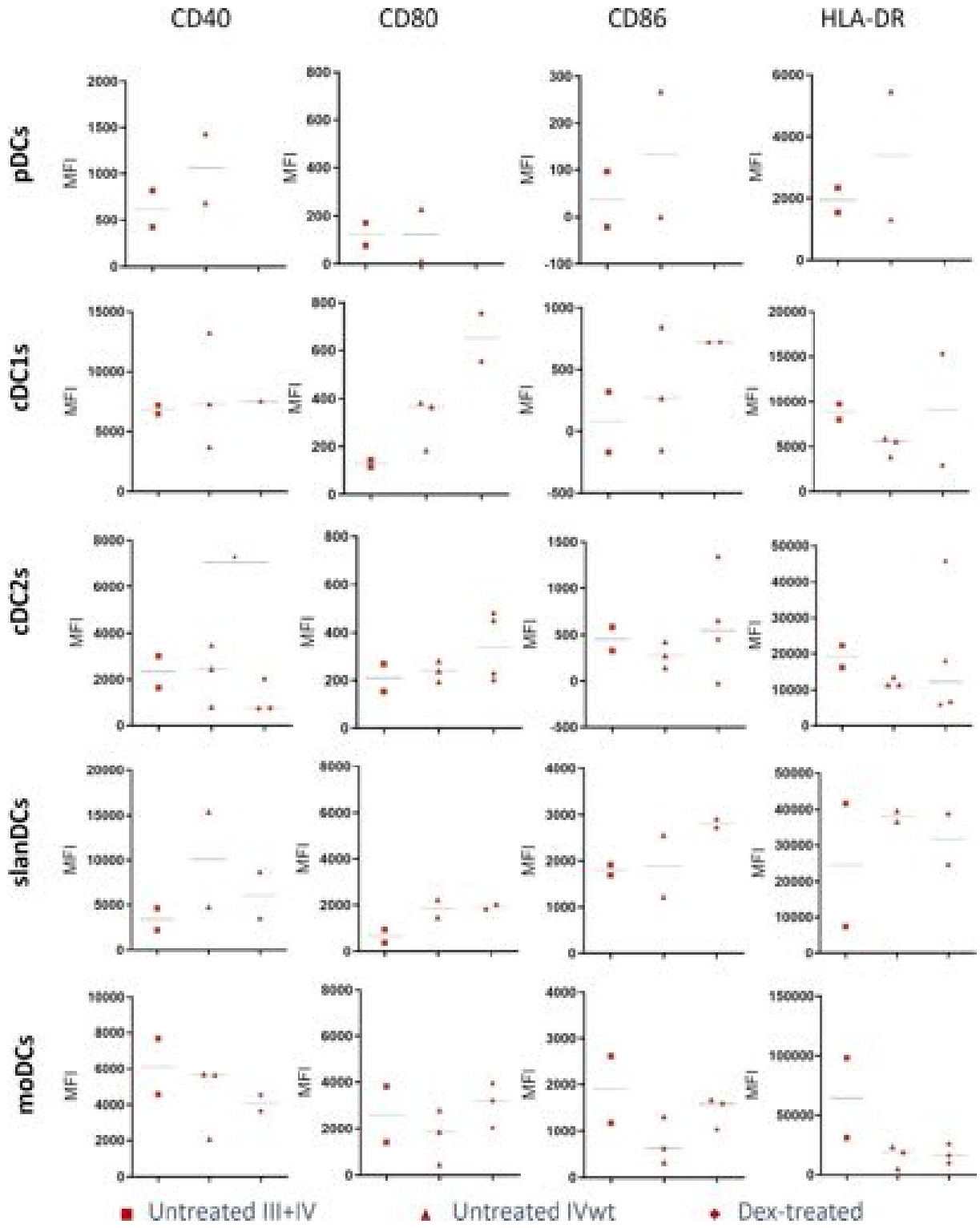

Figure 20. *Surface expression of the activation markers CD40, CD80, CD86 and HLA-DR on DC subsets from tumour samples of HGG patients stratified based on histopathological/molecular features and corticosteroid treatment (red squares, "untreated III+IVmut", n = 2; red triangles, "untreated IVwt", n = 3; red diamonds, "dex-treated", n = 5). The expression levels of the activation molecules were assessed on pDCs, cDC1s, cDC2s, slanDCs, and moDCs, and expressed as Mean Fluorescence Intensity (MFI). Each symbol represents a single sample. Samples with less than 5 events in DC subsets were not included. In each series, the median is also shown. *p < 0.05. Statistical significance calculated using the Mann-Whitney U test.*

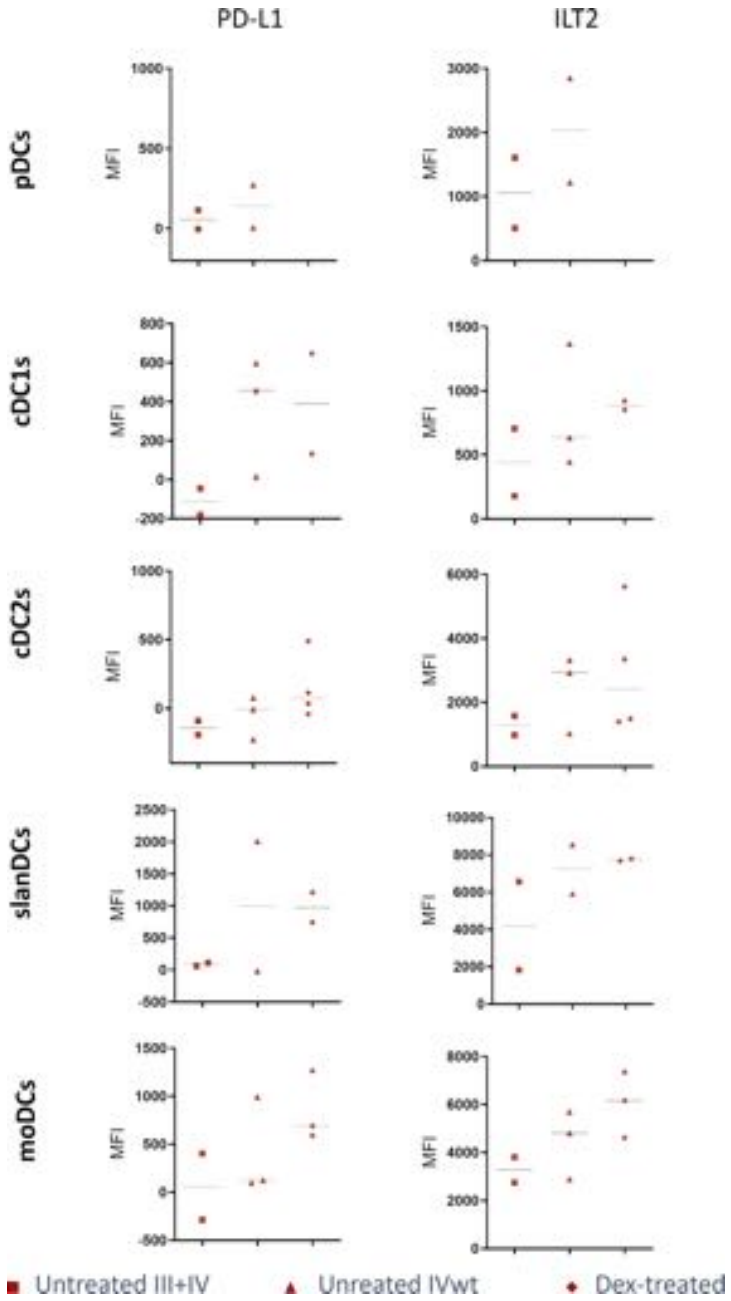

Figure 21. *Surface expression of the inhibitory markers PD-L1 and ILT2 on DC subsets from tumour samples of HGG patients stratified based on histopathological/molecular features and corticosteroid treatment (red squares, "untreated III+IVmut", n = 2; red triangles, "untreated IVwt", n = 3; red diamonds, "dex-treated", n = 5). The expression levels of the inhibitory molecules were assessed on pDCs, cDC1s, cDC2s, slanDCs and moDCs, and expressed as Mean Fluorescence Intensity (MFI). Each symbol represents a single sample. Samples with less than 5 events in DC subsets were not included. In each series, the median is also shown. Statistical significance calculated using the Mann-Whitney U test.*

As regards the TIM-3 expression on DC subsets in tumoral samples, we were not able to evaluate it, for a technical artifact caused by the enzymatic digestion of tissues with collagenase IV. Indeed, as discussed by us in a recent work, and more in detailed in the next section, collagenase IV is able to cut the extracellular domain of TIM-3 protein, causing an unreliable detection of this marker in flow-cytometry (Carenza et al., 2020).

4.1.4.1 Effects of type IV collagenase treatment on TIM-3 expression

Tumour tissues often have to be treated with an enzymatic digestion in order to easily release tumour-infiltrating cells from the tissue structure. By the analysis of these tumour tissues we observed an unexpected low expression of TIM-3 on all subsets of TADCs. A high expression of TIM-3 on the surface of myeloid TADCs has been reported in some human cancers (Chiba et al., 2012; de Mingo Pulido et al., 2018), but most human cancer types remain so far poorly investigated. The observed low expression of TIM-3 on TADCs finds an explanation in the fact that type IV collagenase, the enzyme used for tissue processing, is a protease with a specificity for the X-Gly bond in the sequence R-Pro-(X Gly Pro), where X is most frequently a neutral amino acid (Wood, 1996). By using the protein database of National Center for Biotechnology Information (NCBI), we observed that the cutting site of type IV collagenase was indeed in the extracellular region of the amino acidic sequence of TIM-3, explaining the observed reduction of TIM-3 in tissues treated with type IV collagenase compared with tissues only mechanically processed (Figure 22A). In order to investigate whether in our experimental setting the treatment with type IV collagenase could be responsible for a reduction in TIM-3 expression, we assessed the expression of TIM-3, by using our 18-colour flow-cytometry panel, in peripheral blood of a HD, treated or not treated with Type IV collagenase at a final concentration of 1.6 mg/mL, for 1 hour at 37°C. As shown in Figure 22B we observed, indeed, that TIM-3 expression was downregulated on both cDC subsets by collagenase treatment on peripheral blood DCs.

Afterward, we evaluated possible differences in the processing of the same tumour tissue with either enzymatic (using type IV collagenase) or mechanical dissociation. Applying the same 18-colour flow-cytometry panel, we observed the reduction of TIM-3 expression for both cDC subsets in the tissue digested with type IV collagenase compared with the same tissue processed with mechanical dissociation (Figure 22C).

These data support hypothesis that the low expression of TIM-3 expressed on TADCS of tumor samples digested with Collagenase IV had likely to be ascribed to a technical artifact and suggest the need for a careful setup of all experimental conditions, including the preanalytical phase, when planning the flow cytometric analysis of TADCs.

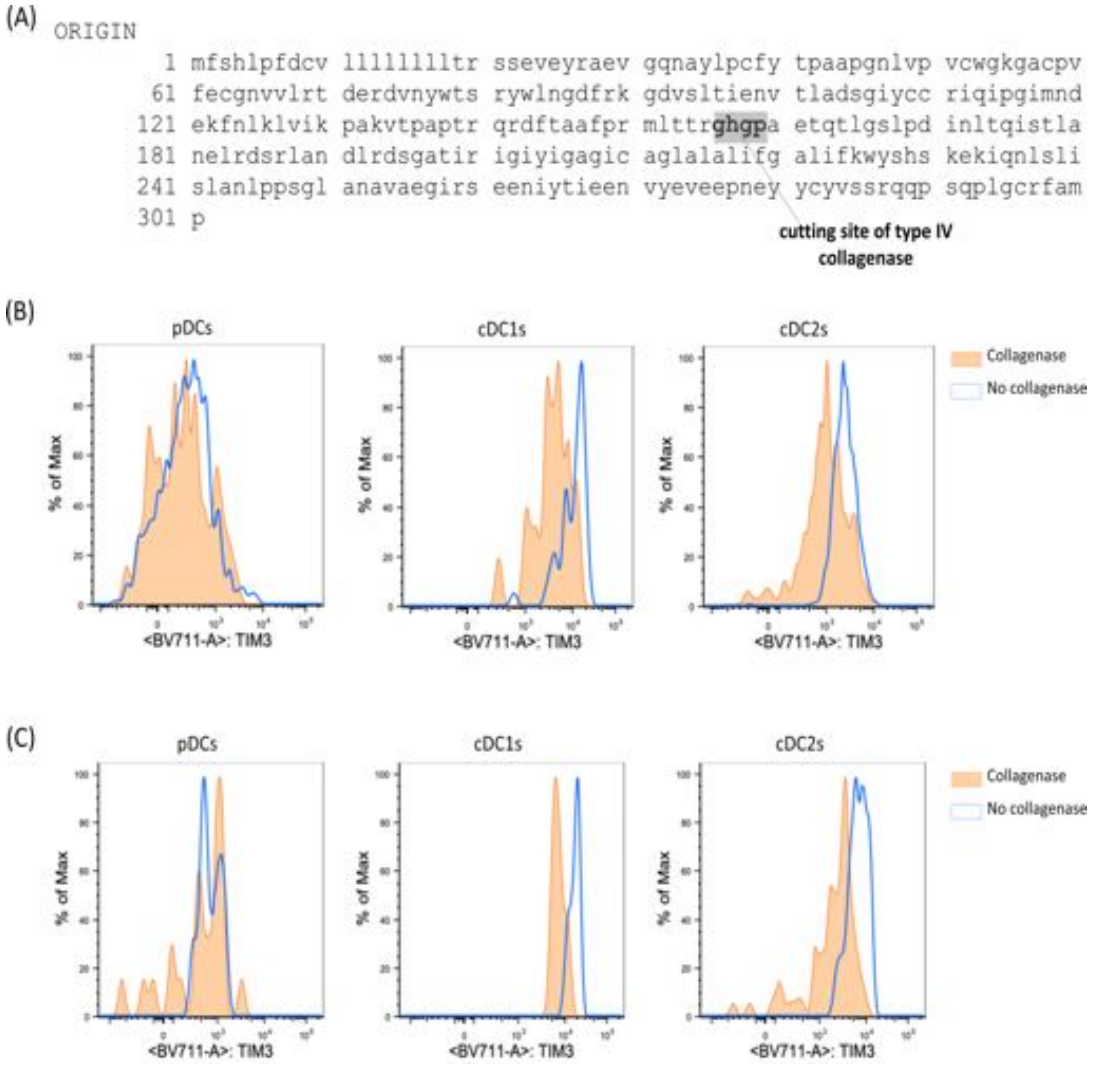

Figure 22. *Effects of incubation with Collagenase type IV on TIM-3 detection by flow cytometry. (A) Protein sequence of TIM-3 and highlighting of the cutting site of collagenase, located in the extracellular portion of the molecule and thus supporting the possibility of TIM-3 cleavage upon collagenase treatment. Comparison of TIM-3 detection on pDCs, cDC1s and cDC2s obtained from (B) whole blood or (C) tumour tissue treated (orange shaded) or not treated (empty) with Collagenase type IV for 1 h. In both cases, the reduction of TIM-3 detection on cDC subsets after incubation with collagenase is evident (adapted from Carenza et al., 2020).*

4.1.5 Visualisation of flow cytometric data by UMAP

In order to visualize the high-dimensional results obtained by flow cytometry, we further analysed our flow cytometric data by using the Uniform Manifold Approximation and Projection (UMAP) algorithm. It is an unsupervised clustering algorithm that allows to reduce the dimensionality of complex data and visualize them in a two-dimension space, evaluating, at single cell level, differences/similarities of marker expression. Data acquired in the gate of viable $CD45^+/lin^-/HLA\text{-}DR^+$ cells, obtained from all the files of peripheral blood and tissue samples of healthy donors and HGG patients were concatenated and displayed in a single UMAP dot plot. In order to improve clarity of visualization and computational time, down-sampled files were used. The UMAP algorithm, on the basis of MFI values of different markers expressed by cells (CD45, CD14, CD16, HLA-DR,

CD11c, CD123, CD141, CD1c, M-DC8, CD1a, costimulatory molecules and immune checkpoints), allowed us to calculate reciprocal interactions among cells, connecting similar cells each other in the same cluster. In the UMAP space also distances among clusters are worthy because similar clusters localize closer than dissimilar ones. Then, we investigated whether DC subsets identified by manual gating strategy had a geographical match with specific clusters within the UMAP generated in an unsupervised manner by the algorithm.

4.1.5.1 Comparison of circulating DCs from HGG patients and HDs using UMAP analysis

By mapping on the UMAP dot plot the MFI of specific markers used in the manual gating strategy for the identification of different DC subset in the blood, we observed that the signal intensity of each marker (CD123 for pDCs, CD141 for cDC1s, CD1c for cDC2s and M-DC8 for slanDCs) localised in a precise area of the UMAP plot, suggesting that in an unsupervised manner, the algorithm clustered together DCs of the same subset. This was true both for whole blood of HDs and HGG patients (Figure 23A and B; Figure 24A and B; Figure 25A and B; Figure 26A and B; Figure 27A and B; upper panels). Then, we evaluated where cells identified by manual gating strategy localised in the UMAP dot plot, and we confirmed that cells belonging to each specific DC subset co-localised in a specific cluster of the UMAP dot plot, corresponding to the area presenting the highest expression of the marker used to the identification of each specific DC subset (Figure 23A and B; Figure 24A and B; Figure 25A and B; Figure 26A and B; Figure 27A and B; lower panels). The observed correspondence strengthened and confirmed our manual gating strategy used to identify DC subsets in our 18-colour flow-cytometry panel.

Moreover, the comparison of UMAP plots representing whole blood samples obtained from HDs and HGG patients confirmed the decrease of DC-lineage DCs in the blood of patients (Figure 23A and B; Figure 24A and B; Figure 25A and B; Figure 26A and B; Figure 27A and B; lower panels). UMAP plots also confirmed the absence of moDCs in the peripheral blood of both patients and HDs. It was also possible to observe how all three subsets of DC-lineage DCs formed three distinct clusters close to each other, but distant from the cluster of slanDCs, thus supporting the different origin of inflammatory DCs. As regards the different expression of activation and inhibitory markers, we did not observed any differences neither in the cluster formation of different DC subsets and between HD and HGG patient samples (data not shown).

4.1.5.2 Identification of DC subsets in tumour tissues of HGG patients

By mapping on the UMAP dot plot the MFI of specific markers used in the manual gating strategy for the identification of different DC subset in tumour tissues, we observed that the signal intensity

of each marker (CD123 for pDCs, CD141 for cDC1s, CD1c for cDC2s, M-DC8 for slanDCs and CD1a for moDCs) localised in a precise area of the UMAP plot, suggesting that in an unsupervised manner, the algorithm clustered together DCs of the same subset. (Figure 23C; Figure 24C; Figure 25C; Figure 26C; Figure 27C; upper panels). Then, we evaluated where cells identified by manual gating strategy localised in the UMAP dot plot, and we confirmed that cells belonging to each specific DC subset co-localised in a specific cluster of the UMAP dot plot, corresponding to the area presenting the highest expression of the marker used to the identification of each specific DC subset (Figure 23C; Figure 24C; Figure 25C; Figure 26C; Figure 27C; lower panels). From the UMAP analysis of cells obtained from tumour tissues, we could confirm that all DC-lineage and inflammatory DC subsets were present in the GME and that they localised in the same geographical area where we identified DC subsets in whole blood of HDs and HGG patients. In particular, as shown in figure 27C, we could confirm the presence of moDCs, which were absent in the peripheral blood. We also observed that cDC2s in tumour tissue was split into 2 different clusters within the UMAP: one in the same position of the cDC2 cluster observed in whole blood, and another one localised in a different position of the UMAP plot, closer to the moDC cluster, suggesting that a subpopulation of cDC2s may acquire a different phenotype within the tumour context (Figure 27C). For this reason, we wonder whether there were differences in the expression of activation and inhibitory markers among the two clusters of cDC2s (namely "cDC2_1", the cluster localised in the same position of cDC2s in peripheral blood, and "cDC2_2", the cluster localised closer to the moDC cluster). As shown in figure 29, cDC2_2 cluster presented a more pronounced inflammatory phenotype, as indicated by the increased expression of HLA-DR, CD40 and ILT2, compared with the cluster of cDC2s more related to peripheral blood cDC2s suggesting that cDC2s could assume different phenotype in the tumour context.

The comparison of tumour infiltrating DCs with those present in healthy brain tissue was not possible because of the absence of DCs in healthy brain parenchyma.

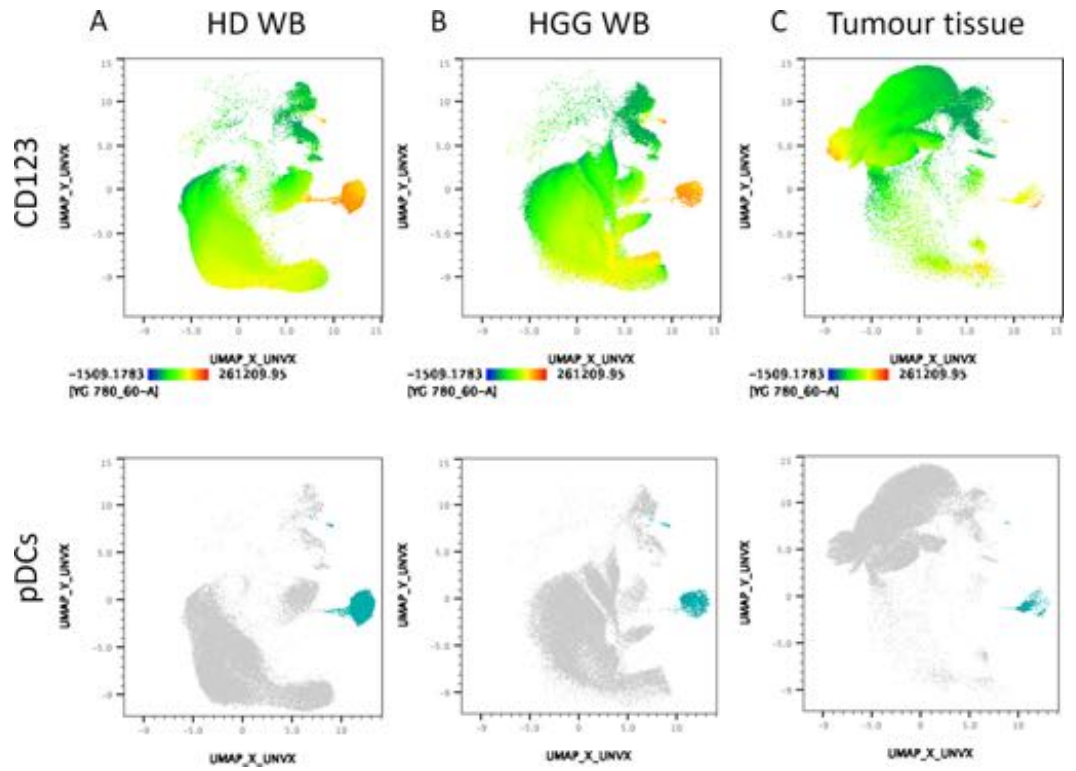

Figure 23. *UMAP plots showing the clustering of DC subsets in whole blood of healthy donors (A) and HGG patients (B) and in tumour tissue (C). Upper panels showing the expression of CD123 in the unsupervised clustering of UMAP. Lower panels showing pDCs as identified with manual gating strategy. Viable CD45$^+$/lin$^-$/HLA-DR$^+$ cells obtained from all samples of healthy donors and patients were down-sampled and concatenated (shown in gray in lower panel). pDCs are highlighted in dark turquoise.*

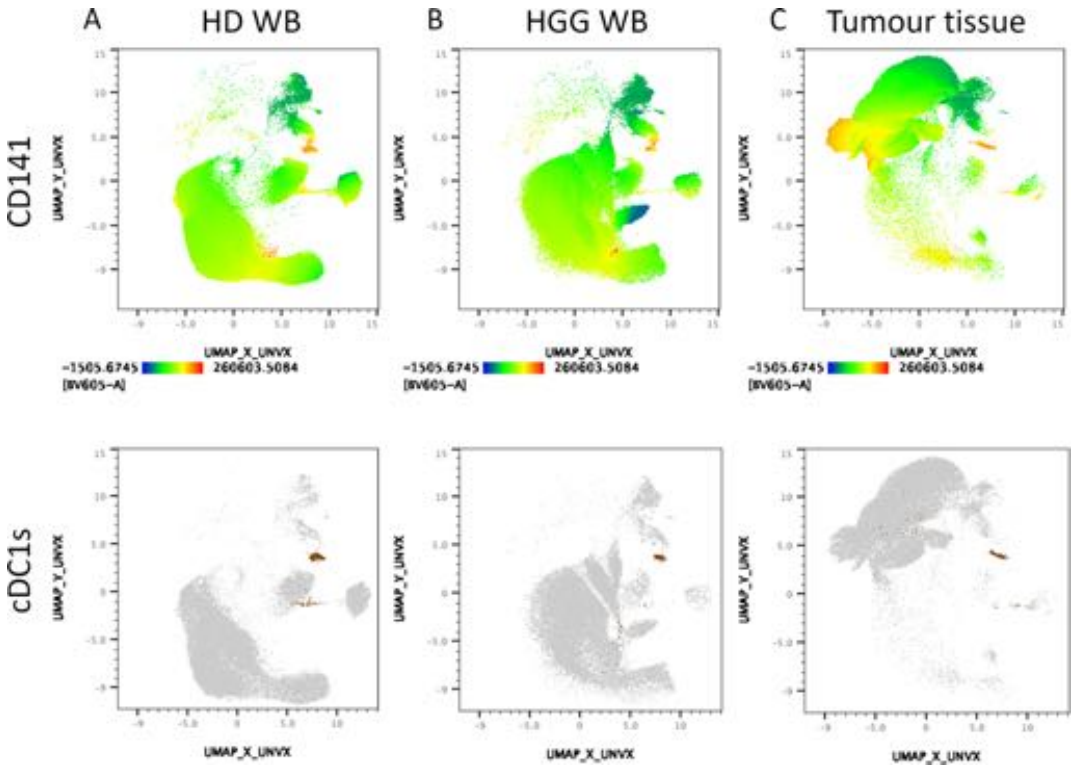

Figure 24. *UMAP plots showing the clustering of DC subsets in whole blood of healthy donors (A) and HGG patients (B) and in tumour tissue (C). Upper panels showing the expression of CD141 in the unsupervised*

clustering of UMAP. Lower panels showing cDC1s as identified with manual gating strategy. Viable CD45^{+}/lin^{-}/HLA-DR^{+} cells obtained from all samples of healthy donors and patients were down-sampled and concatenated (shown in gray in lower panel). cDC1s are highlighted in brown.

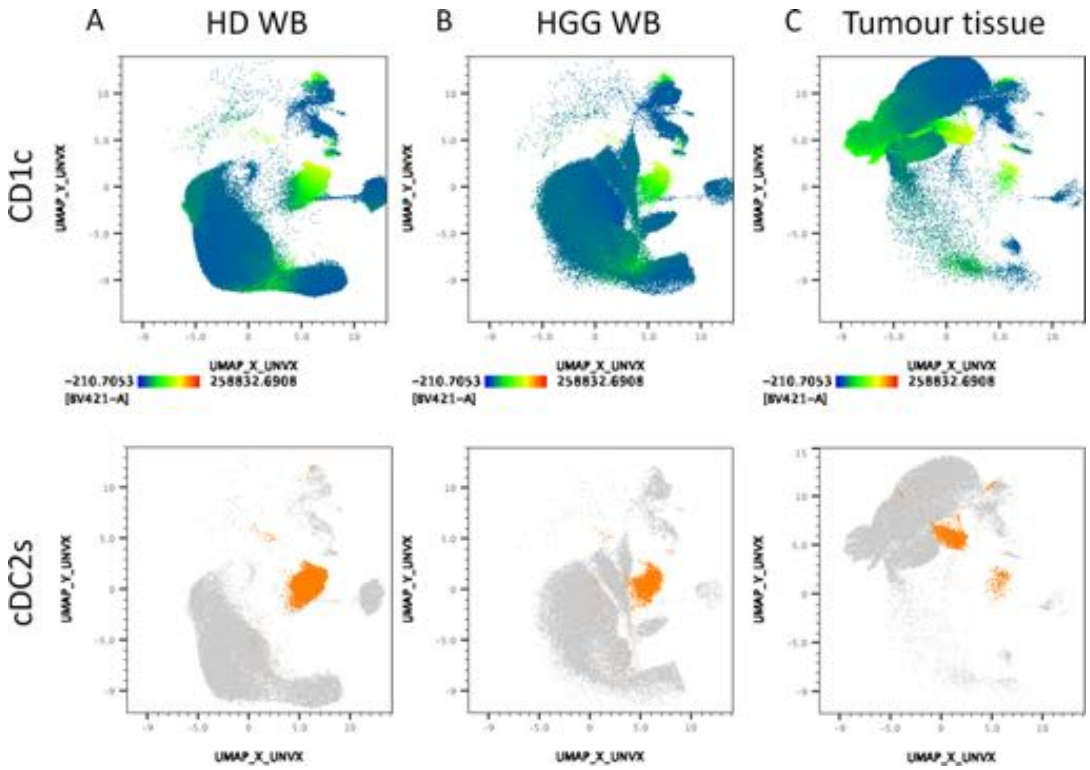

Figure 25. *UMAP plots showing the clustering of DC subsets in whole blood of healthy donors (A) and HGG patients (B) and in tumour tissue (C). Upper panels showing the expression of CD1c in the unsupervised clustering of UMAP. Lower panels showing cDC2s as identified with manual gating strategy. Viable CD45^{+}/lin^{-}/HLA-DR^{+} cells obtained from all samples of healthy donors and patients were down-sampled and concatenated (shown in gray in lower panel). cDC2s are highlighted in orange.*

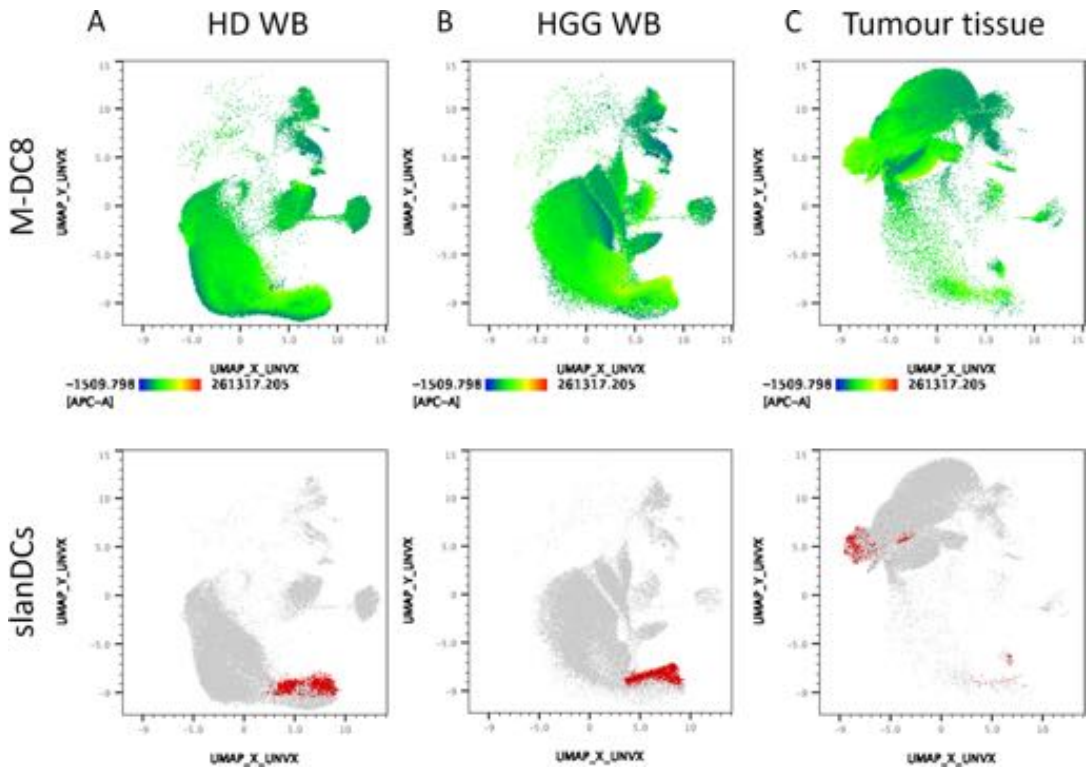

Figure 26. *UMAP plots showing the clustering of DC subsets in whole blood of healthy donors (A) and HGG patients (B) and in tumour tissue (C). Upper panels showing the expression of M-DC8 in the unsupervised clustering of UMAP. Lower panels showing slanDCs as identified with manual gating strategy. Viable CD45$^+$/lin$^-$/HLA-DR$^+$ cells obtained from all samples of healthy donors and patients were down-sampled and concatenated (shown in gray in lower panel). slanDCs are highlighted in red.*

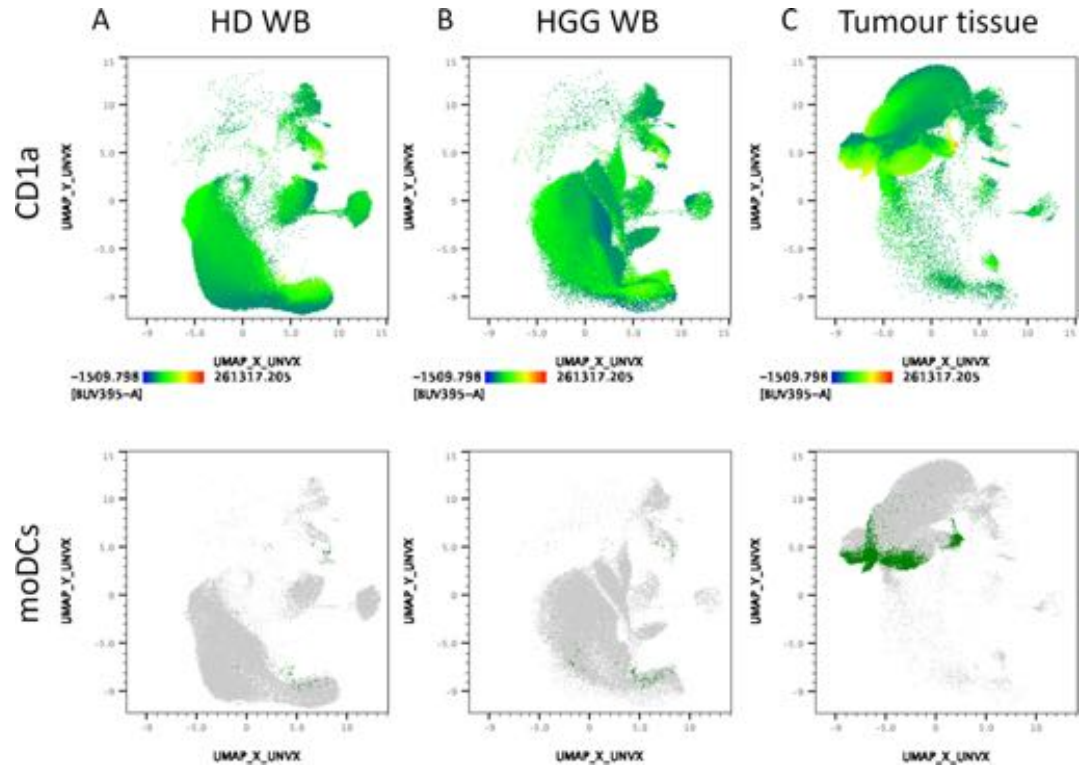

Figure 27. *UMAP plots showing the clustering of DC subsets in whole blood of healthy donors (A) and HGG patients (B) and in tumour tissue (C). Upper panels showing the expression of CD1a in the unsupervised*

clustering of UMAP. Lower panels showing moDCs as identified with manual gating strategy. Viable CD45^{+}/lin^{-}/HLA-DR^{+} cells obtained from all samples of healthy donors and patients were down-sampled and concatenated (shown in gray in lower panel). moDCs are highlighted in green.

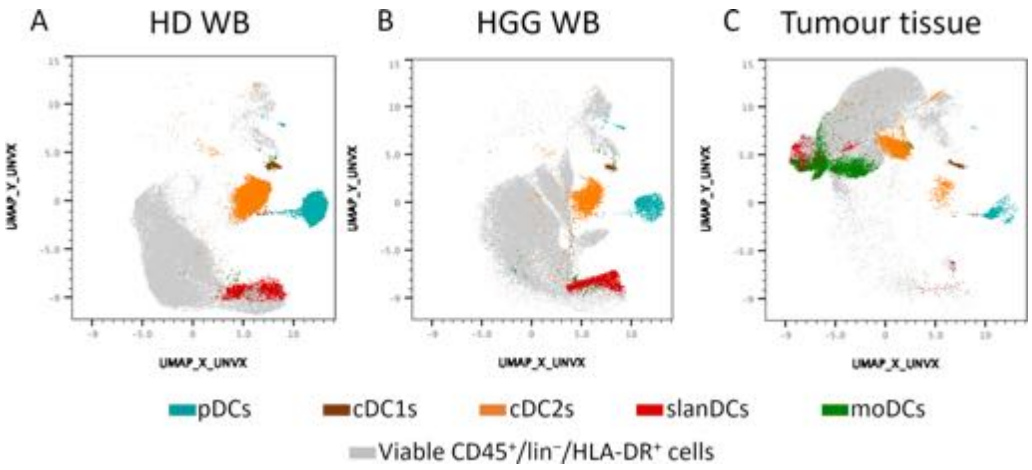

Figure 28. *UMAP plots showing the clustering of DC subsets in whole blood of HDs (A) and HGG patients (B) and in tumour tissue (C) deriving from manual gating strategy and visualized on unsupervised UMAP dot plots. Viable CD45^{+}/lin^{-}/HLA-DR^{+} cells obtained from all samples of healthy donors and patients were down-sampled and concatenated (shown in gray). Colour code as indicated showing different DC subsets.*

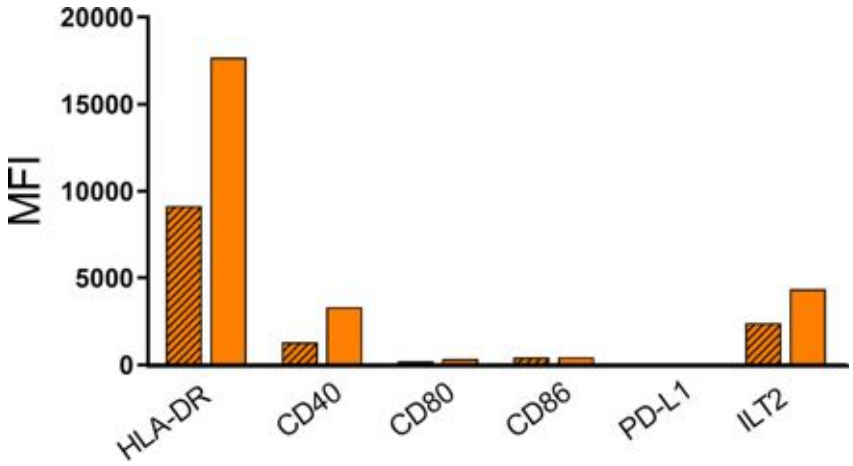

Figure 29. *The expression of HLA-DR, activatory molecules (CD40, CD80, CD86), and inhibitory molecules (PD-L1, ILT2, and TIM-3) was assessed on cDC2_1 cluster (orange angled line bars) and cDC2_2 cluster (orange bars). Data expressed as MFI measured on concatenated files from all tumour samples.*

4.2 Single cell RNA sequencing

In order to further characterise tumour-infiltrating DCs in HGG and validate flow cytometric data concerning the presence of DC subsets in the tumour tissue, single-cell RNA sequencing (scRNAseq) experiments were performed, in collaboration with the Unit of Leukocyte Biology at Humanitas Research Hospital. scRNAseq experiments were performed on 7 tumoral samples and 2 healthy tissue samples derived from 8 different HGG patients. Because of the scarcity of the immune infiltrate in

GME, we performed scRNAseq on CD45$^+$-enriched cells, in order to enrich the immune component. To this aim, we sorted CD45$^+$ and CD45$^-$ cells, and mixed CD45$^+$ sorted cells with a fixed and limited quota (10% in volume) of CD45$^-$ cells, which are mainly composed of parenchymal and tumour cells. These cell preparations were then barcoded and sequenced.

By using the R package "Seurat", the first step of analysis, performed on 39,468 cells which included both CD45$^+$ and CD45$^-$ cells, led to the identification of 33 clusters of immune infiltrating and tumoral cells at resolution 2, as shown in figure 30, of which clusters 15, 16, 17, 23, 25 and 27 were formed by only CD45$^-$ cells, and the others by CD45$^+$ cells.

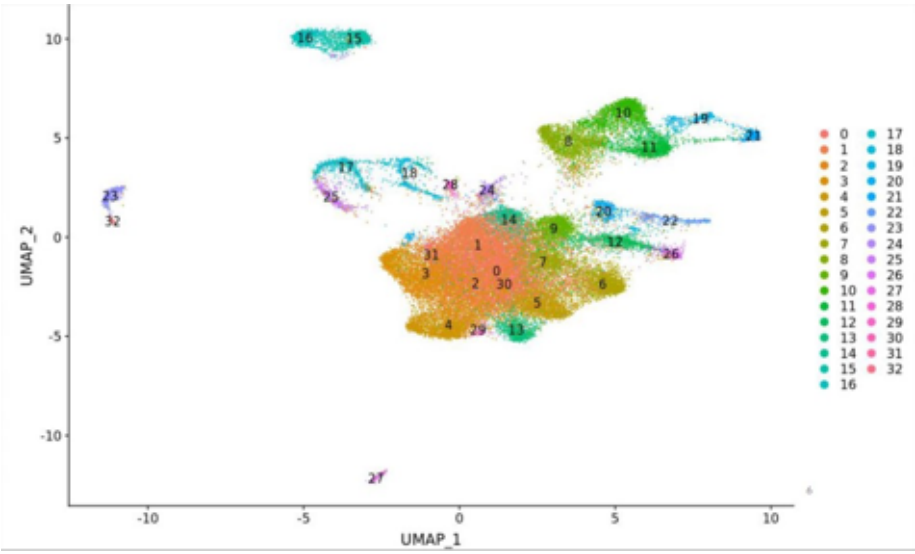

Figure 30. *UMAP visualization of 39,468 cells CD45$^+$ and CD45$^-$ cells from 7 tumor tissues and 2 healthy tissues of 8 HGG patients. Colors indicate unsupervised clustering. Clusters 15, 16, 17, 23, 25 and 27 are those formed by only CD45$^-$ cells; the others by CD45$^+$ cells.*

4.2.1 Identification of DC cluster

The second step of the analysis was performed on 36,237, restricted to CD45$^+$ cells in order to focus the investigation only on immune infiltrating cells, and it led to the identification of 28 sub-clusters (Figure 31). In order to identify different immune cells among the 28 clusters, we used SingleR, an automatic annotation method for scRNAseq data. However, SingleR using different databases for annotation of human cells, like Human Primary Cell Atlas (HPCA) and others (Monaco Immune Data, Novershtern Hematopoietic Data), failed to identify a reliable cluster of DCs, likely because these databases are based on datasets deriving from literature data of bulk sequencing and microarrays. Moreover, DCs are a rare population that lacks specific genes and shares many genes with other immune cells, making their identification difficult. In order to overcome this issue, we proceeded with a manual annotation based on literature data obtained by scRNAseq analyses of sorted DC subsets (Breton et al., 2016; Collin & Bigley, 2018; Villani et al., 2017).

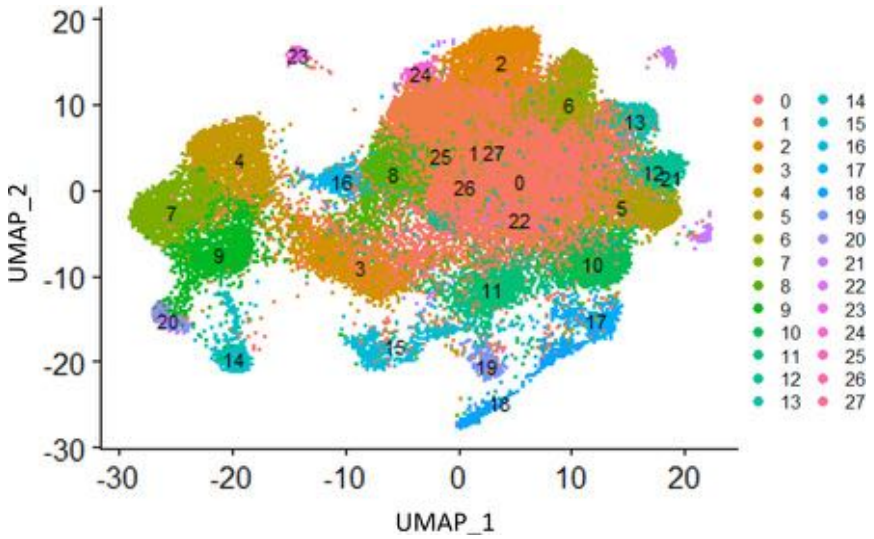

Figure 31. *UMAP visualization of 36,237 CD45⁺ cells from 7 tumor tissues and 2 healthy tissues of 8 HGG patients. Colors indicate unsupervised clustering.*

In particular, we applied to our geneset the gene signature reporting the top markers of different DC subsets identified by Villani and colleagues (Villani *et al.,* 2017). As shown in Figure 32, cluster 19 was characterized by the highest expression of the applied signature, in particular some DC-specific genes (namely, CD1C, FCER1A, CLEC10A, CD1D), compared with other clusters. On this basis, we speculated that cluster 19 may contain DCs.

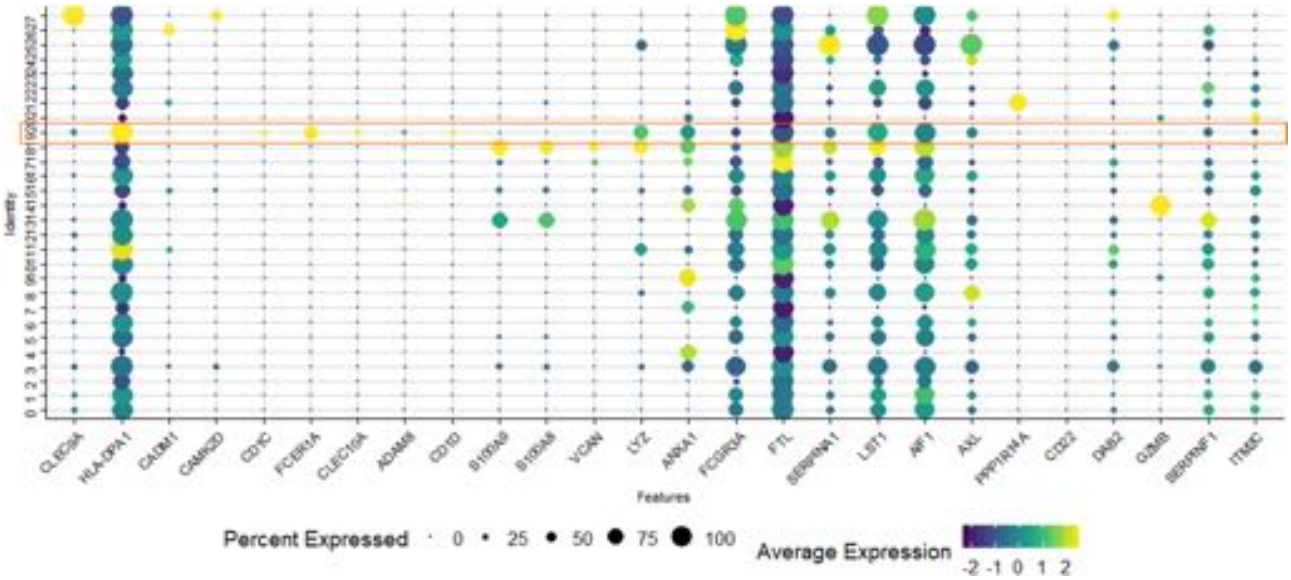

Figure 32. *Dot plot showing the expression level, indicated by the colour scale, and the percentage of positive cells, indicated by circles on the right of the panel, of top marker genes specific for DCs from Villani and colleagues (Villani et al., 2017). Cluster 19 was highlighted. Colour scale indicates the average expression level of genes; the size of dots indicates the percentage of positive cells for each gene.*

To confirm the DC annotation of cluster 19, we applied further analytical strategies. Firstly, we calculated differentially expressed genes (DEGs) between cluster 19 and the other clusters, and

obtained a signature of 56 specific genes for cluster 19 (p-value adjusted < 0.05, $log_2FC > 0.58$) that is represented in the dot plot shown in Figure 33.

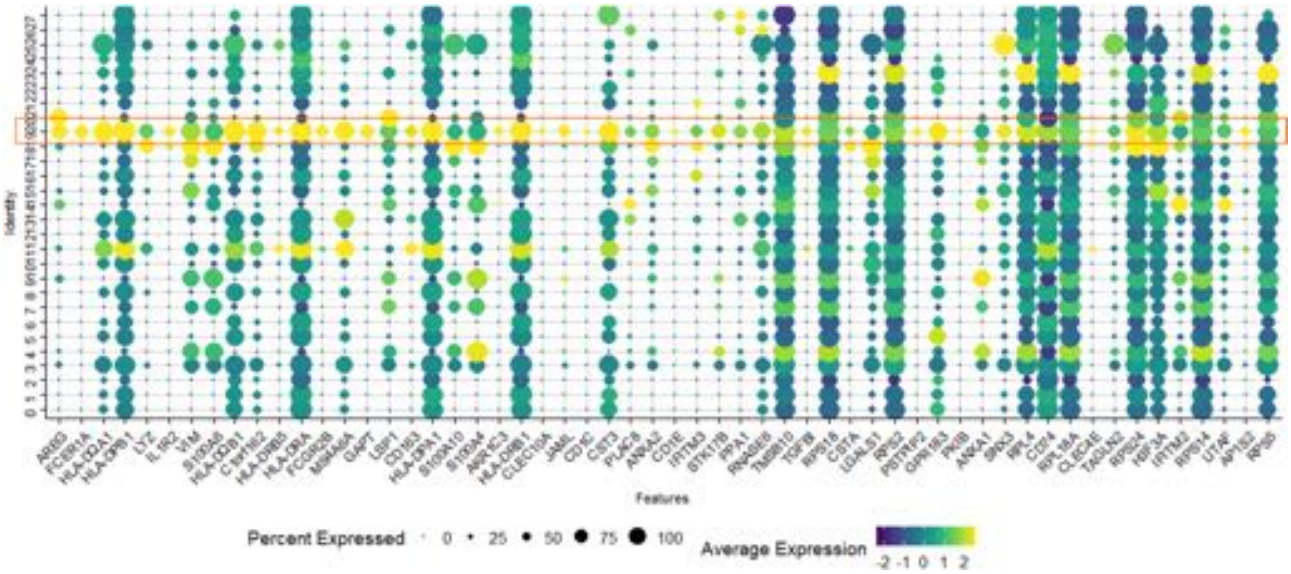

Figure 33. *Dot plot showing the expression level, indicated by the colour scale, and the percentage of positive cells, indicated by circles on the bottom of the panel, of DEGs between cluster 19 and other clusters (n=56 genes, $log_2FC > 0.58$ and p-value adjusted < 0.05). Cluster 19 was highlighted. Colour scale indicates the average expression level of genes; the size of dots indicates the percentage of positive cells for each gene.*

Then, in order to compare this signature among different clusters, we applied in R the "Add Module Score Function" that allows to assess whether a set of genes of interest is overall more expressed in a cluster compared with the general mean of expression in the other clusters. By applying this strategy, we demonstrated that cluster 19 was indeed characterised by an overall higher expression of the virtual signature composed of those 56 genes, as shown in the violin plot reported in Figure 34.

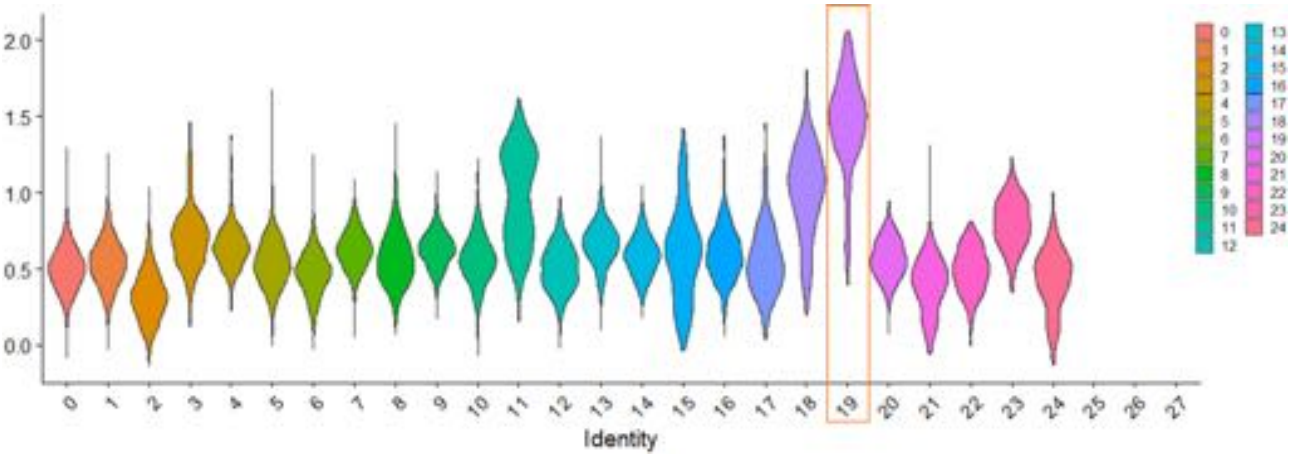

Figure 34. *Violin plots showing the expression level of the overall gene signature specific for cluster 19 in all clusters, obtained with the Add Module Score Function. Cluster 19 is highlighted. The expression level of this signature for clusters 25, 26 and 27 was not available for the very low number of cells composing these three clusters.*

Finally, in order to investigate the genes that composed the identified signature, we took advantage of the Blood Atlas. This is part of The Human Protein Atlas program (v19.1), a database that contains transcriptomic and proteomic information about the circulating immune populations. In this database, we checked each of the 56 genes, and verified that the majority of them was characteristic of, or enriched in, DCs. In this way, we confirmed that cluster 19 was the cluster containing DCs. This finding validated our flow-cytometry data about the presence of infiltrating DCs in tumour samples of HGG patients.

After the step of cluster annotation, we performed the re-clustering of cluster 19, in order to investigate whether different DC subsets falled into different sub-clusters on the basis of their gene expression profile. According to the cluster tree obtained by using Clustree package of R and represented in Figure 35A, DCs formed from 3 to 5 different sub-clusters, depending on the resolution level. For our analyses we chose resolution 0.2 that allowed to appreciate three distinct sub-clusters, numbered from 0 to 2 with cluster 0 containing the highest number of cells (202 cells) followed by cluster 1 (71 cells) and 2 (16 cells) (Figure 35B).

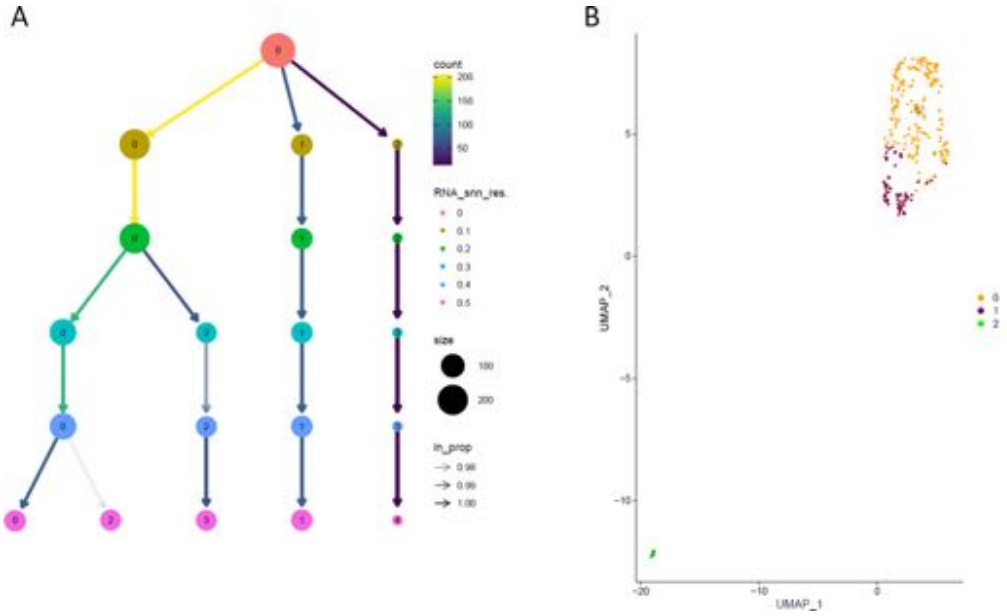

Figure 35. *(A) Cluster tree based on kk-means clustering of the DC cluster (cluster 19). Nodes colored according to the value of k, and sized according to the number of cells they represent. Edges are colored according to the number of cells (from blue representing few to yellow representing many). Cluster labels are randomly assigned by the kk-means algorithm. (B) UMAP representing the geographical position of cluster 0, 1 and 2, in which each dot represents a cell.*

In particular, from this analysis we confirmed that DCs are nearly absent in healthy parenchyma, according to the results obtained by flow-cytometry. Indeed, of the two healthy samples analysed, one was constituted by only 5 cells, spread between cluster 0 and 1; the other sample was composed of 16 cells that formed cluster 2. Because this second sample was superficial and difficult to cut with

the scalpel, we hypothesised that DCs from this sample could derive from meningeal contamination rather than from brain parenchyma. On this basis, we decided to exclude cluster 2 from the next steps of analysis.

Focusing our analysis on cluster 0 and 1, in order to investigate whether the different clusters reflected the division in DC subsets, we analysed the expression of transcription factors and genes that from the literature are known to be characteristic of/enriched in different DC subsets (Breton et al., 2016; Collin & Bigley, 2018; van Leeuwen-Kerkhoff et al., 2017; Villani et al., 2017; Q. Zhang et al., 2019). As shown in Figure 36, we observed the expression of genes characterising all single DC subsets in both cluster 0 and cluster 1, thus confirming with an experimental approach different from flow-cytometry, that all subsets of DC-lineage DCs and inflammatory DCs were present in the tumor infiltrate. However, the expression of those characterizing genes was scattered between cluster 0 and 1, suggesting that the sub-clustering of cluster 19 did not reflect a cell clustering based on DC ontogenesis, but it could be driven by other factors.

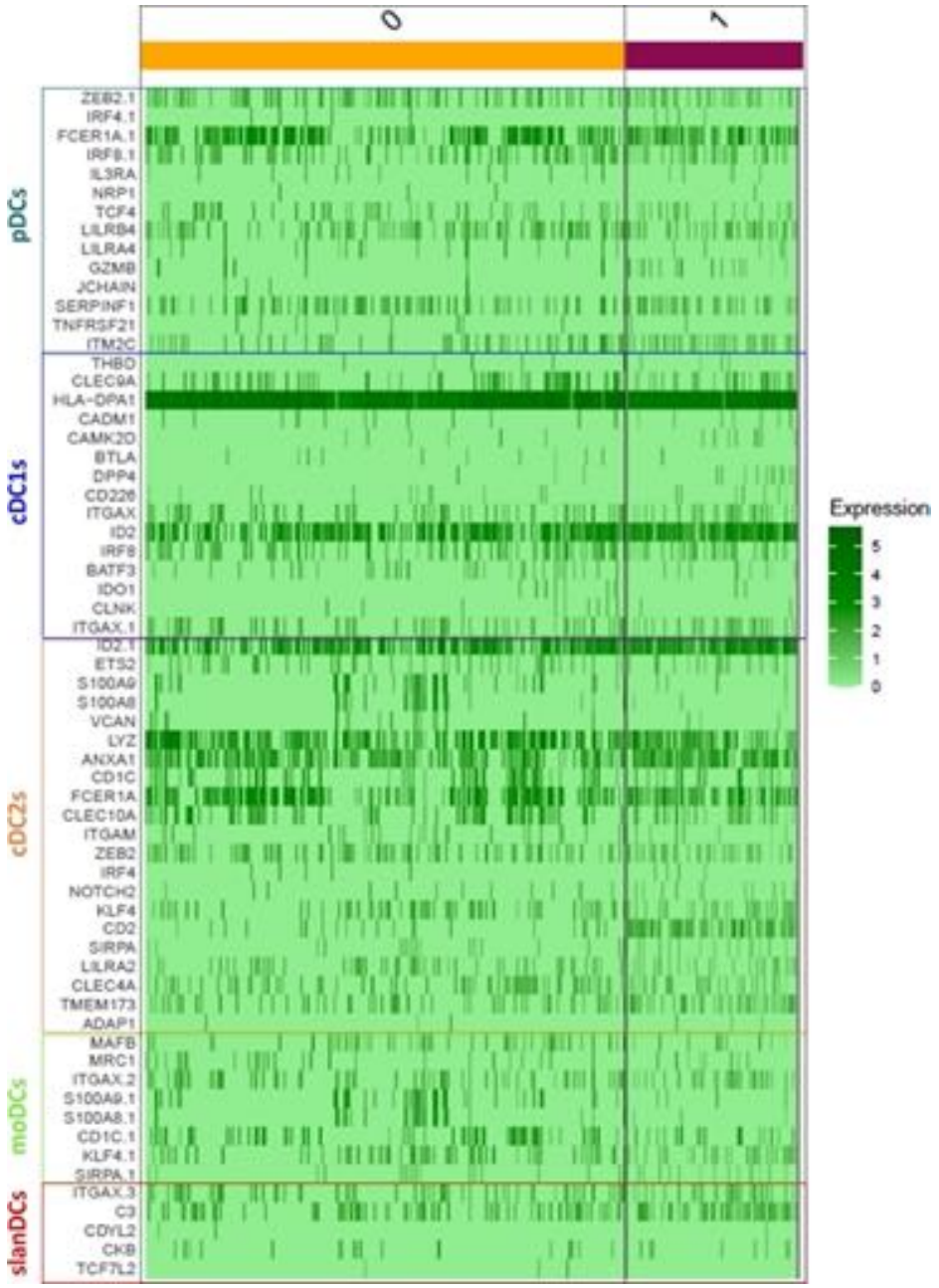

Figure 36. *Heatmap showing the mean expression of some genes characteristic of each DC subset (reported on the left side of the heatmap) in each cell composing sub-clusters 0 and 1.*

4.2.2 Ingenuity Pathway Analysis

In order to assess the factors that could drive the sub-clustering of tumour-infiltrating DCs into cluster 0 and 1, and to investigate the functional meaning of the differential expression profile of the two clusters, we calculated DEGs between clusters 0 and 1 (p-value adjusted < 0.01, $log_2FC > 0.58$ or $log_2FC < -0.58$), and plotted them in the volcano plot shown in Figure 37.

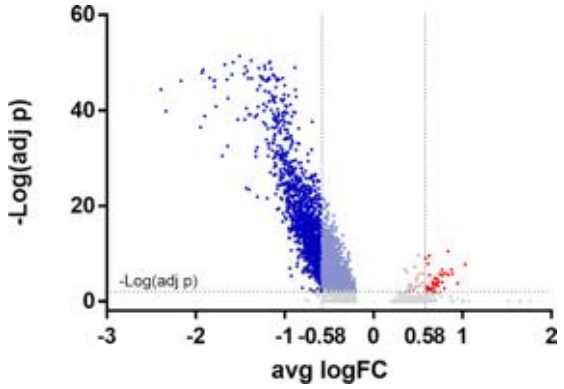

Figure 37. *Volcano plot showing DEGs between cluster 0 and 1. Grey dots indicate genes that were not differentially expressed (-Log(0,01) < 2); red dots indicate significantly up-regulated genes ($log_2FC > 0,58$), and blue dots indicate significantly down-regulated genes ($log_2FC < -0,58$).*

DEGs were further analyzed by using Ingenuity pathway analysis (IPA) software. IPA is an all-in-one, web-based software application that enables the analysis, integration, and understanding of data from gene expression, miRNA, SNP, metabolomics, proteomics, and RNAseq experiments. In particular, the comparison analysis between cluster 0 and 1 was performed taking advantage of the *Canonical Pathways* (CPs) and *Diseases and Functions* (DFs) tools.

4.2.2.1 Canonical Pathway analysis

Firstly, we compared cluster 0 and 1 with CP analysis, which predicts pathways that changed based on the differential expression of the uploaded gene dataset. We considered only CPs with a p-value < 0.05 and z-score < -1.5 (indicating a down-regulation) or z-score > 1.5 (indicating an up-regulation). Based on the category CPs belong to, we gathered them in three main sub-categories: i) *pro-inflammatory mediator production and maturation*; ii) *signal transduction*; iii) *cytoskeleton rearrangement, motility and cell interactions* (Figure 38, Figure 39, Figure 40).

As shown in (Figure 38A, Figure 39A, Figure 40A), the CPs related to *all the three sub-categories mentioned above* were down-regulated in cluster 0, the largest one, compared with cluster 1. This observation was also confirmed by the "Add Module Score Function" that compared the expression of the overall gene signature of the sub-categories between cluster 0 and 1, and was represented in the violin plot shown in Figure 38B, Figure 39B, Figure 40B. In particular, pathways related to NF-kB signalling, to DC maturation or to signal transduction involved in the activation of inflammatory responses, and pathways involved in actinomyosin organization and cell proliferation, like cdc42, Paxillin or PAK signalling, or pathways related to leukocyte migration, like leukocyte extravasation signalling, were downregulated in cluster 0.

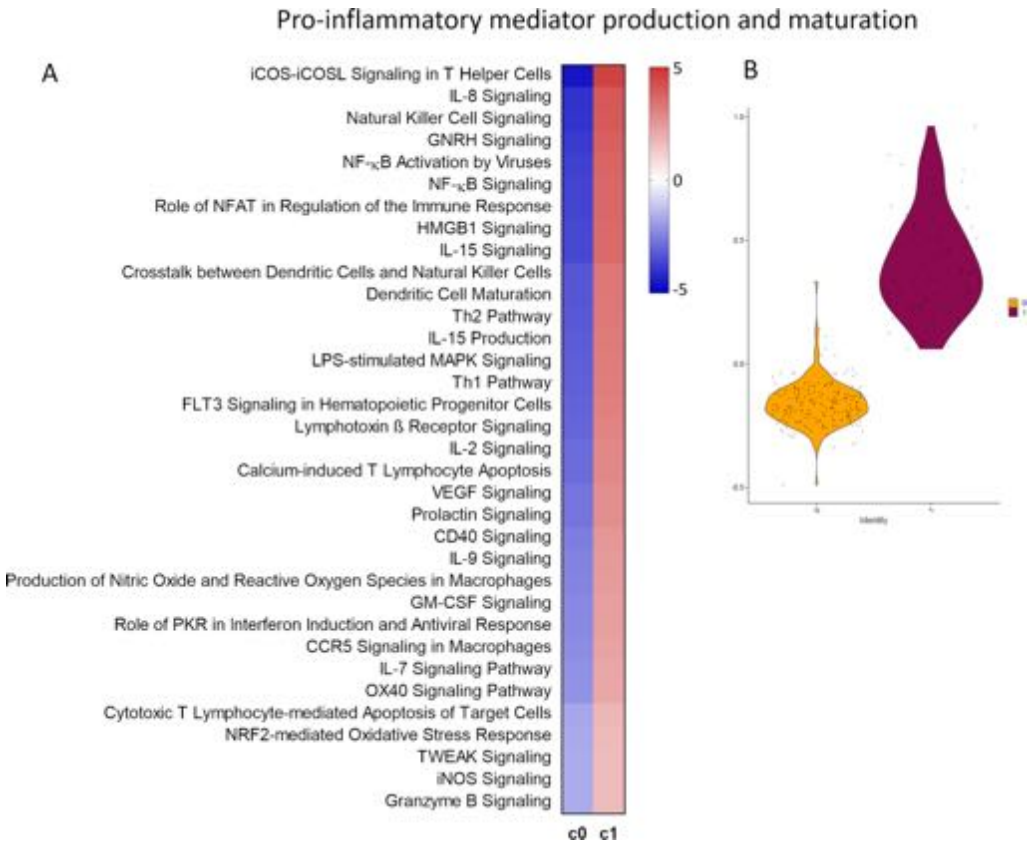

Figure 38. *(A)Heatmap showing the CPs of the sub-category "Pro-inflammatory mediator production and maturation" that were differentially regulated in cluster 0 compared with cluster1. The pathways of the sub-category are listed on the left side of the heatmap. Pathways are ranked according to the z-score that predicts a down-regulation (blue, z-score < -1.5) or an up-regulation (red, z-score > 1.5). (B) Violin plot indicating the overall gene expression of the sub-category "Pro-inflammatory mediator production and maturation" in cluster 0 and 1.*

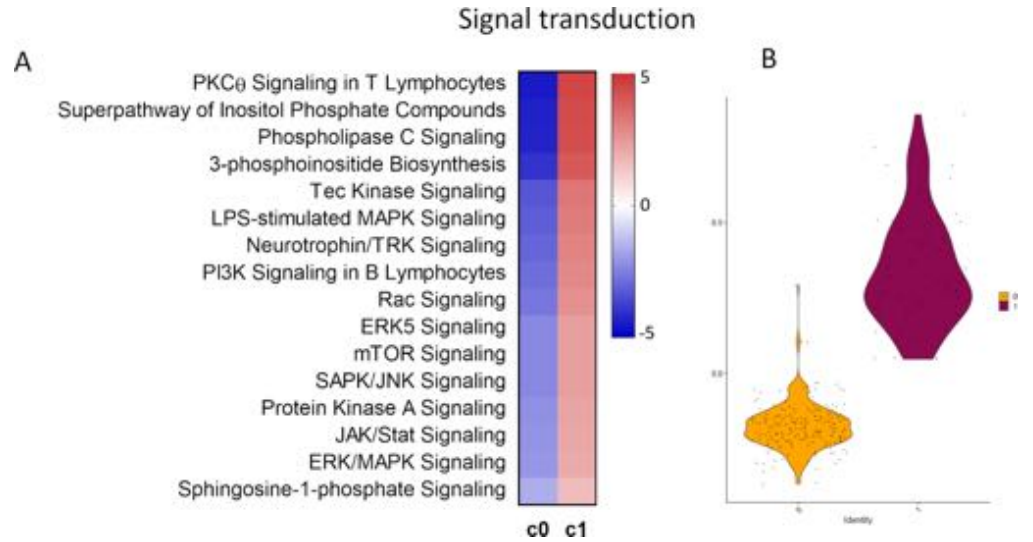

Figure 39. *(A) Heatmap showing the CPs of the sub-category "Signal transduction" that were differentially regulated in cluster 0 compared with cluster1. The pathways of the sub-category are listed on the left side of the heatmap. Pathways are ranked according to the z-score that predicts a down-regulation (blue, z-score < -1.5) or an up-regulation (red, z-score > 1.5). (B) Violin plot indicating the overall gene expression of the sub-category "Signal transduction" in cluster 0 and 1.*

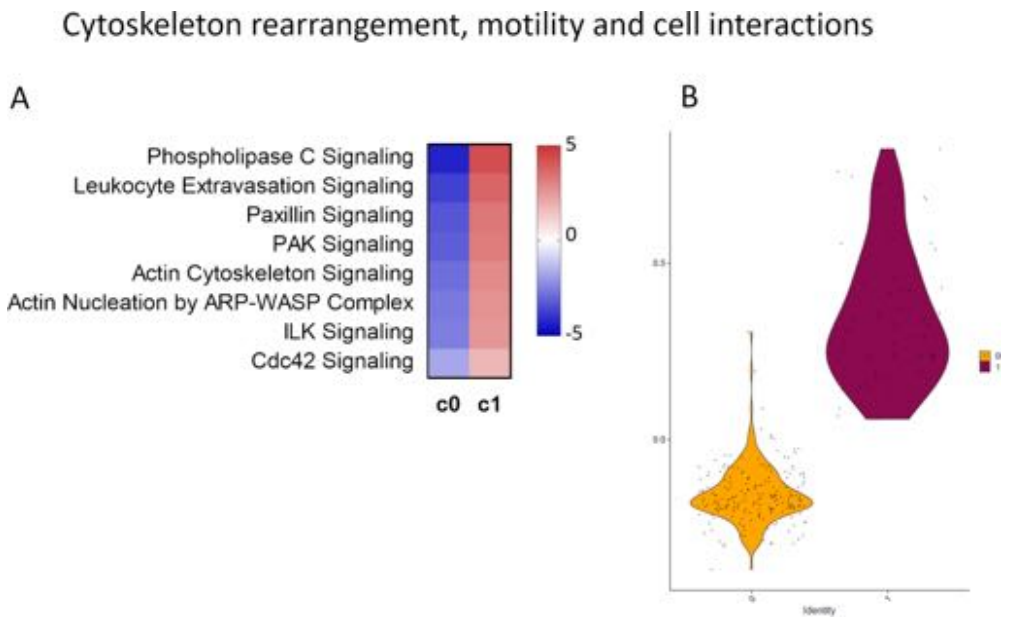

Figure 40. *(A) Heatmap showing the CPs of the sub-category "Cytoskeleton rearrangement, motility and cell interactions" that were differentially regulated in cluster 0 compared with cluster1. The pathways of the sub-category are listed on the left side of the heatmap. Pathways are ranked according to the z-score that predicts a down-regulation (blue, z-score < -1.5) or an up-regulation (red, z-score > 1.5). (B) Violin plot indicating the overall gene expression of the sub-category "Cytoskeleton rearrangement, motility and cell interactions" in cluster 0 and 1.*

In order to better understand and investigate the complexity of the involvement of these CP sub-categories in tumour-infiltrating DCs, we focused our attention on those genes that could have a higher biological relevance in these pathways.

The biologically relevant genes selected in the CP sub-categories *pro-inflammatory mediator production and maturation* and *signal transduction are reported in* Figure 41 and Figure 42, respectively.

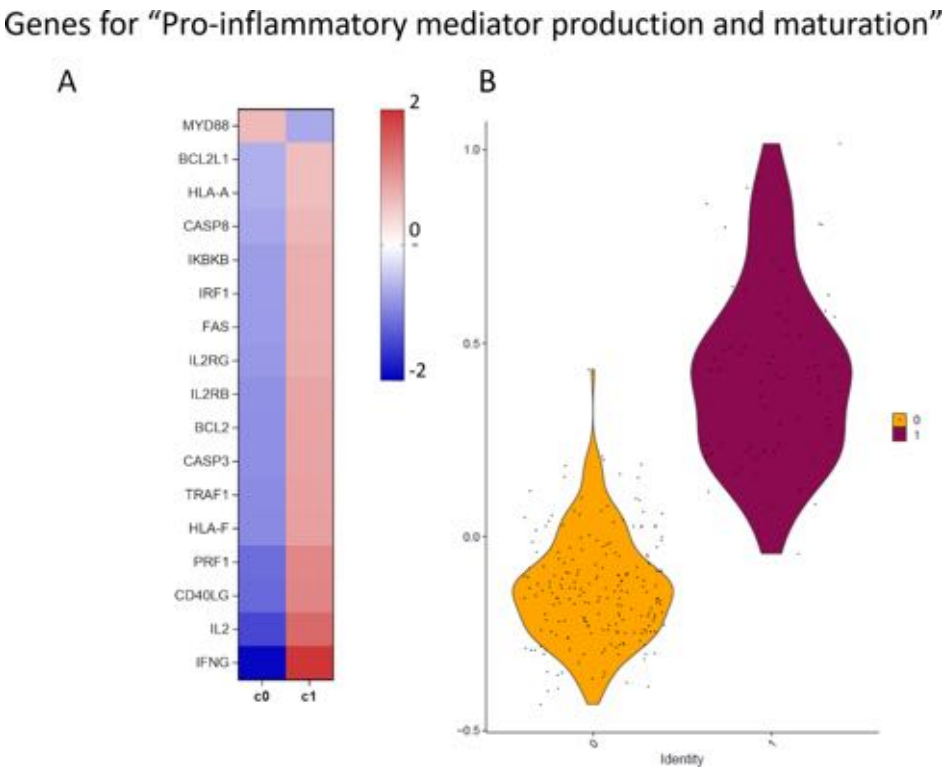

Figure 41. *(A)Heatmap showing the biologically relevant genes of the sub-category "Pro-inflammatory mediator production and maturation" that were differentially regulated in cluster 0 compared with cluster1. The gene names of the sub-category are listed on the left side of the heatmap. Genes are ranked according to the log_2FC that predicts a down-regulation (blue, $log_2FC < -0.58$) or an up-regulation (red, $log_2FC > 0.58$). (B) Violin plot indicating the overall gene expression of the sub-category "Pro-inflammatory mediator production and maturation" in cluster 0 and 1.*

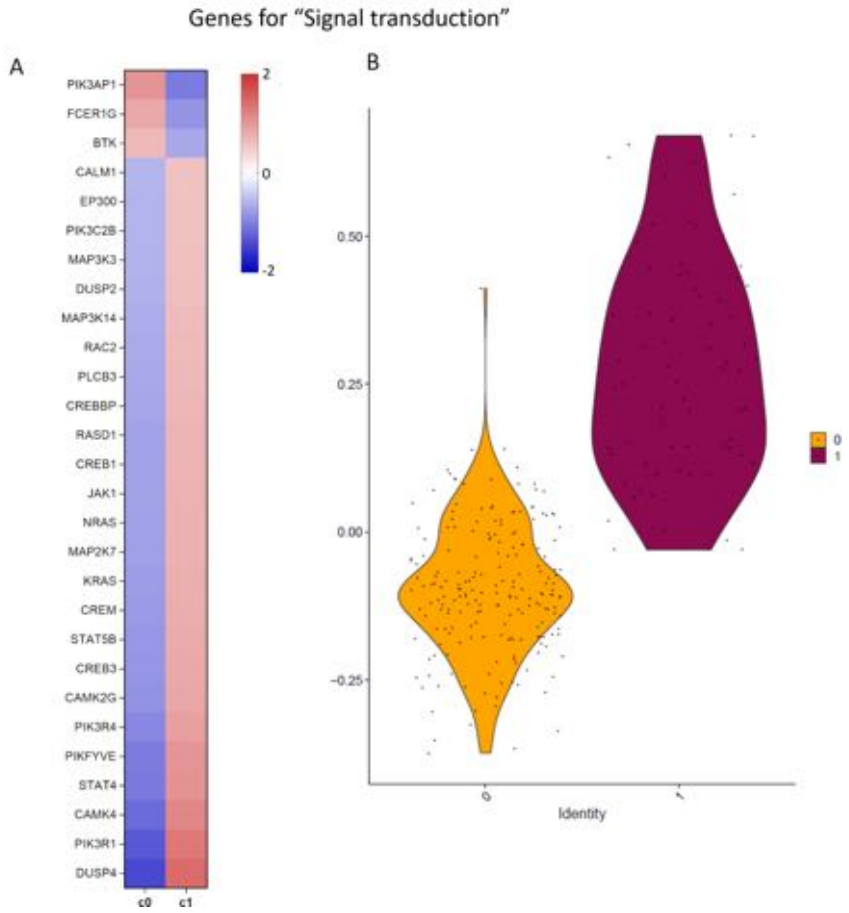

Figure 42. *(A) Heatmap showing the biologically relevant genes of the sub-category "Signal transduction" that were differentially regulated in cluster 0 compared with cluster1. The gene names of the sub-category are listed on the left side of the heatmap. Genes are ranked according to the log_2FC that predicts a down-regulation (blue, $log_2FC < -0.58$) or an up-regulation (red, $log_2FC > 0.58$). (B) Violin plot indicating the overall gene expression of the sub-category "Signal transduction" in cluster 0 and 1.*

As shown in Figure 41 and Figure 42, we observed an overall down-regulation of the genes involved in NF-kB signalling in cluster 0. NF-kB is a transcription factor that regulates the expression of several inflammatory genes, including those encoding cytokines and chemokines, and regulates multiple aspects of innate and adaptive immune responses, as survival, activation and maturation of innate immune cells (Liu et al., 2017). Among DEGs between cluster 0 and 1 there were several genes related to NF-kB pathway down-regulated in cluster 0, including EP300, CREBBP, CREB1, CREB3, CAMK4, CAMK2G and TRAF1. This observation is relevant because the transcription co-activators CREB-binding protein (CBP, encoded by CREBBP) or p300 (encoded by EP300) act by binding to the NF-kB component RelA and inducing the transcription of pro-inflammatory mediators (Wen et al., 2010).

Moreover, CAMK-IV (encoded by CAMK4) and CAMK-II (encoded by CAMK2G), induced by intracellular Ca^{2+} that binds to its receptor calmodulin (encoded by CALM1 gene), phosphorilates

CREB proteins that interact with CBP or p300, inducing the transcription of genes involved in the proliferation, survival and differentiation of immune cells (Illario et al., 2008; Wen et al., 2010).
TRAF1 is a member of the TNF receptor (TNFR)-associated factor (TRAF) protein family. TRAF proteins associate with, and mediate the signal transduction from, distinct receptors of the TNFR superfamily. Indeed, TRAF1 is upregulated in response to NF-kB and AP1 activation by inflammatory mediators (e.g. TNFa, CD40L, LPS). TRAF1 is important in the promotion of cell survival and it is absent in resting cells (Arron et al., 2002; Edilova et al., 2018; Oyoshi et al., 2007).
Other genes, as those related to MAP kinase family (like MAP2K7, MAP3K3, MAP3K14), CREB, JAK1, and DUSP2, which are involved in the regulation of inflammatory responses, were all down-regulated in cluster 0. Moreover, also genes encoding for the family of Phosphoinositide-3 kinases (PI3Ks), like PIK3C3, PIK3C2B, PIK3R1, PIK3R4, and involved in the regulation of antigen processing and presentation in antigen presenting cells, were down-regulated in cluster 0. Only BCAP (PIK3AP1) and BTK resulted up-regulated in cluster 0 (Aksoy et al., 2018; Leone et al., 2017).
Overall, these finding suggested that DCs within cluster 0 could be in a less active or resting state compared with DCs in cluster 1, and this finding was also supported by the "Add Module Score Function" that in violin plots represented the overall expression of these biologically relevant genes (Figure 41B, Figure 42B). For this reason, we checked the expression of those genes regulating the apoptosis and cell cycle, and observed that both anti-apoptotic (BCL2, BCL2L1) and pro-apoptotic genes (FAS, CASP3, CASP8) were downregulated in cluster 0, likely suggesting that these cells were not going in apoptosis. Therefore, we hypothesized that DCs in cluster 0 may be in a quiescent/G0 phase. In support of this hypothesis, we observed that in our whole geneset several genes crucial to the maintenance of mitotic competence (MC) and the exit from G0 phase were downregulated in cluster 0 (Figure 43A).

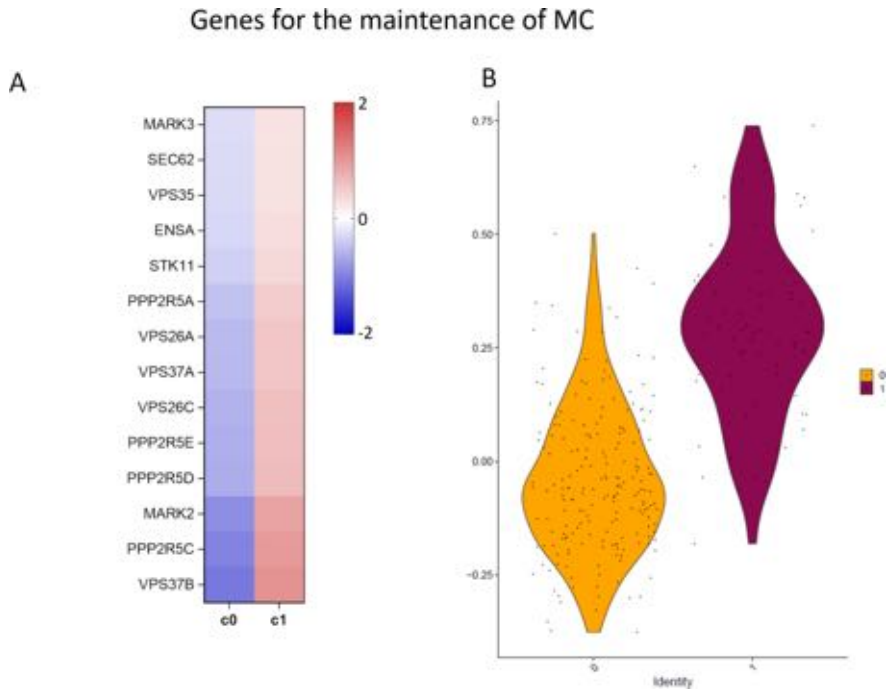

Figure 43. *(A) Heatmap showing the biologically relevant genes involved in the maintenance of mitotic competence (MC) that were differentially regulated in cluster 0 compared with cluster1. The gene names are listed on the left side of the heatmap. Genes are ranked according to the log_2FC that predicts a down-regulation (blue, $log_2FC < -0.58$) or an up-regulation (red, $log_2FC > 0.58$). (B) Violin plot indicating the overall gene expression of genes involved in the MC in cluster 0 and 1.*

In particular, these genes, such as MARK2, MARK3, SEC62, STK11, VPS35, VPS37A, VPS37B, regulate cell polarization and vesicular transport and their down-regulation could impair cellular ability to quickly move from G0 to M phase ((Aono et al., 2019; Dumont et al., 2015; Linxweiler et al., 2017; Sajiki et al., 2018; Y. Wang et al., 2019; G. Zhang et al., 2020; H. X. Zhang et al., 2018).

In order to gain insights into the comprehension of the involvement of the CP sub-category *cytoskeleton rearrangement, motility and cell interactions* in tumour-infiltrating DCs, also in this case we focused our attention on the genes with a higher biological relevance in these pathways. As shown in Figure 44A, we observed that ACTN4, PXN and genes belonging to Rho GTPase family (including ARGHGEF6, RAC2, RHOT2, RHOT2), as well as genes involved in cell-cell contact and adhesion (including ITGA1, ITGA4, ITGAL) were all down-regulated in cluster 0. This observation was also confirmed when we applied the "Add Module Score Function" that compared the expression of the overall gene signature between cluster 0 and 1, represented in the violin plot shown in Figure 44B. All together, these observations supported our hypothesis that DCs in cluster 0, which contained a larger number of cells compared with cluster 1, were characterized by impaired motility, migration and capacity to interact with other cells present in the GME.

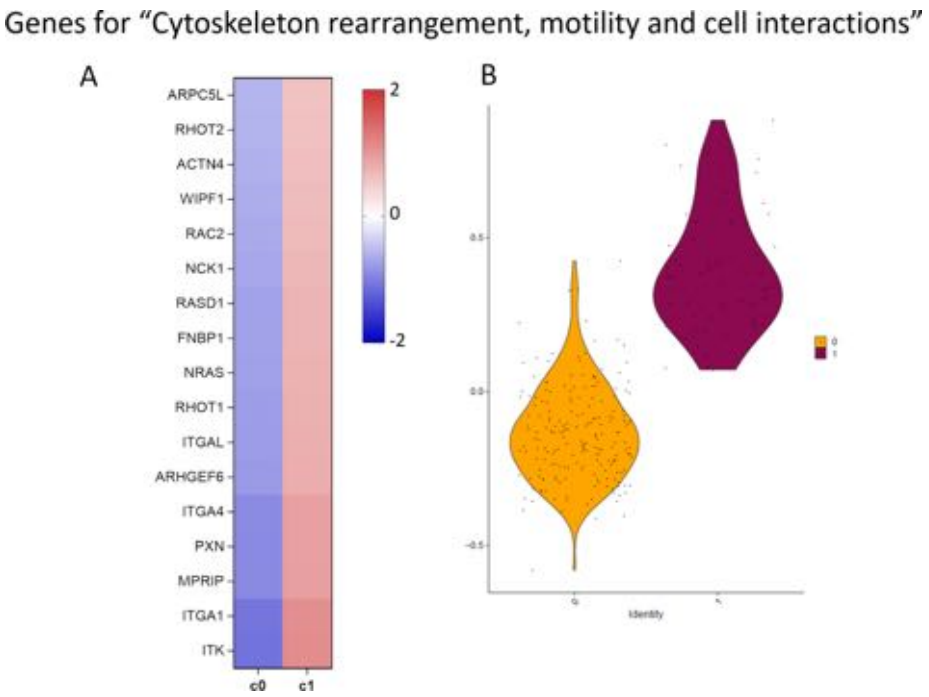

Figure 44. *(A) Heatmap showing the biologically relevant genes of the sub-category "Cytoskeleton rearrangement, motility and cell interactions" that were differentially regulated in cluster 0 compared with cluster1. The gene names of the sub-category are listed on the left side of the heatmap. Genes are ranked according to the log_2FC that predicts a down-regulation (blue, $log_2FC < -0.58$) or an up-regulation (red, $log_2FC > 0.58$). (B) Violin plot indicating the overall gene expression of the sub-category "Cytoskeleton rearrangement, motility and cell interactions" in cluster 0 and 1.*

4.2.2.2 Diseases and Functions (DF) Analysis

We then compared cluster 0 and 1 performing the DF analysis that predicts which cellular processes and biological functions are affected, based on gene expression of the cluster. We considered only DFs with a p-value < 0.05 and z-score < -1.5 (indicating a down-regulation) or z-score > 1.5 (indicating an up-regulation). Based on the category DFs belonged to, we divided them into three main sub-categories: i) *activation state*; ii) *cell viability and cell cycle progression*; iii) *cell movement and cell interactions* (Figure 45; Figure 46; Figure 47). The sub-category *activation state* was composed of biological processes involved in cell activation, leukocyte stimulation, and interactions of antigen presenting cells. All these biological processes were down-regulated in cluster 0 compared with cluster 1. Moreover, functions related to the flux of Ca^{2+} and other ions, that have a preeminent role in the activation of immune responses, were also down-regulated in cluster 0 (Figure 44A). This observation was also confirmed by the "Add Module Score Function" that demonstrated a down-regulated expression of the overall *activation state* gene signature in cluster 0 compared with cluster 1, as shown in the violin plot reported in Figure 45B, suggesting that DCs in cluster 0 were characterized by an impaired activation state.

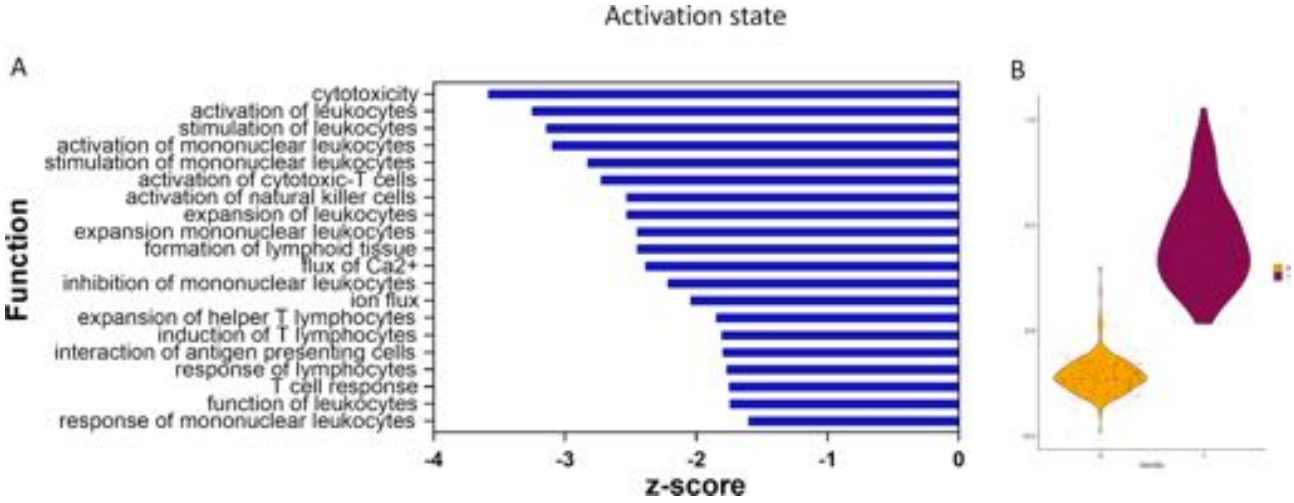

Figure 45. *(A) Bar plot showing DFs of the sub-category "Activation state", that were differentially regulated in cluster 0 compared with cluster1. The functions of the sub-category are listed on the left side of the barplot. Functions are ranked according to the z-score that predicts a down-regulation (blue, z-score < -1.5) or an up-regulation (red, z-score > 1.5). (B) Violin plot indicating the overall gene expression of the sub-category "Activation state" in cluster 0 and 1.*

A similar scenario was also observed when considering the DF category named *cell viability and cell cycle progression*. As shown in (Figure 46A), all functions typical of this category were down-regulated in cluster 0, thus supporting the results described in the Canonical Pathways analysis where we observed in the same cluster a down-regulated expression of the genes involved in the maintenance of mitotic capacity, and suggesting that DCs in cluster 0 were in a resting rather than active state. This observation was also confirmed by "Add Module Score Function" as shown in the violin plot reported in Figure 46B.

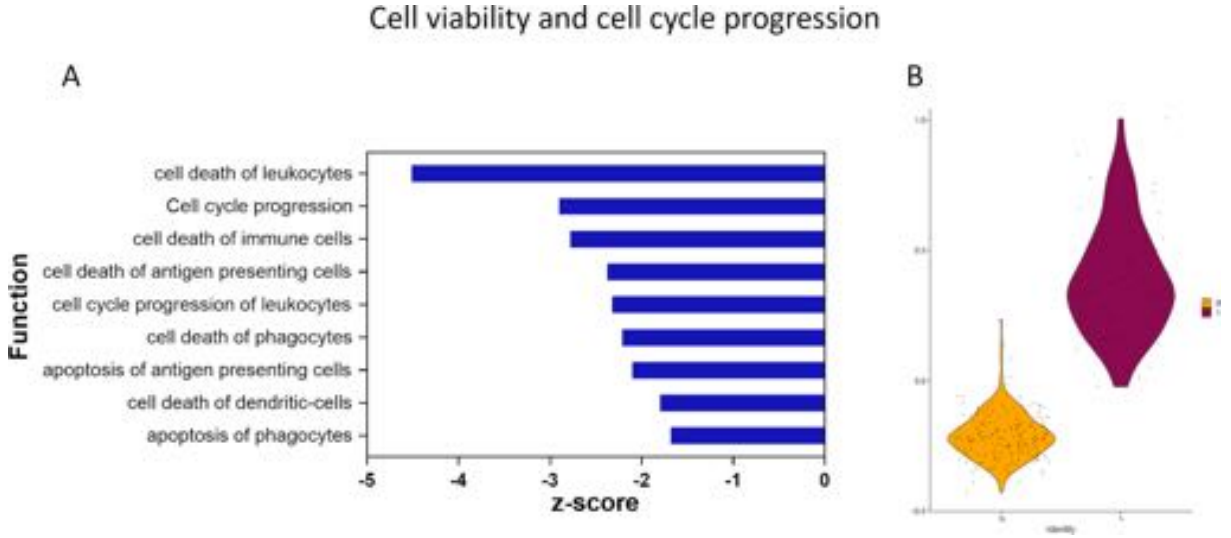

Figure 46. *(A) Bar plot showing DFs of the sub-category "Cell viability and cell cycle progression" that were differentially regulated in cluster 0 compared with cluster1. The functions of the sub-category are listed on the left side of the barplot. Functions are ranked according to the z-score that predicts a down-regulation (blue, z-score < -1.5) or an up-regulation (red, z-score > 1.5). (B) Violin plot indicating the overall gene expression of the sub-category "Cell viability and cell cycle progression" in cluster 0 and 1.*

Finally, as for the CPs related to *cytoskeletal rearrangement, cell motility and migration*, also for DFs related to *cell movement and cell interactions* we observed a down-regulation in cluster 0 of several functions related to migration, homing, adhesion and binding of immune cells (Figure 47A). As shown in the violin plot represented in figure 47B, the "Add Module Score Function" confirmed an overall down-regulation of the overall gene signature related to this category, suggesting that tumour-infiltrating DCs belonging to cluster 0 were characterized by impaired functions related to cell interactions and migration.

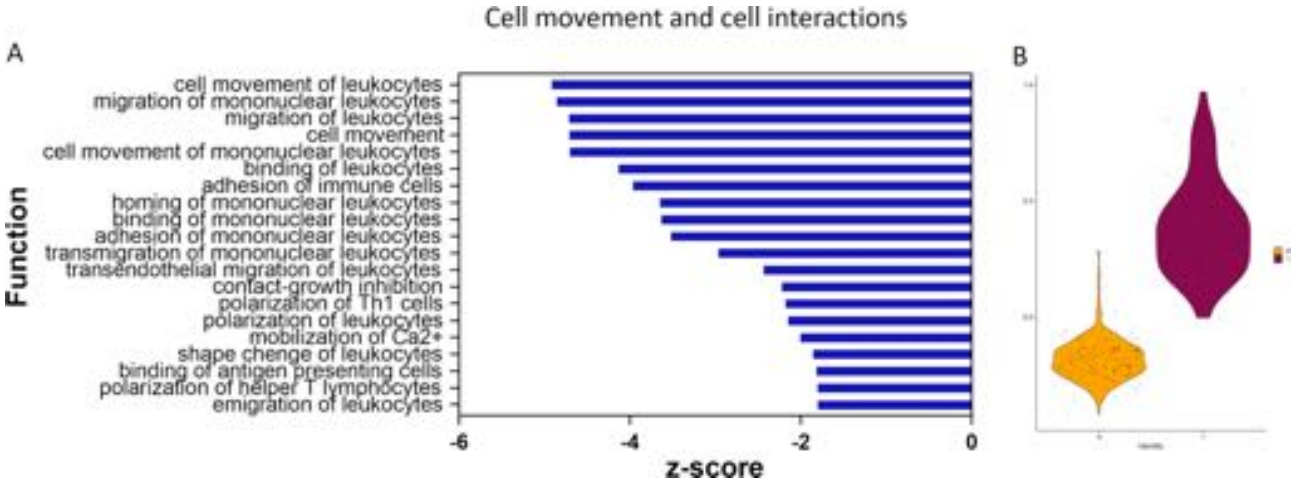

Figure 47. *(A) Bar plot showing DFs of the sub-category "Cell movement and cell interactions" that were differentially regulated in cluster 0 compared with cluster1. The functions of the sub-category are listed on the left side of the barplot. Functions are ranked according to the z-score that predicts a down-regulation (blue, z-score < -1.5) or an up-regulation (red, z-score > 1.5). (B) Violin plot indicating the overall gene expression of the sub-category "Cell movement and cell interactions" in cluster 0 and 1.*

4.3 Analysis of circulating DC subsets in a cohort of HGG patients treated with immunotherapeutic approaches

As a parallel part of the above study that allowed the characterization of different DC subsets in HGG patients at their first diagnosis, we also analysed a small cohort of 17 HGG relapsed patients that were enrolled by the Unit of Neuro-Oncology at Humanitas Research Hospital and were included in multi-cohort pharmacological ieCTs.

This work was part of a bigger clinical study (under submission) aimed at evaluating data of all consecutive patients with a diagnosis of recurrent HGGs treated into multi-cohort ieCTs between 2014 and 2019, and investigating the prognostic and predictive value of a large series of clinical, laboratory, and molecular variables. In a subset of these patients, circulating immune cells, were also prospectively monitored correlating their baseline values and dynamic changes during treatment with clinical outcomes.

In particular, given the importance that immunotherapeutic strategies have in modulating immune system against cancer and the crucial role that DCs play in the activation of immune responses, it could be interesting to investigate whether these new ieCTs had an impact on the modulation of DCs and how it could be correlated with patient prognosis.

Therefore, in this study, we analysed circulating DCs in a cohort of patients with relapsed IV grade gliomas who were followed from July 2018, to February 2020. These patients were enrolled in different ieCTs: 2 of them received anti CSFR-1; 5 received the experimental combination regimen anti CSFR-1 + anti-PD-1 and 10 the anti CD38 + anti PD-L1.

In this study, patients were evaluated before the treatment (T0) and at different time points after the treatment (T1, T2, T3, T4, T5) in order to investigate whether immunotherapeutic treatments could have an impact on absolute counts and activatory/inhibitory phenotype of circulating DC-lineage DCs. No statistically significant differences were observed in absolute counts of cDCs, cDC2s and pDCs among different observation time points, only cDC1s showed a significant decrease between T1 and T2 (Figure 48). Also for the phenotype, we did not observe any statistically significant differences among different observation time points in DC subsets, just cDC1s showed a significant decrease in the expression of CD80 between T0 and T2 (T0 vs T2: mean±std err; 152.96±17.92 vs 122.05±27.74; p-value=0.031). This could probably due to the heterogeneity in the treatments (data not shown).

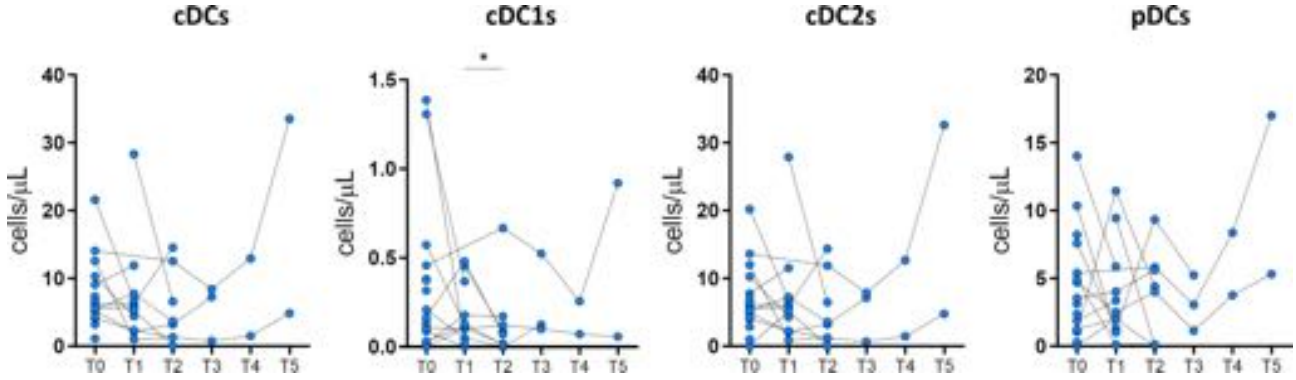

Figure 48. *The absolute count of DC subsets in whole blood samples obtained from 17 patients with relapsed IV grade gliomas, was expressed as number of cells per µL of whole blood. Patients were followed for different time points after treatments (T1, T2, T3, T4, T5). Each symbol represents a single sample. *p < 0.05. Statistical significance calculated using the Wilcoxon signed rank test.*

However, in order to establish whether DC population characteristics could represent a predictive or prognostic marker for the outcome of these patients, we evaluated the correlation between above mentioned parameters (absolute counts and phenotype) and patient overall survival (OS) at T1 and at the final observation time point of each patient (Tf). Although we did not observe any correlation between activatory or inhibitory profile of any DC-lineage DC subsets and OS, we observed that patients who have an increase of total cDCs at T1 with respect to T0 (ΔT1) showed a better clinical outcome (HR=0.25, P= 0.063). Moreover, patients characterised by a positive variation of cDCs at Tf with respect to T0 (ΔTf) had a significantly higher OS (p= 0.035), as shown in Kaplan-Meier curves in Figure 49.

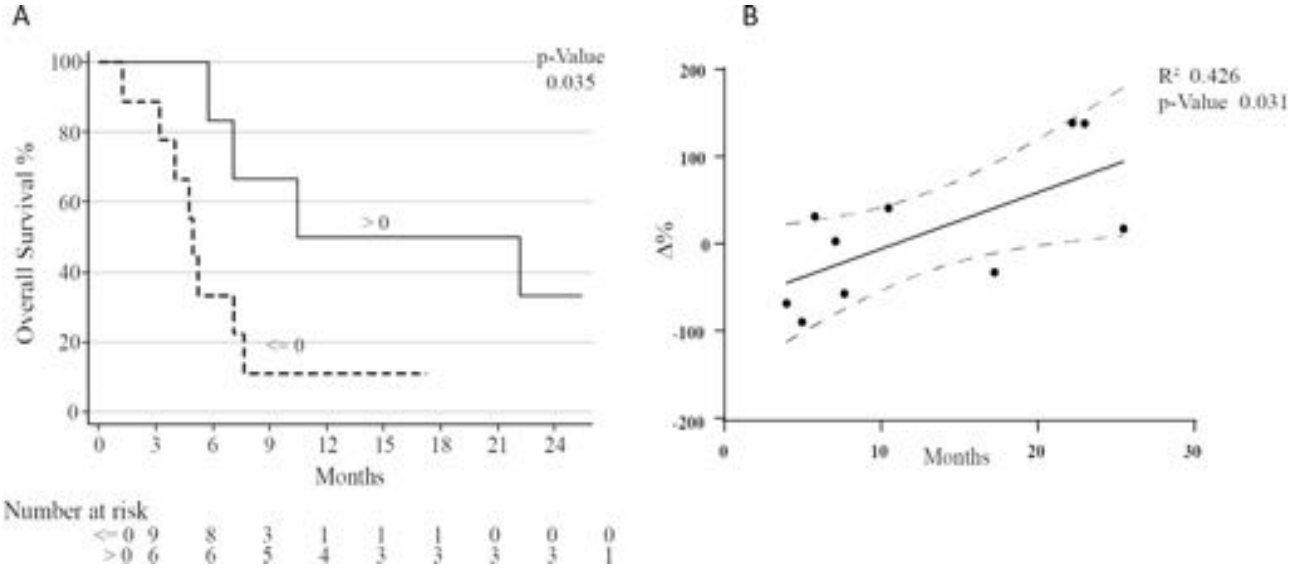

Figure 49. *(A) Kaplan-Meier survival curves of cDCs at ΔTF stratified according to the cut-off level of 0. Size of each patient group and the p-value were given below the figure. (B) Scatter plot showing di percentage variation between Tf and T0 of cDCs correlated with OS. R2 and p-value were shown in the figure.*

For other observation time points no other statistically significant differences were observed in patient outcome (data not shown). Even if these data have to be assessed and confirmed in a larger cohort of

patients, they suggested that patients that benefit of immunotherapeutic agents as demonstrated by the increased OS presented an increase of cDCs.

However, from the analysis of these patients we did not observe any correlation between activatory/inhibitory phenotype of circulating DCs and patient outcomes. Also, when we analysed DCs in patients stratified according to corticosteroid administration, allowed for these patients only in low dose regimen, we did not observe any correlations with OS, maybe for the reduced sample size.

5. Discussion

Discussion

Gliomas represent the 80% of malignant primary brain tumours. Among them, HGGs that belong to grades III or IV, share an aggressive and infiltrating nature (Hart et al., 2019). In particular, the IV grade glioma or GBM with the wild type isoform of IDH enzyme represent the most aggressive form and the patient prognosis is extremely poor (only 14.6 months), despite a standard of care treatment comprising maximal safe surgical resection, radiotherapy, and chemotherapy with the DNA-alkylating agent temozolomide (Stupp et al., 2005). Indeed, so far, there is not a curative intervention, leading clinicians in trying a wide spectrum of therapeutic approaches, like off-label therapies. Moreover, the enrolment of these patients in clinical trials is often denied by strict inclusion criteria. However, the great interest in cancer immunotherapy, with its own concept of boosting antitumour immunity, is growing leading to the development of several trials involving, among others, DC-based vaccines. Among several tumours in which their efficacy has been proven, HGGs have shown the highest susceptibility (Garg et al., 2016; Prins et al., 2011) . Even though life expectancy of these patients remains poor, the use of DC-based therapies is also supported by the fact that DCs have a role, as potent APCs, in initiating and shaping anti-tumoral responses. Accordingly, it has been observed that DC presence within the TME is associated with better survival across multiple types of human cancer (Broz et al., 2014). However, because TME is often immunosuppressive in many tumours including HGGs, the future challenge of DC-based immunotherapy will be to improve the efficacy of treatment by reprogramming tumour-infiltrating DCs directly *in vivo,* in order to switch their behaviour from tumour-induced immunosuppression to promotion of tumour rejection (Benencia et al., 2014; Palucka & Banchereau, 2012). In order to successfully use these strategies in HGG patients, a deep knowledge of the DC subsets that are specifically recruited to the tumour site, and the impact of GME on the activatory/tolerogenic profile of DCs is needed. Therefore, this project aimed at providing a detailed comprehension of circulating and infiltrating DCs in HGG patients, including the molecular pathways of DC activation that may be impaired in these patients. This characterisation would bring novel insights into the comprehension of the intricate interactions between HGGs and the immune system, and would provide the basis for improving the efficacy of DC-based therapies in these patients.

To this aim, we have used two approaches that allow a multi-parametric cell characterisation: flow-cytometry and scRNA sequencing techniques.

By using an 18-colour flow-cytometry panel optimised in our laboratory (Carenza et al., 2019), we compared the frequency and phenotype of DC subsets in the whole blood of HGG patients and HDs, in order to investigate whether circulating DCs underwent any changes in patients. We observed that frequencies and phenotype of circulating DC subsets from HDs were similar to values reported in

previous studies by us and other authors (Adhikaree et al., 2019; Carenza et al., 2019). As expected, we also observed no moDCs in the peripheral blood of both HDs and HGG patients(Collin & Bigley, 2018).

In HGG patients, we observed a significant decrease in the frequency of circulating cDC1s, cDC2s and pDCs compared with HDs. The decrease in circulating DC-lineage DCs was confirmed also by UMAP analysis. This analysis is based on an algorithm of dimensionality reduction that allows to visualize high-dimensional data in a two-dimension space. In particular, by using an unsupervised clustering algorithm UMAP evaluates, at single cell level, differences/similarities of marker expression. By visualising on UMAP plots the expression of markers used to identify different DC subsets with a manual gating strategy, we confirmed that cells belonging to each specific DC subset co-localised in a specific cluster of the UMAP plot. The observed correspondence strengthened and confirmed our manual gating strategy used to identify DC subsets.

Our observation that circulating DC subsets are reduced in HGG patients is in accordance with some previous studies addressing this issue, though with minor differences. For instance, Adhikaree and colleagues reported a reduction in circulating cDC2s and pDCs, but no changes in cDC1c and slanDCs in 16 GBM patients (Adhikaree et al., 2019).

Gousias and colleagues reported a reduction of total myeloid DCs and pDCs, but no differences were observed in cDC1s and cDC2s (Gousias et al., 2013). Notably, another study reported opposing results, showing an increase, rather than a decrease, of circulating pDCs in a cohort of glioma patients affected by I, II, III or IV grade gliomas; the reasons of this discrepancy being poorly evident (Wang 2014).

In our study, we further demonstrated that the reduction of all DC-lineage DC subsets were only evident in patients affected by IV grade IDHwt glioma, which is the most severe type of HGG, whereas patients with III grade or IV grade IDHmut HGG had DC frequencies similar to healthy controls. This result may have different explanations. One possibility is that the reduced frequency of DC subsets observed in our patients may depend on the effects of VEGF released by the tumour (Weathers and de Grout, 2015). Indeed, VEGF is known to inhibit DC development in the bone marrow (D. Gabrilovich et al., 1998). According to this hypothesis, it has been reported that the expression of VEGF is higher in IDHwt than IDH mutated GBM (Polívka et al., 2018). Another mechanism possibly explaining the reduction of circulating DCs in IV IDHwt patients may be represented by the recruitment of DCs into the tumour microenvironment. This possibility may be supported by our observation that DCs, and in particular cDC1s, are more abundant in tumour tissues obtained from patients with IV IDHwt gliomas than the other HGGs.

When we stratified our patients according to corticosteroid treatment, we observed that patients treated with dexamethasone at the time of surgery had a marked reduction of all DC subsets, similar to frequencies observed in patients with IV grade IDHwt HGG. Unfortunately, we were not able to assess whether DC reduction was ascribable to the corticosteroid treatment or to the histopathological/molecular features of the tumour, because the majority of patients included in this group (10 out to 11) were affected by IV grade IDHwt glioma. It should be noted, however, that a reduction of cDC2s and pDCs in the blood of corticosteroid-treated GBM patients has also been reported in a previous study (Adhikaree et al., 2019). This observation, together with the demonstration that one single dose of dexamethasone administered to healthy individuals induces an acute reduction of circulating cDCs (Bain et al., 2018), seems to support a role for corticosteroid treatment in the reduction of circulating DCs observed in our patients. Further supporting a negative impact of dexamethasone treatment on DCs was our observation that also tumour-infiltrating DCs were markedly reduced in steroid-receiving patients. The reduction was particularly evident for cDC1s that are the DC subset mostly implicated in the activation of anti-tumoral cytotoxic T cell responses. And in the case of tumour-infiltrating DCs it could be clearly ascribed to dexamethasone treatment. Dexamethasone is a potent synthetic corticosteroid drug considered to be the gold standard for managing tumour-induced cerebral oedema and its neurological manifestations (Raslan & Bhardwaj, 2007). In HGG patients, it is commonly used perioperatively and frequently continued throughout subsequent treatment in order to improve the neurological patient conditions. However, a retrospective analysis aimed at investigating the prognostic role of corticosteroid administration clearly demonstrated that dexamethasone was an independent predictor of poor outcome in three independent GBM patient cohorts, providing evidence against the traditional use of steroids in brain tumour patients (Pitter et al., 2016). Several mechanisms may underly the negative association between corticosteroid treatment and clinical outcomes (Lukas et al., 2019). Our demonstration that dexamethasone treatment reduces HGG-infiltrating cDC1s demonstrated a further mechanisms involved in the negative impact of corticosteroid treatment in HGG patients, and strongly supports the recommendation of identifying alternative agents for managing oedema in these patients, as already suggested by Pitter and colleagues (Pitter et al., 2016). Indeed, among drugs that have demonstrated to possibly replace corticosteroids for managing oedema, there are VEGF inhibitors. These molecules, like bevacizumab, have been tested in newly diagnosed GBM patients but failed to prolong their survival (Verhoeff et al., 2009). However, it has been observed that bevacizumab or cediranib (a pan-VEGF receptor inhibitor) normalized vessel size and permeability, leading to a reduction of oedema in patients, supporting their use as alternative drug to corticosteroids for oedema management (Batchelor et al., 2007; Sorensen et al., 2009).

Regarding the immunophenotype of circulating DCs, the only consistent difference between HGG patients and HDs resulting from our study was a significant reduction of ILT2 expression on circulating pDCs and cDC2s in patients compared with HDs. This lower expression of ILT2 was apparently unaffected by histopathological or molecular HGG features, or by corticosteroid treatment. ILT molecules represent Ig-like transcripts of activating and inhibitory receptors that are involved in the regulation of immune cell activation and that control the function of immune cells. ILTs are categorized into three groups: i) inhibitory, those containing a cytoplasmic immunoreceptor tyrosine-based inhibitory motif (ITIM) and transducing an inhibitory signal (ILT2, ILT3, ILT4, ILT5, and LIR8); ii) activating, those containing a short cytoplasmic tail and a charged amino acid residue in the transmembrane domain (ILT1, ILT7, ILT8, and LIR6a) and delivering an activating signal through the cytoplasmic immunoreceptor tyrosine-based activating motif (ITAM) of the associated common γ chain of Fc receptor; and iii) the soluble molecule ILT6 lacking the transmembrane domain. Several studies have highlighted immunoregulatory roles for ILTs on the surface of antigen-presenting cells. ILT2 is expressed on the surface of various immune cell types, including myeloid and plasmacytoid DCs (Wu & Horuzsko, 2009). It binds both classical (HLA-A, -B, and -C) and non-classical MHC class I molecules, with a preferential affinity for HLA-G (Villa-Álvarez et al., 2018), and it exerts mainly inhibitory functions through ITIM signalling (Colonna M et al., 2000). The relevance of the inhibitory role of ILT2 in DCs is supported by the demonstration that ILT2 is upregulated on human tolerogenic DCs (Della Bella et al., 2004), and it is diminished on peripheral blood DCs of patients with autoimmune diseases (Monsiváis-Urenda et al., 2013). Downregulation of ILT2 expression on pDCs and moDCs has been reported to occur upon activation of DCs upon exposure to inflammatory stimuli, suggesting that ILT2 downregulation may accompany the transition from a tolerogenic to an immunogenic DC phenotype (Ju et al., 2004). Because in our patients ILT2 downregulation was not associated with a consistent upregulation of costimulatory molecules, further studies will be needed in order to investigate the role of isolated ILT2 downregulation on circulating DCs of HGG patients.

By using the same flow-cytometry approach described above, we investigate the ability of DCs and their subsets to infiltrate the tumour in HGG patients. We compared the frequency of DC subsets between tumoral and healthy cerebral tissues obtained from HGG patients. We observed that the presence of DCs of any subsets was negligible in healthy tissues. This virtual absence of DCs in human healthy brain parenchyma is an important observation that adds another piece to the poor knowledge available at present on human brain DCs. Indeed, our knowledge on brain DCs is largely limited to murine models, where DC populations have been mainly described in meninges and choroid plexus, where DCs capture antigens in the interstice and migrate to cervical lymph nodes

(D'Agostino et al., 2012). Notably, the juxta-vascular location of these cells supports the idea that brain DCs come from a vascular source and are not derived from the brain, suggesting that endogenous DCs in normal brain are most likely to arise from pre-DCs that enter the brain perivascular regions at an early stage (Colton, 2013). In this scenario, our data seem to confirm that DC subsets do not infiltrate human brain parenchyma in homeostatic conditions.

On the other hand, our results clearly demonstrated the accumulation of all myeloid DC subsets, including cDC1s, cDC2s, slanDCs and moDCs in HGG tumour tissues. The presence of HGG-infiltrating DC subsets has already been reported in the few previous studies addressing this issue. In particular, one study reported the presence of pDCs in patients with grade I-III glioma, but lack of these cells in IV grade patients (Dey et al., 2015). Notably, in our study HGG-infiltrating pDCs were detected only in few patients. We are not able to explain the reasons for these different results. It should be noted, however, that in Dey's study, pDCs were identified by immunohistochemistry as $BDCA2^{+}$ cells. Another study demonstrated by flow-cytometry the presence of HGG-infiltrating cDC2 (Hussain et al., 2006). Our results confirm that observation, and provide further information. In fact, by performing UMAP analysis we could further demonstrate that cDC2 subset in tumour tissue localized in 2 clusters within the UMAP: one in the same position of cDC2 cluster observed in whole blood, and another one localised in a different position of UMAP plot, closer to moDC cluster, suggesting a different phenotype of these cells in the tumour context, supported by the fact that the second cluster presented a more pronounced inflammatory phenotype, as indicated by the increased expression of HLA-DR, CD40 and ILT2, compared with the cluster of cDC2s more related to peripheral blood cDC2s. This observation is at least in part in accordance with data obtained by high dimensional single-cell protein and RNA analysis that suggested that moDCs may be more related to cDC2s rather than to monocytes (Dutertre et al., 2019; Sander et al., 2017).

Moreover, in our study we could provide some information on the activatory and inhibitory state of HGG-infiltrating DCs. Although it was not possible to compare the phenotype of tissue-infiltrating DC subsets between healthy and tumour tissues, because of the lack of DCs in healthy tissues, we could compare the phenotype of tumour-infiltrating DCs among the three groups of patients, stratified based on their histopathological/molecular features and corticosteroid treatment. However, given the exiguity of tumoral samples, we did not observe consistent differences in the expression of activatory molecules among patient groups. We just observed a slight increase in the expression of PD-L1 in tumour-infiltrating cDC2s and moDCs in the group of "dex-treated" patients. This slight trend in increased PD-L1 levels on cDC1s could be in accordance with other studies in which it has been demonstrated that, upon uptake of tumour antigens, tumour-infiltrating cDC1s can upregulate PD-L1 and become tolerogenic by activating a regulatory program (Maier et al., 2020). If dexamethasone

could have a role in this increase in HGG-infiltrating DCs requires further investigations, even if it is known the immunosuppressive role of corticosteroids in inducing an impairment in DC maturation (Franchimont, 2004). As regards the TIM-3 expression on DC subsets in tumoral samples, we were not able to evaluate it, for a technical artifact caused by the enzymatic digestion of tissues with collagenase IV. Indeed, as discussed by us in a recent work, collagenase IV, the enzyme used to digest tumoral specimens, was able to cut the extracellular domain of TIM-3 protein, causing an unreliable detection of this marker in flow-cytometry. This suggests the need for a careful setup of all experimental conditions, including the preanalytical phase, when planning the flow-cytometry analyses of TADCs (Carenza et al., 2020).

Finally, in order to further characterise HGG-infiltrating DCs we performed scRNAseq experiments on 7 tumoral samples and 2 healthy cerebral tissues derived from 8 HGG patients. The identification of DCs infiltrating tumour tissues in scRNAseq experiments was challenging, due to the fact that DCs are a rare population that lacks specific genes and shares many genes with other myeloid populations. However, by taking advantage of literature data related to the gene signature of sorted DC subsets (Villani et al., 2017) , we were able to identify, among the different immune cell clusters, the cluster containing DCs (Cluster 19). The identification of DC cluster was also confirmed by the expression of differentially expressed genes (DEGs) between cluster 19 and the other clusters, that we confirmed to be specific for or enriched in DC subsets, by using the Human Protein Atlas Database. In this way we could also provide a gene signature that could help in the discrimination of DCs in other studies or pathological contexts.

Once identified the DC cluster, in order to deepen our characterisation of infiltrating DCs, we performed a re-clustering of cluster 19 obtaining, at resolution 0.2, 3 distinct sub-clusters, of which, according their numeration, cluster 0 contained the highest number of cells followed by cluster 1 and 2.. In particular, from this analysis, we confirmed that DCs are nearly absent in healthy parenchyma, as observed by flow cytometry. Indeed, of the two healthy samples analysed, one was constituted by just 5 cells which spread between cluster 0 and 1, and the other, was composed by 16 cells which formed cluster 2. Since this last sample was superficial and difficult to cut with the scalpel, we hypothesised that DCs from it could derive from a meningeal contamination rather than from their real presence in the brain parenchyma. Therefore, we decided to exclude cluster 2 from the next steps of analysis. Focusing on clusters 0 and 1, we did not observe any stratification in the distribution of patients between the two clusters on the basis of the grade of disease or the corticosteroid treatment.

In order to investigate whether the sub-clustering reflected the division of DCs into distinct subsets, we further analysed the expression of transcription factors and genes that from the literature were known to be characteristic of/enriched in different DC subsets, observing that there was a scattered

expression of these genes in all sub-clusters and actually confirming the presence of all distinct DC subsets in every cluster. This allowed us to conclude that DCs did not form clusters on the basis of their ontogeny, but on the basis of their functional state in the GME, as supported by the following analyses on IPA software. With these analyses we validated the presence of DCs in the tumour tissue, making us the first to demonstrate the presence of all distinct DC subsets in the core of the pathological lesion of HGG patients with both flow-cytometry and sequencing techniques. Indeed, just other two works which took advantage of scRNA sequencing to study immune populations in GME identified only the presence of TADCs, without making a distinction in their subsets (Darmanis et al., 2017; Q. Wang et al., 2017).

Bu using IPA software tools Canonical Pathways (CPs) and Diseases and Functions (DFs), we performed a comparison analysis of DEGs between cluster 0 and 1. From the CP analysis, we observed that cluster 0, that was the largest one, was characterised by an overall state of inactivation and dormancy for pathways related to the following sub-categories: *pro-inflammatory mediator production and maturation*; ii) *signal transduction*; iii) *cytoskeleton rearrangement, motility and cell interactions*. In particular, pathways related to NF-kB signalling, to DC maturation or to signal transduction involved in the activation of inflammatory responses, and pathways related to actinomyosin organization and cell proliferation, like cdc42, Paxillin or PAK signalling, or pathways related to leukocyte migration, like leukocyte extravasation signalling, are downregulated in cluster 0 compared with cluster 1. As also confirmed by the expression of several biologically relevant genes characteristics of these pathways.

Particularly interesting were those genes implicated in NF-kB signalling. NF-kB is a transcription factor that regulates the expression of several inflammatory genes, including those encoding cytokines and chemokines, and regulates multiple aspects of innate and adaptive immune responses, as survival, activation and maturation of innate immune cells (Liu et al., 2017). Among DEGs between cluster 0 and 1 there were several ones related to NF-kB pathway down-regulated in cluster 0, such as EP300, CREBBP, CREB1, CREB3, CAMK4, CAMK2G, CALM1 and TRAF1. These are all genes regulating the transcription of pro-inflammatory mediators (Wen et al., 2010) and involved in cell proliferation, survival and differentiation of immune cells (Illario et al., 2008; Wen et al., 2010).

Another crucial gene in immune responses is TRAF1. It is a member of the TNF receptor (TNFR) associated factor (TRAF) protein family. TRAF proteins associate with, and mediate the signal transduction from various receptors of the TNFR superfamily. Indeed, TRAF1 is upregulated in response to NF-kB and AP1 activation by inflammatory mediators (e.g. TNFα, CD40L, LPS). It is important in promoting survival and it is absent in resting cells. Moreover, it has been observed in

mice that TRAF$^{-/-}$ DCs were more apoptotic, presented a marked deficiency in NF-kB activation, and TRAF$^{-/-}$ mice were also deficient in recruitment of DCs in the lung after LPS inhalation (Arron et al., 2002; Edilova et al., 2018; Oyoshi et al., 2007).

Other genes, as those related to MAP kinase family (like MAP2K7, MAP3K3, MAP3K14), CREB, JAK1, DUSP2 which are involved in the regulation of inflammatory responses, were all down-regulated in cluster 0. Moreover, also genes encoding for the family of phosphoinositide-3 kinases (PI3Ks), like PIK3C3, PIK3C2B, PIK3R1, PIK3R4, involved in the regulation of antigen processing and presentation in APCs, were down-regulated in cluster 0. In particular, it has been observed that deficient mice for PIK3C3 presented a reduction of CD8^{+}DCs (cDC1s) and a reduction of antigen cross-presentation of dying cell-associated antigens (Aksoy et al., 2018; Leone et al., 2017). Only BCAP (PIK3AP1) and BTK resulted up-regulated in cluster 0. Accordingly, Miao and colleagues observed that BCAP was able to negatively regulate DC maturation induced by TLR stimulation (Miao et al., 2020). On the other hand, Kawakami and colleagues demonstrated that DCs from BTK$^{-/-}$ mice presented a major stimulatory activity (Kawakami et al., 2006). All these findings suggested that DCs within cluster 0 could be in a less active or resting state compared with DCs in cluster 1, as also confirmed by the downregulation in cluster 0 of pro- and anti-apoptotic genes and those genes involved in the maintenance of MC, such as MARK2, MARK3, SEC62, STK11, VPS35, VPS37A, VPS37B. These genes regulate cell migration, polarization and vesicular transport and their down-regulation could impair cellular ability to quickly move from G0 to M phase (Aono et al., 2019; Dumont et al., 2015; Linxweiler et al., 2017; Sajiki et al., 2018; Y. Wang et al., 2019; G. Zhang et al., 2020; H. X. Zhang et al., 2018). All these data also found confirmation in the down-regulation of those pathways and genes involved in the regulation of cytoskeletal rearrangement, like actomyosin organization, cell proliferation and cell interactions, including genes like ACTN4, PXN, or genes belonging to Rho GTPase family (like ARGHGEF6, RAC2, RHOT2, RHOT2), or still genes involved in cell-cell contact and adhesion (like ITGA1, ITGA4, ITGAL) (Biro et al., 2014; López-Colomé et al., 2017; Melendez et al., 2011; Nobes & Marsh, 2000; Schittenhelm et al., 2017; Shurin et al., 2005). All these observations supported our hypothesis that DCs in cluster 0, constituted by the largest number of cells compared with cluster 1, were characterized by impaired motility, migration and capacity to interact with other cells present in GME. All these findings were also supported by the analysis of DFs related to biological processes regulating immune activation state, cell cycle progression and cell movement and interactions, indicating that DCs in cluster 0 were almost in a state of dormancy characterised by impaired immune functions and impaired ability to migrate and to interact with other cells present in GME, compared with DCs in cluster 1 which was constituted by a lower number of cells that presumably could exert an anti-tumoral activity. In particular,

differently from other two works in which by scRNAseq the authors studied the microenvironment of human GBM and in which they identified cells with a signature of DCs (Darmanis et al., 2017; Q. Wang et al., 2017), we were able, for the first time to our knowledge, to characterise the functional state of TADCs in a very delicate and difficult context like that of human brain.

In this step of analysis it could was not possible to perform comparison analyses in order to investigate eventual differences occurring in tumour-infiltrating DCs from patients treated or not with corticosteroids, due to the scarce number of cells that this stratification would have led to, making the results not reliable.

Moreover, in this study we also analysed DCs in a cohort of relapsed HGG patients who were enrolled in a multi-cohort ieCTs in which patients received anti CSFR-1 or the experimental combination regimen anti CSFR-1 + anti-PD-1 or the combination of anti CD38 + anti PD-L1. These data were part of another study (under submission) aimed at reviewing data of a larger cohort of patients with a diagnosis of recurrent HGGs and at monitoring different circulating immune cells, correlating their baseline values and changes during the treatment with clinical outcomes. Data on total cDCs, suggested that patients that benefit of immunotherapeutic agents, as demonstrated by the increased OS, presented an increase of circulating cDCs. Our findings are in accordance with previous reports on NSCLC patients treated with immune-checkpoint blockade (Donahue et al., 2017; Möller et al., 2020), composing a scenario in which the activation of DCs in HGGs, and in general the activation of innate immunity, is crucial for deriving benefit from immunotherapeutic approaches. However, from the analysis of these patients we could not observe any correlation between activatory/inhibitory phenotype of circulating DCs and patient outcomes. Also, when we analysed DCs in patients stratified according to corticosteroid administration, allowed for these patients only in low dose regimen, we did not observed any correlations with OS, maybe for the reduced sample size. On the contrary, a recent work by Iorgulescu and colleagues analysed, in a retrospective study, the effect of concurrent dexamethasone on survival of patients affected by IDH wild-type GBM and treated with PD-(L)1 blockade. They observed that baseline dexamethasone administration was the strongest predictor of poor survival. Even if, they did not investigate correlations between patient DCs or other immune populations and dexamethasone treatment in patients, in mice models of GBM treated with anti-PD-1 therapy they observed that some myeloid immune populations, like TAMs, monocytes and DCs, trended downward, particularly if dexamethasone was added to anti–PD-1 (Iorgulescu et al., 2021).

In conclusion, our data on circulating and tumour-infiltrating DCs of a first cohort of patients affected by non-recurrent HGGs have brought new insights into the knowledge of this rare population that we observed to be able to infiltrate tumour tissues, but not the healthy brain parenchyma. In particular, we observed that the frequency of circulating DCs was affected only in HGG patients with the most

severe disease and how corticosteroid treatment markedly reduced the amount of tumour-infiltrating DCs, in particular cDC1s which are DCs mostly implicated in the activation of anti-tumoral cytotoxic T cell responses, suggesting a negative role of dexamethasone administration in HGG patients, and supporting the recommendation of identifying alternative agents for managing oedema in HGG patients. In addition, from data on transcriptomic profile of TADCs and taking advantage of new bioinformatic tools, like IPA software, we were able to observe how the majority of TADCs were characterised by an impairment in their functions that may make them unable to interact and communicate with other tumour-infiltrating immune cells or to leave GME for the presentation of tumour antigens in secondary lymphoid organs in order to establish a potent anti-tumour immune response. On the basis of these findings, our results could pave the way and support the manipulation and reprogramming of TADCs, directly *in vivo,* so that they could present tumour antigens and potentially activate CTLs and other cytotoxic immune cells, like NK cells, promoting anti-tumour immunity and hindering tumour growth (Yang et al., 2021).

For the future, we are approaching in the study of the interactions that could occur between DCs and tumoral cells or between DCs and other immune populations infiltrating the tumour and that could be responsible for the observed phenotype of TADCs. This will be made possible by using new bioinformatic tools like NicheNet which is a recent computational tool able to predict which ligands influence the expression in another cell, which target genes are affected by each ligand and which signalling mediators may be involved (Browaeys et al., 2020). In this way, it will be possible to investigate the reciprocal interaction between DCs and other cells, and predict their functional state and how tumour could influence this crosstalk. This could provide further information crucial for improving therapeutic strategies.

Moreover, we could observe in a second cohort of relapsed HGG patients treated with different immunotherapeutic strategies how patients who benefited of immunotherapeutic agents, in terms of increased OS, presented an increase of circulating cDCs.

Although HGG patients have still few effective therapeutic options at recurrence and the minor improvements in OS over the last decades, there will be the need to encourage the enrolment into early-phase trials in order to catch early signs of activity, pushing forward only promising strategies. Moreover, it will be also necessary to better and deepen characterise the innate immunity in the brain, given our still poor knowledge about it, in order to develop new strategies to manipulate immune cells in such a way that immune responses can attack effectively glioma cells.

6. References

Adhikaree, J., Franks, H. A., Televantos, C., Vaghela, P., Kaur, A. P., Walker, D., Schmitz, M., Jackson, A. M., & Patel, P. M. (2019). Impaired circulating myeloid CD1c+ dendritic cell function in human glioblastoma is restored by p38 inhibition–implications for the next generation of DC vaccines. *OncoImmunology*, *8*(7), 1–12. https://doi.org/10.1080/2162402X.2019.1593803

Aksoy, E., Saveanu, L., & Manoury, B. (2018). The isoform selective roles of PI3Ks in dendritic cell biology and function. *Frontiers in Immunology*, *9*(NOV), 1–7. https://doi.org/10.3389/fimmu.2018.02574

Alexander, B. M., & Cloughesy, T. F. (2017). Adult glioblastoma. *Journal of Clinical Oncology*, *35*(21), 2402–2409. https://doi.org/10.1200/JCO.2017.73.0119

Aono, S., Haruna, Y., Watanabe, Y. hei, Mochida, S., & Takeda, K. (2019). The fission yeast Greatwall–Endosulfine pathway is required for proper quiescence/G 0 phase entry and maintenance. *Genes to Cells*, *24*(2), 172–186. https://doi.org/10.1111/gtc.12665

Arron, J. R., Pewzner-Jung, Y., Walsh, M. C., Kobayashi, T., & Choi, Y. (2002). Regulation of the subcellular localization of tumor necrosis factor receptor-associated factor (TRAF)2 by TRAF1 reveals mechanisms of TRAF2 signaling. *Journal of Experimental Medicine*, *196*(7), 923–934. https://doi.org/10.1084/jem.20020774

Aspelund, A., Antila, S., Proulx, S. T., Karlsen, T. V., Karaman, S., Detmar, M., Wiig, H., & Alitalo, K. (2015). A dural lymphatic vascular system that drains brain interstitial fluid and macromolecules. *Journal of Experimental Medicine*, *212*(7), 991–999. https://doi.org/10.1084/jem.20142290

Bain, C. R., Draxler, D. F., Taylor, R., Wallace, S., Gouldthorpe, O., Corcoran, T. B., Myles, P. S., L. Medcalf, R., & Bozaoglu, K. (2018). The early in-vivo effects of a single anti-emetic dose of dexamethasone on innate immune cell gene expression and activation in healthy volunteers. *Anaesthesia*, *73*(8), 955–966. https://doi.org/10.1111/anae.14306

Baleeiro, R. B., Anselmo, L. B., Soares, F. A., Pinto, C. A. L., Ramos, O., Gross, J. L., Haddad, F., Younes, R. N., Tomiyoshi, M. Y., Bergami-Santos, P. C., & Barbuto, J. A. M. (2008). High frequency of immature dendritic cells and altered in situ production of interleukin-4 and tumor necrosis factor-α in lung cancer. *Cancer Immunology, Immunotherapy*, *57*(9), 1335–1345. https://doi.org/10.1007/s00262-008-0468-7

Batchelor, T. T., Sorensen, A. G., di Tomaso, E., Zhang, W. T., Duda, D. G. G., Cohen, K. S., Kozak, K. R., Cahill, D. P., Chen, P. J., Zhu, M., Ancukiewicz, M., Mrugala, M. M., Plotkin, S., Drappatz, J., Louis, D. N., Ivy, P., Scadden, D. T. T., Benner, T., Loeffler, J. S., … Jain, R. K. (2007). AZD2171, a Pan-VEGF Receptor Tyrosine Kinase Inhibitor, Normalizes Tumor Vasculature and Alleviates Edema in Glioblastoma Patients. *Cancer Cell*, *11*(1), 83–95. https://doi.org/10.1016/j.ccr.2006.11.021

Benencia, F., Muccioli, M., & Alnaeeli, M. (2014). Perspectives on reprograming cancer-associated dendritic cells for anti-tumor therapies. *Frontiers in Oncology*, *4 APR*(April), 1–5. https://doi.org/10.3389/fonc.2014.00072

Berger, M. S., Bruce, J. N., Chen, T. C., & Zadeh, G. (2014). Glioblastoma: An update on pathophysiology and management strategies. *Neurosurgical Focus*, *37*(6), 14677. https://doi.org/10.3171/2014.9.FOCUS14677

Biro, M., Munoz, M. A., & Weninger, W. (2014). Targeting Rho-GTPases in immune cell migration and inflammation. *British Journal of Pharmacology*, *171*(24), 5491–5506. https://doi.org/10.1111/bph.12658

Blacher, E., Baruch, B. Ben, Levy, A., Geva, N., Green, K. D., Garneau-Tsodikova, S., Fridman, M., & Stein, R. (2015). Inhibition of glioma progression by a newly discovered CD38 inhibitor. *International Journal of Cancer*, *136*(6), 1422–1433. https://doi.org/10.1002/ijc.29095

Bradshaw, A., Wickremsekera, A., Tan, S. T., Peng, L., Davis, P. F., & Itinteang, T. (2016). Cancer Stem Cell Hierarchy in Glioblastoma Multiforme. *Frontiers in Surgery*, *3*(April), 1–15. https://doi.org/10.3389/fsurg.2016.00021

Breton, G., Zheng, S., Valieris, R., da Silva, I. T., Satija, R., & Nussenzweig, M. C. (2016). Human dendritic cells (DCs) are derived from distinct circulating precursors that are precommitted to become CD1c+ or CD141+ DCs. *Journal of Experimental Medicine*, *213*(13), 2861–2870. https://doi.org/10.1084/jem.20161135

Browaeys, R., Saelens, W., & Saeys, Y. (2020). NicheNet: modeling intercellular communication by linking ligands to target genes. In *Nature Methods* (Vol. 17, Issue 2, pp. 159–162). https://doi.org/10.1038/s41592-019-0667-5

Broz, M. L., Binnewies, M., Boldajipour, B., Nelson, A. E., Pollack, J. L., Erle, D. J., Barczak, A., Rosenblum, M. D., Daud, A., Barber, D. L., Amigorena, S., van'tVeer, L. J., Sperling, A. I., Wolf, D. M., & Krummel, M. F. (2014). Dissecting the Tumor Myeloid Compartment Reveals Rare Activating Antigen-Presenting Cells Critical for T Cell Immunity. *Cancer Cell*, *26*(5), 638–652. https://doi.org/10.1016/j.ccell.2014.09.007

Buchbinder, E. I., & Desai, A. (2016). CTLA-4 and PD-1 pathways similarities, differences, and implications of their inhibition. *American Journal of Clinical Oncology: Cancer Clinical Trials*, *39*(1), 98–106.

https://doi.org/10.1097/COC.0000000000000239

Cairncross, G., Wang, M., Shaw, E., Jenkins, R., Brachman, D., Buckner, J., Fink, K., Souhami, L., Laperriere, N., Curran, W., & Mehta, M. (2013). Phase III trial of chemoradiotherapy for anaplastic oligodendroglioma: Long-term results of RTOG 9402. *Journal of Clinical Oncology*, *31*(3), 337–343. https://doi.org/10.1200/JCO.2012.43.2674

Cao, W., & Bover, L. (2010). Signaling and ligand interaction of ILT7: Receptor-mediated regulatory mechanisms for plasmacytoid dendritic cells. *Immunological Reviews*, *234*(1), 163–176. https://doi.org/10.1111/j.0105-2896.2009.00867.x

Carenza, C., Calcaterra, F., Oriolo, F., Di Vito, C., Ubezio, M., Porta, M. G. Della, Mavilio, D., & Bella, S. Della. (2019). Costimulatory molecules and immune checkpoints are differentially expressed on different subsets of dendritic cells. *Frontiers in Immunology*, *10*(JUN), 1–15. https://doi.org/10.3389/fimmu.2019.01325

Carenza, C., Franzese, S., Calcaterra, F., Mavilio, D., & Della Bella, S. (2020). Comprehensive Phenotyping of Dendritic Cells in Cancer Patients by Flow Cytometry. *Cytometry Part A*, *6*, 1–13. https://doi.org/10.1002/cyto.a.24245

Carson, M. J., Doose, J. M., Melchior, B., Schmid, C. D., & Ploix, C. C. (2006). CNS immune privilege: Hiding in plain sight. *Immunological Reviews*, *213*(1), 48–65. https://doi.org/10.1111/j.1600-065X.2006.00441.x

Cheray, M., Bégaud, G., Deluche, E., Nivet, A., Battu, S., Lalloué, F., Verdier, M., Bessette, B. (2017). *Glioblastoma. Cancer StemLike Cells in Glioblastoma.* In: Glioblastoma. Brisbane: Codon Publications. pp 59-72.

Chiba, S., Baghdadi, M., Akiba, H., Yoshiyama, H., Kinoshita, I., Dosaka-Akita, H., Fujioka, Y., Ohba, Y., Gorman, J. V., Colgan, J. D., Hirashima, M., Uede, T., Takaoka, A., Yagita, H., & Jinushi, M. (2012). Tumor-infiltrating DCs suppress nucleic acid-mediated innate immune responses through interactions between the receptor TIM-3 and the alarmin HMGB1. *Nature Immunology*, *13*(9), 832–842. https://doi.org/10.1038/ni.2376

Collin, M., & Bigley, V. (2018). Human dendritic cell subsets: an update. *Immunology*, *154*(1), 3–20. https://doi.org/10.1111/imm.12888

Collin, M., Mcgovern, N., & Haniffa, M. (2013). Human dendritic cell subsets. *Immunology*, *140*(1), 22–30. https://doi.org/10.1111/imm.12117

Colonna M, Nakajima H, & Cella M. (2000). A family of inhibitory and activating Ig-like receptors that modulate function of lymphoid and myeloid cells. *Seminars in Immunology*, *12*, 121–127.

Colton, C. A. (2013). Immune heterogeneity in neuroinflammation: Dendritic cells in the brain. *Journal of Neuroimmune Pharmacology*, *8*(1), 145–162. https://doi.org/10.1007/s11481-012-9414-8

Curiel, T. J., Cheng, P., Mottram, P., Alvarez, X., Moons, L., Evdemon-Hogan, M., Wei, S., Zou, L., Kryczek, I., Hoyle, G., Lackner, A., Carmeliet, P., & Zou, W. (2004). Dendritic cell subsets differentially regulate angiogenesis in human ovarian cancer. *Cancer Research*, *64*(16), 5535–5538. https://doi.org/10.1158/0008-5472.CAN-04-1272

D'Agostino, P. M., Gottfried-Blackmore, A., Anandasabapathy, N., & Bulloch, K. (2012). Brain dendritic cells: Biology and pathology. *Acta Neuropathologica*, *124*(5), 599–614. https://doi.org/10.1007/s00401-012-1018-0

Darmanis, S., Sloan, S. A., Croote, D., Mignardi, M., Chernikova, S., Samghababi, P., Zhang, Y., Neff, N., Kowarsky, M., Caneda, C., Li, G., Chang, S. D., Connolly, I. D., Li, Y., Barres, B. A., Gephart, M. H., & Quake, S. R. (2017). Single-Cell RNA-Seq Analysis of Infiltrating Neoplastic Cells at the Migrating Front of Human Glioblastoma. *Cell Reports*, *21*(5), 1399–1410. https://doi.org/10.1016/j.celrep.2017.10.030

Davis, M. E. (2018). Epidemiology and Overview of Gliomas. *Seminars in Oncology Nursing*, *34*(5), 420–429. https://doi.org/10.1016/j.soncn.2018.10.001

de Mingo Pulido, Á., Gardner, A., Hiebler, S., Soliman, H., Rugo, H. S., Krummel, M. F., Coussens, L. M., & Ruffell, B. (2018). TIM-3 Regulates CD103+ Dendritic Cell Function and Response to Chemotherapy in Breast Cancer. *Cancer Cell*, *33*(1), 60-74.e6. https://doi.org/10.1016/j.ccell.2017.11.019

Della Bella, S., Nicola, S., Timofeeva, I., Villa, M. L., Santoro, A., & Berardi, A. C. (2004). Are interleukin-16 and thrombopoietin new tools for the in vitro generation of dendritic cells? *Blood*, *104*(13), 4020–4028. https://doi.org/10.1182/blood-2004-03-0885

Dey, M., Chang, A. L., Miska, J., Wainwright, D. A., Ahmed, A. U., Balyasnikova, I. V., Pytel, P., Han, Y., Tobias, A., Zhang, L., Qiao, J., & Lesniak, M. S. (2015). Dendritic Cell–Based Vaccines that Utilize Myeloid Rather than Plasmacytoid Cells Offer a Superior Survival Advantage in Malignant Glioma. *The Journal of Immunology*, *195*(1), 367–376. https://doi.org/10.4049/jimmunol.1401607

Dimitrov, L., Hong, C. S., Yang, C., Zhuang, Z., & Heiss, J. D. (2015). New developments in the pathogenesis and therapeutic targeting of the IDH1 mutation in glioma. *International Journal of Medical Sciences*, *12*(3), 201–213.

https://doi.org/10.7150/ijms.11047

Dolecek, T. A., Propp, J. M., Stroup, N. E., & Kruchko, C. (2012). CBTRUS statistical report: Primary brain and central nervous system tumors diagnosed in the United States in 2005-2009. *Neuro-Oncology*, *14*(SUPPL.5). https://doi.org/10.1093/neuonc/nos218

Domogalla, M. P., Rostan, P. V., Raker, V. K., & Steinbrink, K. (2017). Tolerance through education: How tolerogenic dendritic cells shape immunity. *Frontiers in Immunology*, *8*(DEC), 1–14. https://doi.org/10.3389/fimmu.2017.01764

Donahue, R. N., Lepone, L. M., Grenga, I., Jochems, C., Fantini, M., Madan, R. A., Heery, C. R., Gulley, J. L., & Schlom, J. (2017). Analyses of the peripheral immunome following multiple administrations of avelumab, a human IgG1 anti-PD-L1 monoclonal antibody. *Journal for ImmunoTherapy of Cancer*, *5*(1), 1–16. https://doi.org/10.1186/s40425-017-0220-y

Dumont, N. A., Wang, Y. X., Von Maltzahn, J., Pasut, A., Bentzinger, C. F., Brun, C. E., & Rudnicki, M. A. (2015). Dystrophin expression in muscle stem cells regulates their polarity and asymmetric division. *Nature Medicine*, *21*(12), 1455–1463. https://doi.org/10.1038/nm.3990

Dutertre, C. A., Becht, E., Irac, S. E., Khalilnezhad, A., Narang, V., Khalilnezhad, S., Ng, P. Y., van den Hoogen, L. L., Leong, J. Y., Lee, B., Chevrier, M., Zhang, X. M., Yong, P. J. A., Koh, G., Lum, J., Howland, S. W., Mok, E., Chen, J., Larbi, A., … Ginhoux, F. (2019). Single-Cell Analysis of Human Mononuclear Phagocytes Reveals Subset-Defining Markers and Identifies Circulating Inflammatory Dendritic Cells. *Immunity*, *51*(3), 573-589.e8. https://doi.org/10.1016/j.immuni.2019.08.008

Edilova, M. I., Abdul-Sater, A. A., & Watts, T. H. (2018). TRAF1 Signaling in Human Health and Disease. *Frontiers in Immunology*, *9*(December), 2969. https://doi.org/10.3389/fimmu.2018.02969

Eisenbarth, S. C. (2019). Dendritic cell subsets in T cell programming: location dictates function. *Nature Reviews Immunology*, *19*(2), 89–103. https://doi.org/10.1038/s41577-018-0088-1

Eljamel, M. S., Goodman, C., & Moseley, H. (2008). ALA and Photofrin® Fluorescence-guided resection and repetitive PDT in glioblastoma multiforme: A single centre Phase III randomised controlled trial. *Lasers in Medical Science*, *23*(4), 361–367. https://doi.org/10.1007/s10103-007-0494-2

Fernandes, C., Costa, A., Osório, L., Lago, RC., Linhares, P., Carvalho. B., Caeiro, C. (2017). "Glioblastoma. Current Standards of Care in Glioblastoma Therapy. In: Glioblastoma. Brisbane: Codon Publications. pp. 197-242.

Franchimont, D. (2004). Overview of the actions of glucocorticoids on the immune response: A good model to characterize new pathways of immunosuppression for new treatment strategies. *Annals of the New York Academy of Sciences*, *1024*, 124–137. https://doi.org/10.1196/annals.1321.009

Gabrilovich, D. I., Chen, H. L., Girgis, K. R., Cunningham, H. T., Meny, G. M., Nadaf, S., Kavanaugh, D., & Carbone, D. P. (1996). Production of vascular endothelial growth factor by human tumors inhibits the functional maturation of dendritic cells. *Nature Medicine*, *2*(10), 1096–1103. https://doi.org/10.1038/nm1096-1096

Gabrilovich, D., Ishida, T., Oyama, T., Ran, S., Kravtsov, V., Nadaf, S., & Carbone, D. P. (1998). Vascular endothelial growth factor inhibits the development of dendritic cells and dramatically affects the differentiation of multiple hematopoietic lineages in vivo. *Blood*, *92*(11), 4150–4166. https://doi.org/10.1182/blood.v92.11.4150

Garg, A. D., Coulie, P. G., Van den Eynde, B. J., & Agostinis, P. (2017). Integrating Next-Generation Dendritic Cell Vaccines into the Current Cancer Immunotherapy Landscape. *Trends in Immunology*, *38*(8), 577–593. https://doi.org/10.1016/j.it.2017.05.006

Garg, A. D., Vandenberk, L., Koks, C., Verschuere, T., Boon, L., Van Gool, S. W., & Agostinis, P. (2016). Dendritic cell vaccines based on immunogenic cell death elicit danger signals and T cell-driven rejection of high-grade glioma. *Science Translational Medicine*, *8*(328), 1–16. https://doi.org/10.1126/scitranslmed.aae0105

Gousias, K., von Ruecker, A., Voulgari, P., & Simon, M. (2013). Phenotypical analysis, relation to malignancy and prognostic relevance of ICOS + T regulatory and dendritic cells in patients with gliomas. *Journal of Neuroimmunology*, *264*(1–2), 84–90. https://doi.org/10.1016/j.jneuroim.2013.09.001

Grimm, S. A., & Chamberlain, M. C. (2016). CNS Oncology Anaplastic astrocytoma. *CNS Oncology*, *5*, 145–157.

Harizi, H., & Gualde, N. (2005). The impact of eicosanoids on the crosstalk between innate and adaptive immunity: The key roles of dendritic cells. *Tissue Antigens*, *65*(6), 507–514. https://doi.org/10.1111/j.1399-0039.2005.00394.x

Hart, M. G., Grant, G. R. L., Solyom, E. F., & Grant, R. (2019). Biopsy versus resection for high-grade glioma. *Cochrane Database of Systematic Reviews*, *2019*(6). https://doi.org/10.1002/14651858.CD002034.pub2

Hodi, F.S., O'Day, S.J., McDermott, D.F., et al. (2010). Improved survival with ipilimumab in patients with metastatic melanoma [published correction appears in N Engl J Med. 2010 Sep 23;363(13):1290]. N Engl J Med. 363(8):711-723. https://doi:10.1056/NEJMoa1003466

Hussain, S. F., Yang, D., Suki, D., Aldape, K., Grimm, E., & Heimberger, A. B. (2006). The role of human glioma-infiltrating microglia/macrophages in mediating antitumor immune responses. *Neuro-Oncology*, *8*(3), 261–279. https://doi.org/10.1215/15228517-2006-008

Hwang, B., Lee, J. H., & Bang, D. (2018). Single-cell RNA sequencing technologies and bioinformatics pipelines. *Experimental and Molecular Medicine*, *50*(8). https://doi.org/10.1038/s12276-018-0071-8

Illario, M., Giardino-Torchia, M. L., Sankar, U., Ribar, T. J., Galgani, M., Vitiello, L., Masci, A. M., Bertani, F. R., Ciaglia, E., Astone, D., Maulucci, G., Cavallo, A., Vitale, M., Cimini, V., Pastore, L., Means, A. R., Rossi, G., & Racioppi, L. (2008). Calmodulin-dependent kinase IV links Toll-like receptor 4 signaling with survival pathway of activated dendritic cells. *Blood*, *111*(2), 723–731. https://doi.org/10.1182/blood-2007-05-091173

Jiang, S., Li, X., Hess, N. J., Guan, Y., & Tapping, R. I. (2016). TLR10 Is a Negative Regulator of Both MyD88-Dependent and -Independent TLR Signaling. *The Journal of Immunology*, *196*(9), 3834–3841. https://doi.org/10.4049/jimmunol.1502599

Johanson, C., Stopa, E., Mcmillan, P., Roth, D., Funk, J., & Krinke, G. (2011). The Distributional Nexus of Choroid Plexus to Cerebrospinal Fluid, Ependyma and Brain:Toxicologic/Pathologic Phenomena, Periventricular Destabilization, and Lesion Spread. *Toxicologic Pathology*, *39*(1), 186–212. https://doi.org/10.1177/0192623310394214

Ju, X. S., Hacker, C., Scherer, B., Redecke, V., Berger, T., Schuler, G., Wagner, H., Lipford, G. B., & Zenke, M. (2004). Immunoglobulin-like transcripts ILT2, ILT3 and ILT7 are expressed by human dendritic cells and down-regulated following activation. *Gene*, *331*(1–2), 159–164. https://doi.org/10.1016/j.gene.2004.02.018

Kaminska, B., Czapski, B., Guzik, R., Król, S. K., & Gielniewski, B. (2019). Consequences of IDH1/2 mutations in gliomas and an assessment of inhibitors targeting mutated IDH proteins. *Molecules*, *24*(5), 1–17. https://doi.org/10.3390/molecules24050968

Kawakami, Y., Inagaki, N., Salek-Ardakani, S., Kitaura, J., Tanaka, H., Nagao, K., Kawakami, Y., Xiao, W., Nagai, H., Croft, M., & Kawakami, T. (2006). Regulation of dendritic cell maturation and function by Bruton's tyrosine kinase via IL-10 and Stat3. *Proceedings of the National Academy of Sciences of the United States of America*, *103*(1), 153–158. https://doi.org/10.1073/pnas.0509784103

Kim, J. E., Patel, M. A., Mangraviti, A., Kim, E. S., Theodros, D., Velarde, E., Liu, A., Sankey, E. W., Tam, A., Xu, H., Mathios, D., Jackson, C. M., Harris-Bookman, S., Garzon-Muvdi, T., Sheu, M., Martin, A. M., Tyler, B. M., Tran, P. T., Ye, X., … Lim, M. (2017). Combination therapy with anti-PD-1, anti-TIM-3, and focal radiation results in regression of murine gliomas. *Clinical Cancer Research*, *23*(1), 124–136. https://doi.org/10.1158/1078-0432.CCR-15-1535

Knudsen, E. S., & Wang, J. Y. J. (2010). Targeting the RB-pathway in cancer therapy. *Clinical Cancer Research*, *16*(4), 1094–1099. https://doi.org/10.1158/1078-0432.CCR-09-0787

Kolodziejczyk, A. A., Kim, J. K., Tsang, J. C. H., Ilicic, T., Henriksson, J., Natarajan, K. N., Tuck, A. C., Gao, X., Bühler, M., Liu, P., Marioni, J. C., & Teichmann, S. A. (2015). Single Cell RNA-Sequencing of Pluripotent States Unlocks Modular Transcriptional Variation. *Cell Stem Cell*, *17*(4), 471–485. https://doi.org/10.1016/j.stem.2015.09.011

Koul, D. (2008). PTEN signaling pathways in glioblastoma. *Cancer Biology and Therapy*, *7*(9), 1321–1325. https://doi.org/10.4161/cbt.7.9.6954

Kurts, C., Robinson, B. W. S., & Knolle, P. A. (2010). Cross-priming in health and disease. *Nature Reviews Immunology*, *10*(6), 403–414. https://doi.org/10.1038/nri2780

Lande, R., Gafa, V., Serafini, B., Giacomini, E., Visconti, A., Remoli, M. E., Severa, M., Parmentier, M., Ristori, G., Salvetti, M., Aloisi, F., & Coccia, E. M. (2008). Plasmacytoid dendritic cells in multiple sclerosis: Intracerebral recruitment and impaired maturation in response to interferon-β. *Journal of Neuropathology and Experimental Neurology*, *67*(5), 388–401. https://doi.org/10.1097/NEN.0b013e31816fc975

Larkin, J., Chiarion-Sileni, V., Gonzalez, R., Grob, J. J., Cowey, C. L., Lao, C. D., Schadendorf, D., Dummer, R., Smylie, M., Rutkowski, P., Ferrucci, P. F., Hill, A., Wagstaff, J., Carlino, M. S., Haanen, J. B., Maio, M., Marquez-Rodas, I., McArthur, G. A., Ascierto, P. A., … Wolchok, J. D. (2015). Combined Nivolumab and Ipilimumab or Monotherapy in Untreated Melanoma. *New England Journal of Medicine*, *373*(1), 23–34. https://doi.org/10.1056/nejmoa1504030

Le Rhun, E., Taillibert, S., & Chamberlain, M. (2015). The future of high-grade glioma: Where we are and where are we

going. *Surgical Neurology International*, *6*(2), S9–S44. https://doi.org/10.4103/2152-7806.151331

Leone, D. A., Peschel, A., Brown, M., Schachner, H., Ball, M. J., Gyuraszova, M., Salzer-Muhar, U., Fukuda, M., Vizzardelli, C., Bohle, B., Rees, A. J., & Kain, R. (2017). Surface LAMP-2 Is an Endocytic Receptor That Diverts Antigen Internalized by Human Dendritic Cells into Highly Immunogenic Exosomes. *The Journal of Immunology*, *199*(2), 531–546. https://doi.org/10.4049/jimmunol.1601263

Linxweiler, M., Schick, B., & Zimmermann, R. (2017). Let's talk about secs: Sec61, sec62 and sec63 in signal transduction, oncology and personalized medicine. *Signal Transduction and Targeted Therapy*, *2*(January), 1–10. https://doi.org/10.1038/sigtrans.2017.2

Liu, T., Zhang, L., Joo, D., & Sun, S. C. (2017). NF-κB signaling in inflammation. *Signal Transduction and Targeted Therapy*, *2*(April). https://doi.org/10.1038/sigtrans.2017.23

Locarno, C. V., Simonelli, M., Carenza, C., Capucetti, A., Stanzani, E., Lorenzi, E., Persico, P., Della Bella, S., Passoni, L., Mavilio, D., Bonecchi, R., Locati, M., & Savino, B. (2020). Role of myeloid cells in the immunosuppressive microenvironment in gliomas. *Immunobiology*, *225*(1), 151853. https://doi.org/10.1016/j.imbio.2019.10.002

Lombardi, M.Y., Assem, M. (2017). Glioblastoma Genomics: A Very Complicated Story. In: Glioblastoma. Brisbane: Codon Publications. pp3-26.

López-Colomé, A. M., Lee-Rivera, I., Benavides-Hidalgo, R., & López, E. (2017). Paxillin: A crossroad in pathological cell migration. *Journal of Hematology and Oncology*, *10*(1), 1–15. https://doi.org/10.1186/s13045-017-0418-y

Louis, D. N., Perry, A., Reifenberger, G., von Deimling, A., Figarella-Branger, D., Cavenee, W. K., Ohgaki, H., Wiestler, O. D., Kleihues, P., & Ellison, D. W. (2016). The 2016 World Health Organization Classification of Tumors of the Central Nervous System: a summary. *Acta Neuropathologica*, *131*(6), 803–820. https://doi.org/10.1007/s00401-016-1545-1

Louveau, A., Harris, T. H., & Kipnis, J. (2015). Revisiting the Mechanisms of CNS Immune Privilege. *Trends in Immunology*, *36*(10), 569–577. https://doi.org/10.1016/j.it.2015.08.006

Louveau, A., Smirnov, I., Keyes, T. J., Eccles, J. D., Rouhani, S. J., Peske, J. D., Derecki, N. C., Castle, D., Mandell, J. W., Lee, K. S., Harris, T. H., & Kipnis, J. (2015). Structural and functional features of central nervous system lymphatic vessels. *Nature*, *523*(7560), 337–341. https://doi.org/10.1038/nature14432

Lu, C., Ward, P. S., Kapoor, G. S., Rohle, D., Turcan, S., Abdel-Wahab, O., Edwards, C. R., Khanin, R., Figueroa, M. E., Melnick, A., Wellen, K. E., Oğrourke, D. M., Berger, S. L., Chan, T. A., Levine, R. L., Mellinghoff, I. K., & Thompson, C. B. (2012). IDH mutation impairs histone demethylation and results in a block to cell differentiation. *Nature*, *483*(7390), 474–478. https://doi.org/10.1038/nature10860

Lukas, R. V., Wainwright, D. A., Horbinski, C. M., Iwamoto, F. M., & Sonabend, A. M. (2019). Immunotherapy Against Gliomas: is the Breakthrough Near? *Drugs*, *79*(17), 1839–1848. https://doi.org/10.1007/s40265-019-01203-z

Lun, M. P., Monuki, E. S., & Lehtinen, M. K. (2015). Development and functions of the choroid plexus-cerebrospinal fluid system. *Nature Reviews Neuroscience*, *16*(8), 445–457. https://doi.org/10.1038/nrn3921

Ma, D. Y., & Clark, E. A. (2009). The role of CD40 and CD40L in Dendritic Cells. *Semin Immunol*, *21*(5), 265–272. https://doi.org/10.1016/j.smim.2009.05.010.The

Macri, C., Pang, E. S., Patton, T., & O'Keeffe, M. (2018). Dendritic cell subsets. *Seminars in Cell and Developmental Biology*, *84*, 11–21. https://doi.org/10.1016/j.semcdb.2017.12.009

Maier, B., Leader, A. M., Chen, S. T., Tung, N., Chang, C., LeBerichel, J., Chudnovskiy, A., Maskey, S., Walker, L., Finnigan, J. P., Kirkling, M. E., Reizis, B., Ghosh, S., D'Amore, N. R., Bhardwaj, N., Rothlin, C. V., Wolf, A., Flores, R., Marron, T., … Merad, M. (2020). A conserved dendritic-cell regulatory program limits antitumour immunity. *Nature*, *580*(7802), 257–262. https://doi.org/10.1038/s41586-020-2134-y

Mansouri, A., Hachem, L. D., Mansouri, S., Nassiri, F., Laperriere, N. J., Xia, D., Lindeman, N. I., Wen, P. Y., Chakravarti, A., Mehta, M. P., Hegi, M. E., Stupp, R., Aldape, K. D., & Zadeh, G. (2019). MGMT promoter methylation status testing to guide therapy for glioblastoma: Refining the approach based on emerging evidence and current challenges. *Neuro-Oncology*, *21*(2), 167–178. https://doi.org/10.1093/neuonc/noy132

Mariathasan, S., Turley, S. J., Nickles, D., Castiglioni, A., Yuen, K., Wang, Y., Kadel, E. E., Koeppen, H., Astarita, J. L., Cubas, R., Jhunjhunwala, S., Banchereau, R., Yang, Y., Guan, Y., Chalouni, C., Ziai, J., Şenbabaoğlu, Y., Santoro, S., Sheinson, D., … Powles, T. (2018). TGFβ attenuates tumour response to PD-L1 blockade by contributing to exclusion of T cells. *Nature*, *554*(7693), 544–548. https://doi.org/10.1038/nature25501

McInnes, L., Healy, J., & Melville, J. (2018). UMAP: Uniform manifold approximation and projection for dimension reduction. *ArXiv*.

McLendon, R., Friedman, A., Bigner, D., Van Meir, E. G., Brat, D. J., Mastrogianakis, G. M., Olson, J. J., Mikkelsen, T., Lehman, N., Aldape, K., Yung, W. K. A., Bogler, O., Weinstein, J. N., VandenBerg, S., Berger, M., Prados, M., Muzny, D., Morgan, M., Scherer, S., … Thomson, E. (2008). Comprehensive genomic characterization defines human glioblastoma genes and core pathways. *Nature*, *455*(7216), 1061–1068. https://doi.org/10.1038/nature07385

Melendez, J., Grogg, M., & Zheng, Y. (2011). Signaling role of Cdc42 in regulating mammalian physiology. *Journal of Biological Chemistry*, *286*(4), 2375–2381. https://doi.org/10.1074/jbc.R110.200329

Mellman, I. (2013). Dendritic cells: master regulators of the immune response. *Cancer Immunology Research*, *1*(3), 145–149. https://doi.org/10.1158/2326-6066.CIR-13-0102

Miao, Y., Jiang, M., Qi, L., Yang, D., Xiao, W., & Fang, F. (2020). BCAP Regulates Dendritic Cell Maturation Through the Dual-Regulation of NF-κB and PI3K/AKT Signaling During Infection. *Frontiers in Immunology*, *11*(February), 1–13. https://doi.org/10.3389/fimmu.2020.00250

Micheletti, A., Finotti, G., Calzetti, F., Lonardi, S., Zoratti, E., Bugatti, M., Stefini, S., Vermi, W., & Cassatella, M. A. (2016). slan/M-DC8+ cells constitute a distinct subset of dendritic cells in human tonsils. *Oncotarget*, *7*(1), 161–175. https://doi.org/10.18632/ONCOTARGET.6660

Mitchell, D. A., Batich, K. A., Gunn, M. D., Huang, M. N., Sanchez-Perez, L., Nair, S. K., Congdon, K. L., Reap, E. A., Archer, G. E., Desjardins, A., Friedman, A. H., Friedman, H. S., Herndon, J. E., Coan, A., McLendon, R. E., Reardon, D. A., Vredenburgh, J. J., Bigner, D. D., & Sampson, J. H. (2015). Tetanus toxoid and CCL3 improve dendritic cell vaccines in mice and glioblastoma patients. *Nature*, *519*(7543), 366–369. https://doi.org/10.1038/nature14320

Möller, M., Turzer, S., Schütte, W., Seliger, B., & Riemann, D. (2020). Blood Immune Cell Biomarkers in Patient with Lung Cancer Undergoing Treatment with Checkpoint Blockade. *Journal of Immunotherapy*, *43*(2), 57–66. https://doi.org/10.1097/CJI.0000000000000297

Monsiváis-Urenda, A., Gómez-Martin, D., Santana-de-Anda, K., Cruz-Martínez, J., Alcocer-Varela, J., & González-Amaro, R. (2013). Defective expression and function of the ILT2/CD85j regulatory receptor in dendritic cells from patients with systemic lupus erythematosus. *Human Immunology*, *74*(9), 1088–1096. https://doi.org/10.1016/j.humimm.2013.05.006

Mueller, W. M., Yetkin, F. Z., Hammeke, T. A., Morris, G. L., Swanson, S. J., Reichert, K., Cox, R., & Haughton, V. M. (1996). Functional magnetic resonance imaging mapping of the motor cortex in patients with cerebral tumors. *Neurosurgery*, *39*(3), 515–521. https://doi.org/10.1227/00006123-199609000-00015

Munn, D. H., Sharma, M. D., Hou, D., Baban, B., Lee, J. R., Antonia, S. J., Messina, J. L., Chandler, P., Koni, P. A., & Mellor, A. L. (2004). Expression of indoleamine 2,3-dioxygenase by plasmacytoid dendritic cells in tumor-draining lymph nodes. *Journal of Clinical Investigation*, *114*(2), 280–290. https://doi.org/10.1172/JCI200421583

Nobes, C., & Marsh, M. (2000). Dendritic cells: New roles for Cdc42 and Rac in antigen uptake? *Current Biology*, *10*(20), 739–741. https://doi.org/10.1016/S0960-9822(00)00736-3

O'Keeffe, M., Mok, W. H., & Radford, K. J. (2015). Human dendritic cell subsets and function in health and disease. *Cellular and Molecular Life Sciences*, *72*(22), 4309–4325. https://doi.org/10.1007/s00018-015-2005-0

Ostrom, Q. T., Gittleman, H., Farah, P., Ondracek, A., Chen, Y., Wolinsky, Y., Stroup, N. E., Kruchko, C., & Barnholtz-Sloan, J. S. (2013). CBTRUS statistical report: Primary brain and central nervous system tumors diagnosed in the United States in 2006-2010. *Neuro-Oncology*, *15*(SUPPL.2). https://doi.org/10.1093/neuonc/not151

Oyoshi, M. K., Barthel, R., & Tsitsikov, E. N. (2007). TRAF1 regulates recruitment of lymphocytes and, to a lesser extent, neutrophils, myeloid dendritic cells and monocytes to the lung airways following lipopolysaccharide inhalation. *Immunology*, *120*(3), 303–314. https://doi.org/10.1111/j.1365-2567.2006.02499.x

Palucka, K., & Banchereau, J. (2012). Cancer immunotherapy via dendritic cells. *Nature Reviews Cancer*, *12*(4), 265–277. https://doi.org/10.1038/nrc3258

Parsons, D. W., Jones, S., Zhang, X., Lin, J. C. H., Leary, R. J., Angenendt, P., Mankoo, P., Carter, H., Siu, I. M., Gallia, G. L., Olivi, A., McLendon, R., Rasheed, B. A., Keir, S., Nikolskaya, T., Nikolsky, Y., Busam, D. A., Tekleab, H., Diaz, L. A., … Kinzler, K. W. (2008). An integrated genomic analysis of human glioblastoma multiforme. *Science*, *321*(5897), 1807–1812. https://doi.org/10.1126/science.1164382

Pellerino A, Franchino F, Soffietti R, Rudà R. Overview on current treatment standards in high-grade gliomas. Q J Nucl Med Mol Imaging. 2018;62(3):225-238. https://doi:10.23736/S1824-4785.18.03096-0.

Pitter, K. L., Tamagno, I., Alikhanyan, K., Hosni-Ahmed, A., Pattwell, S. S., Donnola, S., Dai, C., Ozawa, T., Chang, M., Chan, T. A., Beal, K., Bishop, A. J., Barker, C. A., Jones, T. S., Hentschel, B., Gorlia, T., Schlegel, U., Stupp,

R., Weller, M., … Hambardzumyan, D. (2016). Corticosteroids compromise survival in glioblastoma. *Brain*, *139*(5), 1458–1471. https://doi.org/10.1093/brain/aww046

Platten, M., Schilling, D., Bunse, L., Wick, A., Bunse, T., Riehl, D., Green, E., Sanghvi, K., Karapanagiotou-Schenkel, I., Harting, I., Sahm, F., Steinbach, J., Weyerbrock, A., Hence, J., Misch, M., Krex, D., Stevanovic, S., Tabatabai, G., Von Deimling, A., Schmitt, M., Wick, W. (2018). A first-in-man multicenter phase i clinical trial of the german neurooncology working group evaluating a mutation-specific peptide vaccine targeting idh1r132h in patients with newly diagnosed malignant astrocytomas. Neuro Oncol. Nov;20(Suppl 6):Vi8–9. Epub 2018 Nov 5. https://doi:10.1093/Neuonc/Noy148.028

Polívka, J., Pešta, M., Pitule, P., Hes, O., Holubec, L., Polívka, J., Kubíková, T., & Tonar, Z. (2018). IDH1 mutation is associated with lower expression of VEGF but not microvessel formation in glioblastoma multiforme. *Oncotarget*, *9*(23), 16462–16476. https://doi.org/10.18632/oncotarget.24536

Prabhakar, U., Maeda, H., K. Jain, R., Sevick-Muraca, E. M., Zamboni, W., Farokhzad, O. C., Barry, S. T., Gabizon, A., Grodzinski, P., & Blakey, D. C. (2013). Challenges and key considerations of the enhanced permeability and retention effect for nanomedicine drug delivery in oncology. *Cancer Research*, *73*(8), 2412–2417. https://doi.org/10.1158/0008-5472.CAN-12-4561

Preusser, M., De Ribaupierre, S., Wöhrer, A., Erridge, S. C., Hegi, M., Weller, M., & Stupp, R. (2011). Current concepts and management of glioblastoma. *Annals of Neurology*, *70*(1), 9–21. https://doi.org/10.1002/ana.22425

Preusser, M., Lim, M., Hafler, D. A., Reardon, D. A., & Sampson, J. H. (2015). Prospects of immune checkpoint modulators in the treatment of glioblastoma. *Nature Reviews Neurology*, *11*(9), 504–514. https://doi.org/10.1038/nrneurol.2015.139

Prins, R. M., Soto, H., Konkankit, V., Odesa, S. K., Eskin, A., Yong, W. H., Nelson, S. F., & Liau, L. M. (2011). Gene expression profile correlates with T-cell infiltration and relative survival in glioblastoma patients vaccinated with dendritic cell immunotherapy. *Clinical Cancer Research*, *17*(6), 1603–1615. https://doi.org/10.1158/1078-0432.CCR-10-2563

Quail, D. F., & Joyce, J. A. (2017). The Microenvironmental Landscape of Brain Tumors. *Cancer Cell*, *31*(3), 326–341. https://doi.org/10.1016/j.ccell.2017.02.009

Rampling, R., Peoples, S., Mulholland, P. J., James, A., Al-Salihi, O., Twelves, C. J., McBain, C., Jefferies, S., Jackson, A., Stewart, W., Lindner, J., Kutscher, S., Hilf, N., McGuigan, L., Peters, J., Hill, K., Schoor, O., Singh-Jasuja, H., Halford, S. E., & Ritchie, J. W. A. (2016). A cancer research UK first time in human phase i trial of IMA950 (novel multipeptide therapeutic vaccine) in patients with newly diagnosed glioblastoma. *Clinical Cancer Research*, *22*(19), 4776–4785. https://doi.org/10.1158/1078-0432.CCR-16-0506

Ransohoff, R. M., & Engelhardt, B. (2012). The anatomical and cellular basis of immune surveillance in the central nervous system. *Nature Reviews Immunology*, *12*(9), 623–635. https://doi.org/10.1038/nri3265

Raslan, A., & Bhardwaj, A. (2007). Management of cerebral Edema. *Neurosurgical Focus*, *22*(5), 1–12. https://doi.org/10.1542/pir.4-7-217

Reizis, B. (2019). Plasmacytoid Dendritic Cells: Development, Regulation, and Function. *Immunity*, *50*(1), 37–50. https://doi.org/10.1016/j.immuni.2018.12.027

Ronkainen, J., & Tervonen, O. (2006). Cost analysis of an open low-field (0.23T) MRI unit: Effect of procedure shares in combined imaging, interventional, and neurosurgical use. *Acta Radiologica*, *47*(4), 359–365. https://doi.org/10.1080/02841850500537698

Saeed, M., Gao, J., Shi, Y., Lammers, T., & Yu, H. (2019). Engineering nanoparticles to reprogram the tumor immune microenvironment for improved cancer immunotherapy. *Theranostics*, *9*(26), 7981–8000. https://doi.org/10.7150/thno.37568

Sajiki, K., Tahara, Y., Uehara, L., Sasaki, T., Pluskal, T., & Yanagida, M. (2018). Genetic regulation of mitotic competence in G0 quiescent cells. *Science Advances*, *4*(8), 1–9. https://doi.org/10.1126/sciadv.aat5685

Sallusto, F., & Lanzavecchia, A. (2002). The instructive role of dendritic cells on T-cell responses. *Arthritis Research*, *4*, S127–S132. https://doi.org/10.1186/ar567

Sander, J., Schmidt, S. V., Cirovic, B., McGovern, N., Papantonopoulou, O., Hardt, A. L., Aschenbrenner, A. C., Kreer, C., Quast, T., Xu, A. M., Schmidleithner, L. M., Theis, H., Thi Huong, L. Do, Sumatoh, H. R. Bin, Lauterbach, M. A. R., Schulte-Schrepping, J., Günther, P., Xue, J., Baßler, K., … Schultze, J. L. (2017). Cellular Differentiation of Human Monocytes Is Regulated by Time-Dependent Interleukin-4 Signaling and the Transcriptional Regulator NCOR2. *Immunity*, *47*(6), 1051-1066.e12. https://doi.org/10.1016/j.immuni.2017.11.024

Santos, and B. (2018). Dendritic cell-based cancer vaccines. *The Journal of Immunology*, *200*, 443–449. https://doi.org/10.4049/jimmunol.1701024

Sasaki, M., Knobbe, C. B., Itsumi, M., Elia, A. J., Harris, I. S., Chio, I. I. C., Cairns, R. A., Mccracken, S., Wakeham, A., Haight, J., Ten, A. Y., Snow, B., Ueda, T., Inoue, S., Yamamoto, K., Ko, M., Rao, A., Yen, K. E., Su, S. M., & Mak, T. W. (2012). D-2-hydroxyglutarate produced by mutant Idh1 perturbs collagen maturation and basement membrane function. *Genes and Development*, *26*(18), 2038–2049. https://doi.org/10.1101/gad.198200.112

Schittenhelm, L., Hilkens, C. M., & Morrison, V. L. (2017). B2 Integrins As Regulators of Dendritic Cell, Monocyte, and Macrophage Function. *Frontiers in Immunology*, *8*(DEC). https://doi.org/10.3389/fimmu.2017.01866

Schlitzer, A., McGovern, N., & Ginhoux, F. (2015). Dendritic cells and monocyte-derived cells: Two complementary and integrated functional systems. *Seminars in Cell and Developmental Biology*, *41*, 9–22. https://doi.org/10.1016/j.semcdb.2015.03.011

Segura, E., & Amigorena, S. (2013). Inflammatory dendritic cells in mice and humans. *Trends in Immunology*, *34*(9), 440–445. https://doi.org/10.1016/j.it.2013.06.001

Seliger, C., Luber, C., Gerken, M., Schaertl, J., Proescholdt, M., Riemenschneider, M. J., Meier, C. R., Bogdahn, U., Leitzmann, M. F., Klinkhammer-Schalke, M., & Hau, P. (2019). Use of metformin and survival of patients with high-grade glioma. *International Journal of Cancer*, *144*(2), 273–280. https://doi.org/10.1002/ijc.31783

Serot, J. M., Foliguet, B., Béné, M. C., & Faure, G. C. (1997). Ultrastructural and immunohistological evidence for dendritic-like cells within human choroid plexus epithelium. *NeuroReport*, *8*(8), 1995–1998. https://doi.org/10.1097/00001756-199705260-00039

Shurin, G. V., Tourkova, I. L., Chatta, G. S., Schmidt, G., Wei, S., Djeu, J. Y., & Shurin, M. R. (2005). Small Rho GTPases Regulate Antigen Presentation in Dendritic Cells. *The Journal of Immunology*, *174*(6), 3394–3400. https://doi.org/10.4049/jimmunol.174.6.3394

Simonelli, M., Persico, P., Perrino, M., Zucali, P. A., Navarria, P., Pessina, F., Scorsetti, M., Bello, L., & Santoro, A. (2018). Checkpoint inhibitors as treatment for malignant gliomas: "A long way to the top." *Cancer Treatment Reviews*, *69*(March), 121–131. https://doi.org/10.1016/j.ctrv.2018.06.016

Simonetti, G., Gaviani, P., Botturi, A., Innocenti, A., Lamperti, E., & Silvani, A. (2015). Clinical management of grade III oligodendroglioma. *Cancer Management and Research*, *7*, 213–223. https://doi.org/10.2147/CMAR.S56975

Sorensen, A. G., Batchelor, T. T., Zhang, W. T., Chen, P. J., Yeo, P., Wang, M., Jennings, D., Wen, P. Y., Lahdenranta, J., Ancukiewicz, M., Di Tomaso, E., Duda, D. G., & Jain, R. K. (2009). A "vascular normalization index" as potential mechanistic biomarker to predict survival after a single dose of cediranib in recurrent glioblastoma patients. *Cancer Research*, *69*(13), 5296–5300. https://doi.org/10.1158/0008-5472.CAN-09-0814

Srivastava, S., Jackson, C., Kim, T., Choi, J., & Lim, M. (2019). A characterization of dendritic cells and their role in immunotherapy in glioblastoma: From preclinical studies to clinical trials. *Cancers*, *11*(4). https://doi.org/10.3390/cancers11040537

Stupp, R., Mason, W. P., van den Bent, M. J., Weller, M., Fisher, B., Taphoorn, M. J. B., Belanger, K., Brandes, A. A., Marosi, C., Bogdahn, U., Curschmann, J., Janzer, R. C., Ludwin, S. K., Gorlia, T., Allgeier, A., Lacombe, D., Cairncross, J. G., Eisenhauer, E., & Mirimanoff, R. O. (2005). Radiotherapy plus Concomitant and Adjuvant Temozolomide for Glioblastoma. *New England Journal of Medicine*, *352*(10), 987–996. https://doi.org/10.1056/nejmoa043330

Suárez-García, J. G., Hernández-López, J. M., Moreno-Barbosa, E., & de Celis-Alonso, B. (2020). A simple model for glioma grading based on texture analysis applied to conventional brain MRI. *PLoS ONE*, *15*(5), 1–19. https://doi.org/10.1371/journal.pone.0228972

Sugawa, N., Ekstrand, A. J., James, C. D., & Collins, V. P. (1990). Identical splicing of aberrant epidermal growth factor receptor transcripts from amplified rearranged genes in human glioblastomas. *Proceedings of the National Academy of Sciences of the United States of America*, *87*(21), 8602–8606. https://doi.org/10.1073/pnas.87.21.8602

Tamimi, A.F., Juweid M. (2017). *Glioblastoma. Epidemiology and Outcome of Glioblastoma.* In: Glioblastoma. Brisbane: Codon Publications. pp143154.

Tamura, T., Kurotaki, D., & Koizumi, S. ichi. (2015). Regulation of myelopoiesis by the transcription factor IRF8. *International Journal of Hematology*, *101*(4), 342–351. https://doi.org/10.1007/s12185-015-1761-9

Tauriello, D. V. F., Palomo-Ponce, S., Stork, D., Berenguer-Llergo, A., Badia-Ramentol, J., Iglesias, M., Sevillano, M., Ibiza, S., Cañellas, A., Hernando-Momblona, X., Byrom, D., Matarin, J. A., Calon, A., Rivas, E. I., Nebreda, A. R., Riera, A., Attolini, C. S. O., & Batlle, E. (2018). TGFβ drives immune evasion in genetically reconstituted colon

cancer metastasis. *Nature*, *554*(7693), 538–543. https://doi.org/10.1038/nature25492

Van Der Maaten, L. (2015). Accelerating t-SNE using tree-based algorithms. *Journal of Machine Learning Research*, *15*, 3221–3245.

van Leeuwen-Kerkhoff, N., Lundberg, K., Westers, T. M., Kordasti, S., Bontkes, H. J., de Gruijl, T. D., Lindstedt, M., & van de Loosdrecht, A. A. (2017). Transcriptional profiling reveals functional dichotomy between human slan + non-classical monocytes and myeloid dendritic cells . *Journal of Leukocyte Biology*, *102*(4), 1055–1068. https://doi.org/10.1189/jlb.3ma0117-037r

Verger, A., Langen, K.J. (2017). PET Imaging in Glioblastoma: Use in Clinical Practice. In: Glioblastoma. Brisbane: Codon Publications. pp155-174.

Verhoeff, J. J. C., Van Tellingen, O., Claes, A., Stalpers, L. J. A., Van Linde, M. E., Richel, D. J., Leenders, W. P. J., & Van Furth, W. R. (2009). Concerns about anti-angiogenic treatment in patients with glioblastoma multiforme. *BMC Cancer*, *9*, 1–9. https://doi.org/10.1186/1471-2407-9-444

Villa-Álvarez, M., Sordo-Bahamonde, C., Lorenzo-Herrero, S., Gonzalez-Rodriguez, A. P., Payer, A. R., Gonzalez-Garcia, E., Villa-Álvarez, M. C., López-Soto, A., & Gonzalez, S. (2018). Ig-Like Transcript 2 (ILT2) Blockade and Lenalidomide Restore NK Cell Function in Chronic Lymphocytic Leukemia. *Frontiers in Immunology*, *9*(December), 2917. https://doi.org/10.3389/fimmu.2018.02917

Villani, A. C., Satija, R., Reynolds, G., Sarkizova, S., Shekhar, K., Fletcher, J., Griesbeck, M., Butler, A., Zheng, S., Lazo, S., Jardine, L., Dixon, D., Stephenson, E., Nilsson, E., Grundberg, I., McDonald, D., Filby, A., Li, W., De Jager, P. L., … Hacohen, N. (2017). Single-cell RNA-seq reveals new types of human blood dendritic cells, monocytes, and progenitors. *Science*, *356*(6335). https://doi.org/10.1126/science.aah4573

Vredenburgh, J. J., Desjardins, A., Herndon, J. E., Marcello, J., Reardon, D. A., Quinn, J. A., Rich, J. N., Sathornsumetee, S., Gururangan, S., Sampson, J., Wagner, M., Bailey, L., Bigner, D. D., Friedman, A. H., & Friedman, H. S. (2007). Bevacizumab plus irinotecan in recurrent glioblastoma multiforme. *Journal of Clinical Oncology*, *25*(30), 4722–4729. https://doi.org/10.1200/JCO.2007.12.2440

Wang, Q., Hu, B., Hu, X., Kim, H., Squatrito, M., Scarpace, L., deCarvalho, A. C., Lyu, S., Li, P., Li, Y., Barthel, F., Cho, H. J., Lin, Y. H., Satani, N., Martinez-Ledesma, E., Zheng, S., Chang, E., Sauvé, C. E. G., Olar, A., … Verhaak, R. G. W. (2017). Tumor Evolution of Glioma-Intrinsic Gene Expression Subtypes Associates with Immunological Changes in the Microenvironment. *Cancer Cell*, *32*(1), 42-56.e6. https://doi.org/10.1016/j.ccell.2017.06.003

Wang, Y., Du, X., Wei, J., Long, L., Tan, H., Guy, C., Dhungana, Y., Qian, C., Neale, G., Fu, Y. X., Yu, J., Peng, J., & Chi, H. (2019). LKB1 orchestrates dendritic cell metabolic quiescence and anti-tumor immunity. *Cell Research*, *29*(5), 391–405. https://doi.org/10.1038/s41422-019-0157-4

Weathers SP, de Groot J. VEGF Manipulation in Glioblastoma. *Oncology (Williston Park)*. 2015;29(10):720-727. PMID: 26470893

Weller, M., Roth, P., Preusser, M., Wick, W., Reardon, D. A., Platten, M., & Sampson, J. H. (2017). Vaccine-based immunotherapeutic approaches to gliomas and beyond. *Nature Reviews Neurology*, *13*(6), 363–374. https://doi.org/10.1038/nrneurol.2017.64

Weller, R. O., Djuanda, E., Yow, H. Y., & Carare, R. O. (2009). Lymphatic drainage of the brain and the pathophysiology of neurological disease. *Acta Neuropathologica*, *117*(1), 1–14. https://doi.org/10.1007/s00401-008-0457-0

Wen, A. Y., Sakamoto, K. M., & Miller, L. S. (2010). The Role of the Transcription Factor CREB in Immune Function. *The Journal of Immunology*, *185*(11), 6413–6419. https://doi.org/10.4049/jimmunol.1001829

Wesseling, P., & Capper, D. (2018). WHO 2016 Classification of gliomas. *Neuropathology and Applied Neurobiology*, *44*(2), 139–150. https://doi.org/10.1111/nan.12432

Wood, E. J. (1996). Extracellular matrix a practical approach: Edited by M A Haraldson and J R Hassell. pp 404. IRL Press at Oxford University Press, Oxford. 1995. In *Biochemical education* (Vol. 24, Issue 3, p. 189).

Worbs, T., Hammerschmidt, S. I., & Förster, R. (2017). Dendritic cell migration in health and disease. *Nature Reviews Immunology*, *17*(1), 30–48. https://doi.org/10.1038/nri.2016.116

Wu, J., & Horuzsko, A. (2009). Expression and function of ILTs on tolerogenic dendritic cells. *Human Immunology*, *70*(5), 353–356. https://doi.org/10.1016/j.humimm.2009.01.024.Expression

Yang, M., Li, J., Gu, P., & Fan, X. (2021). The application of nanoparticles in cancer immunotherapy: Targeting tumor microenvironment. *Bioactive Materials*, *6*(7), 1973–1987. https://doi.org/10.1016/j.bioactmat.2020.12.010

Zhang, G., Tang, X., Liang, L., Zhang, W., Li, D., Li, X., Zhao, D., Zheng, Y., Chen, Y., Hao, B., Wang, K., Tang, N., & Ding, K. (2020). DNA and RNA sequencing identified a novel oncogene VPS35 in liver hepatocellular carcinoma. *Oncogene*, *39*(16), 3229–3244. https://doi.org/10.1038/s41388-020-1215-6

Zhang, H. X., Xu, Z. S., Lin, H., Li, M., Xia, T., Cui, K., Wang, S. Y., Li, Y., Shu, H. B., & Wang, Y. Y. (2018). TRIM27 mediates STAT3 activation at retromer-positive structures to promote colitis and colitis-associated carcinogenesis. *Nature Communications*, *9*(1). https://doi.org/10.1038/s41467-018-05796-z

Zhang, Q., He, Y., Luo, N., Patel, S. J., Han, Y., Gao, R., Modak, M., Carotta, S., Haslinger, C., Kind, D., Peet, G. W., Zhong, G., Lu, S., Zhu, W., Mao, Y., Xiao, M., Bergmann, M., Hu, X., Kerkar, S. P., … Zhang, Z. (2019). Landscape and Dynamics of Single Immune Cells in Hepatocellular Carcinoma. *Cell*, *179*(4), 829-845.e20. https://doi.org/10.1016/j.cell.2019.10.003